

FACILITY FORM 602

N 57-24605
(ACCESSION NUMBER)141
(PAGES)CR-81615
(NASA CR OR TMX OR AD NUMBER)

(THRU)

(CODE)

31
(CATEGORY)

VOLUME 2 OF 8

Final Report**ATS - 4**

PREPARED BY

FAIRCHILD HILLER
SPACE SYSTEMS DIVISION

FOR

NASA
Goddard Space Flight Center

DECEMBER 1966

ATS-4 STUDY PROGRAM
FINAL REPORT
(Contract NASW-1411)
VOLUME TWO OF EIGHT

prepared by
FAIRCHILD HILLER SPACE SYSTEMS DIVISION
Sherman Fairchild Technology Center
Germantown, Maryland
for
GODDARD SPACE FLIGHT CENTER
NATIONAL AERONAUTICS AND SPACE ADMINISTRATION

December 1966

N67 24605

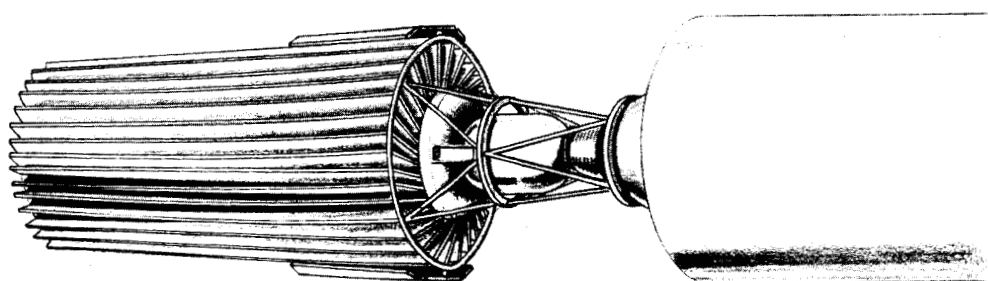
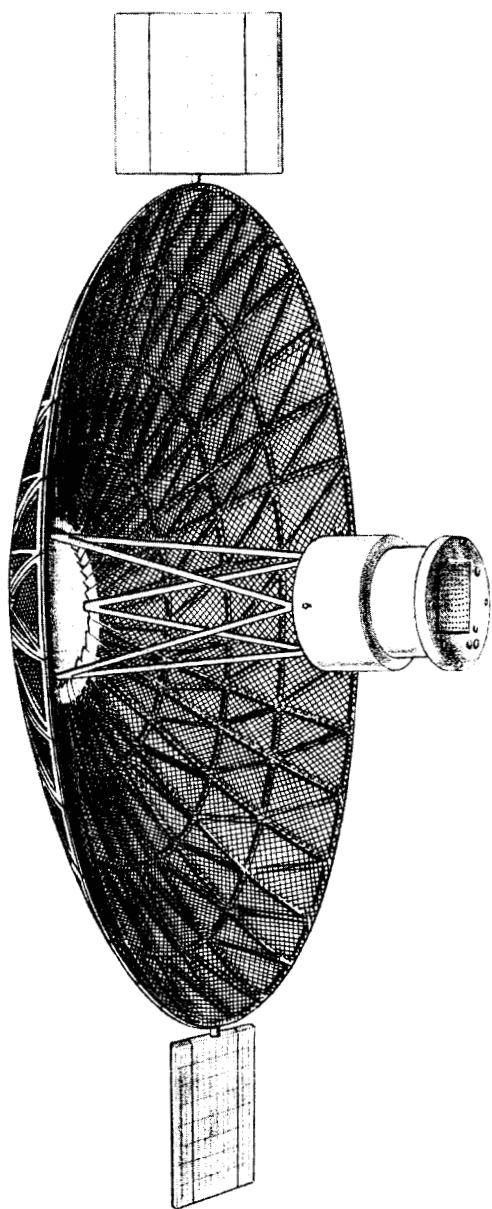


TABLE OF CONTENTS

VOLUME ONE

Section	Title	Page
1.0	Summary	1-1
1.1	Objectives and Justification	1-1
	1.1.1 Utilization	1-2
	1.1.2 Implementation	1-4
1.2	Program Feasibility	1-6
	1.2.1 Parabolic Antenna	1-6
	1.2.2 Stabilization and Control System	1-8
	1.2.3 Phased Array	1-11
	1.2.4 Interferometer	1-12
1.3	Subsystem Summaries	1-13
	1.3.1 Configuration Description	1-13
	1.3.2 Parabolic Reflector	1-19
	1.3.3 Parabolic Antenna Feed	1-22
	1.3.4 Attitude Stabilization and Control System	1-24
	1.3.5 Launch Vehicle - Ascent and Orbit Injection	1-27
	1.3.6 Interferometer System	1-32
	1.3.7 Phased Array	1-33
	1.3.8 In-Orbit Maneuvers and Auxiliary Propulsion System	1-35
	1.3.9 Additional Experiment Capability	1-37

TABLE OF CONTENTS

VOLUME TWO

Section	Title	Page
2.0	Systems Analysis	2-1
2.1	Mission Profile and Operations Plan	2-1
	2.1.1 Mission Profile	2-1
	2.1.2 Operations Plan	2-20
2.2	Experiment Plan	2-20
	2.2.1 Parabolic Antenna Experiment	2-20
	2.2.2 Monopulse System Operation	2-30
	2.2.3 Phased Array Experiment	2-32
	2.2.4 Orientation and Control Experiment	2-45
	2.2.5 Interferometer Experiment	2-49
	2.2.6 Additional Communication Experiments	2-54
2.3	Power Profiles	2-58
	2.3.1 Preorbital Power	2-58
	2.3.2 Experiment Evaluation	2-61
	2.3.3 Experiment Demonstration	2-61
	2.3.4 Power System Margin	2-61
	2.3.5 Experiment Loads	2-64
2.4	Antenna Accuracy Considerations	2-68
	2.4.1 Reflecting Surface Errors	2-68
	2.4.2 Feed Location Errors	2-73
	2.4.3 Frequency Limitations on Gain	2-74
	2.4.4 Summary of Antenna Error Effects	2-76
2.5	Antenna Efficiencies	2-79
	2.5.1 Parabolic Antenna	2-79
	2.5.2 Phased Array Figures of Merit	2-82
2.6	Faisure Modes	2-91
	2.6.1 System Considerations	2-91
	2.6.2 Parabolic Antenna	2-91
	2.6.3 Stabilization and Control System	2-93
	2.6.4 Phased Array	2-98
	2.6.5 Antenna Experiment Electronics	2-100
	2.6.6 Phased Array Monopulse Operation	2-103
2.7	Weight Summaries	2-105

TABLE OF CONTENTS

VOLUME THREE

Section	Title	Page
3.0	Vehicle Engineering	3-1
3.1	Concept Evolution	3-1
	3.1.1 Trade-off Parameters	3-1
	3.1.2 F/D Trade-offs	3-6
	3.1.3 Spacecraft Concepts	3-8
3.2	Concept Evaluation and Reference Concept	3-21
	3.2.1 Launch Vehicle Choice	3-21
	3.2.2 Split Module Concept	3-21
	3.2.3 Reference Concept	3-25
	3.2.4 Concept Comparison	3-29
	3.2.5 Titan IIC Adaptability	3-29
3.3	Reflector Design	3-33
	3.3.1 Design Evolution and Alternate Approaches	3-33
	3.3.2 Petal Hinging Concepts	3-38
	3.3.3 Petal Structural Design	3-40
	3.3.4 Deployment System	3-47
	3.3.5 Tolerance Considerations	3-47
	3.3.6 Reflecting Surface	3-50
	3.3.7 Petal Locking System	3-53
3.4	Reflector Fabrication	3-57
	3.4.1 Fabrication Considerations	3-57
	3.4.2 Aluminum Substructure	3-57
	3.4.3 Wire Mesh Forming	3-59
	3.4.4 Sub-Assemblies	3-60
	3.4.5 Tooling	3-60
	3.4.6 Assembly Procedure	3-64
	3.4.7 Measurement of Surface Deviations	3-65
3.5	Structural and Dynamic Analyses	3-71
	3.5.1 Analytical Methods and Approach	3-71
	3.5.2 Preliminary Analysis	3-77
	3.5.3 Integrated Spacecraft-Launch Configuration	3-104
	3.5.4 Integrated Spacecraft-Orbit Configuration	3-115
	3.5.5 Orbit Maneuvering	3-121

TABLE OF CONTENTS

VOLUME THREE (Continued)

Section	Title	Page
3.6	Thermo/Structural Analysis	3-129
	3.6.1 Thermal Requirements and Approach	3-129
	3.6.2 Design Orbit	3-133
	3.6.3 Petal Thermal Analysis	3-135
	3.6.4 Thermoelastic Analysis of Reflector	3-154
	3.6.5 Feed Mast Thermal Analysis	3-166
	3.6.6 Thermal Deformation of Feed Mast	3-172
	3.6.7 Spacecraft Thermal Control	3-175
3.7	Dimensional Stability	3-178
	3.7.1 Introduction	3-178
	3.7.2 Precision Elastic Limit	3-179
	3.7.3 Residual Stress	3-179
	3.7.4 Design Application	3-180
	3.7.5 References for Dimensional Stability Discussion	3-182
3.8	In-Orbit Measurement of Antenna Surface Accuracy	3-183
	3.8.1 Basic Techniques	3-183
	3.8.2 Operational Considerations	3-183
	3.8.3 Antenna Surface Errors	3-185
	3.8.4 Equipment Location	3-185
	3.8.5 Conceptual Design	3-186
	3.8.6 Error Resolution Requirements	3-189
	3.8.7 Sampling Surface Measurements	3-191
	3.8.8 The Axial Four Camera System	3-192
	3.8.9 Illumination of the Antenna	3-208
	3.8.10 System Operation	3-209
	3.8.11 General Comments	3-209
Appendix		
3A	Expandable Truss Antennas	3-211
3B	Inflatable Antennas	3-225
3C	Rigid Panel Antennas	3-230
3D	Petal Axis of Rotation Determination	3-248

TABLE OF CONTENTS

VOLUME FOUR

Section	Title	Page
4.0	Power Systems	4-1
4.1	Solar Panel Configuration Study	4-2
4.2	Solar Cell Radiation Degradation	4-6
	4.2.1 Radiation Environment	4-6
	4.2.2 Background Flux	4-7
	4.2.3 Power Margin	4-10
4.3	Battery Characteristics	4-10
	4.3.1 Nickel-Cadmium Battery	4-13
	4.3.2 Silver-Cadmium Battery	4-13
	4.3.3 Silver-Zinc Battery	4-15
	4.3.4 Battery Comparison	4-15
4.4	Battery Charging and Control	4-23
	4.4.1 Constant Current Charging	4-23
	4.4.2 Constant Voltage Charging	4-24
	4.4.3 Modified Constant Voltage Charging	4-26
	4.4.4 Tapered Charging	4-26
	4.4.5 Recommendation	4-26
4.5	Concept Power Subsystem	4-28
	4.5.1 Design Approach	4-28
	4.5.2 Battery Complement	4-32
	4.5.3 Solar Array	4-35
	4.5.4 Power Conditioning and Control	4-36
5.0	Orbital Analysis	5-1
5.1	General	5-1
5.2	Apogee Injection Stages	5-2
5.3	Ascent Trajectories	5-4
	5.3.1 Requirements and General Considerations	5-4
	5.3.2 Synchronous Injection - Single Apogee Impulse	5-7
	5.3.3 Subsynchronous Injection - High Altitude Parking Orbit	5-10
	5.3.4 Recommended Centaur Ascent Trajectory	5-18
5.4	Orbit Payloads	5-23
	5.4.1 General	5-23
	5.4.2 SLV3A/Agna and SLV3C/Centaur	5-23

TABLE OF CONTENTS
VOLUME FOUR (Continued)

Section	Title	Page
	5.4.3 Titan IIIC	5-30
	5.4.4 Payload Data Summary	5-30
5.5	Orbit Injection Errors	5-32
	5.5.1 Error Values	5-32
	5.5.2 Associated Latitude-Longitude Deviation	5-33
	5.5.3 Associated Corrective Velocity Impulse Requirements	5-36
5.6	Orbit Perturbations	5-39
	5.6.1 General	5-39
	5.6.2 Earth Oblateness and Extraterrestrial Perturbations	5-39
	5.6.3 Terrestrial Perturbations - Equatorial Ellipticity	5-41
	5.6.4 Associated Corrective Velocity Impulse Requirements	5-45
5.7	Auxiliary Propulsion System	5-48
	5.7.1 Velocity Impulse and Thrust Requirements	5-48
	5.7.2 Initial APS Comparison Study	5-48
5.8	Orbit Guidance	5-57
	5.8.1 General Requirements	5-57
	5.8.2 Orbit Injection Error Correction	5-58
	5.8.3 Station Keeping and Repositioning	5-63
5.9	References and Symbols for Orbital Analysis	5-65
	5.9.1 References	5-65
	5.9.2 List of Symbols	5-67

TABLE OF CONTENTS

VOLUME FIVE

Section	Title	Page
6.0	ATTITUDE STABILIZATION AND CONTROL SYSTEM	6-1
6.1	Attitude Stabilization and Control Requirements	6-1
6.1.1	Mission Requirements	6-1
6.1.2	Pointing Accuracy	6-1
6.1.3	Control Modes	6-1
6.2	Attitude Reference Subsystem	6-2
6.2.1	Alternate Approaches	6-2
6.2.2	Candidate Reference Sensors	6-11
6.2.3	Selected Configuration	6-22
6.2.4	Sensor Performance	6-23
6.3	Disturbance Torque Model	6-25
6.3.1	Meteoroid Impact	6-25
6.3.2	Gravity Gradient	6-34
6.3.3	Magnetic Disturbance	6-35
6.3.4	Internal Rotating Equipment	6-35
6.3.5	Solar Pressure	6-35
6.4	Torquer Subsystem	6-52
6.4.1	Control Impulse Requirements	6-52
6.4.2	Candidate Reaction Jet Types	6-59
6.4.3	Inertia Wheel Subsystem	6-63
6.4.4	Selected Torquer Configuration	6-69
6.5	Computation and Data Handling	6-71
6.5.1	On-Board Computation	6-71
6.5.2	Up-Data Commands	6-71
6.5.3	Down-Data Monitor	6-71
6.6	System Operational Description	6-75
6.6.1	Control Mode Operation	6-75
6.6.2	System Block Diagram	6-85
6.6.3	Sensor Update	6-89
6.7	System Performance	6-90
6.7.1	Pointing Accuracy	6-90
6.7.2	Acquisition	6-93
6.7.3	Control System Dynamics	6-93
6.7.4	Reliability	6-117
6.8	System Physical Description	6-124
Appendix		
6A	Preliminary Control Torque and Impulse Requirements	
6B	Preliminary Reaction Jet Considerations	
6C	Preliminary Inertia Wheel Considerations For Candidate Vehicle Configurations	
6D	Preliminary Combined Wheel/Jet System Considerations	
6E	Preliminary Transfer Orbit Control Mode Analysis	

TABLE OF CONTENTS

VOLUME SIX

Section	Title	Page
7.0	Communications Experiments	7-1
7.1	Parabolic Antenna	7-1
	7.1.1 Beam Scanning	7-1
	7.1.2 Parabolic Antenna Feeds	7-14
	7.1.3 Aperture Blockage	7-32
	7.1.4 Paraboloid Performance	7-42
7.2	Phased Array	7-58
	7.2.1 Transdirective Array	7-59
	7.2.2 The Butler Matrix Array	7-63
	7.2.3 Space Fed (Lens) Array	7-65
	7.2.4 Corporate-Fed Array	7-71
	7.2.5 Corporate-Fed Phased Array Design Considerations	7-79
	7.2.6 Antenna Definition	7-92
	7.2.7 Digital Beam Steering Unit	7-102
	7.2.8 Packaging Configuration	7-108
7.3	Communications Equipment	7-111
	7.3.1 Transmission Parameters	7-111
	7.3.2 Systems Description	7-113
	7.3.3 Weight, Volume and Power Summary	7-134
	7.3.4 System Performance Summary	7-137
Appendix		
7A	Four Paraboloid Off-Set Feed Configuration	7-139
7B	Ionospheric Effects on Wave Polarization	7-147
7C	Separate 100 MHz Antennas	7-159
7D	Communication Components	7-165

TABLE OF CONTENTS

VOLUME SEVEN

Section	Title	Page
8.0	Radio Interferometer Experiment	8-1
8.1	Introduction	8-1
8.2	Study Approach	8-3
8.3	Candidate Interferometer Concepts	8-5
8.4	Candidate Interferometer Systems	8-11
	8.4.1 Selection Criteria	8-11
	8.4.2 System Block Diagrams	8-11
8.5	Selection of Preferred Concept	8-25
	8.5.1 Candidate Evaluation and Selection of Preferred System	8-25
	8.5.2 Phased Array as an Interferometer	8-44
8.6	Design of Preferred Interferometer System	8-48
	8.6.1 General Circuit Description	8-48
	8.6.2 Mechanical and Thermal Design	8-59
	8.6.3 Interferometer Attitude Sensor Interface	8-68
	8.6.4 Physical Characteristics	8-85
8.7	Error Analysis of Preferred Concept	8-86
8.8	Conclusions and Recommendations	8-116
8.9	Bibliography and Glossary	8-117
Appendix		
8A	Interference Reduction by Correlation	8-136
8B	RF Link Calculation	8-138
8C	Interferometer Angular Error Due to Mutual Coupling	8-141
8D	System Polarization	8-146
8E	Derivation of the Received Voltage Phases on an Elliptically Polarized Interferometer Antenna Pair with an Incident Elliptically Polarized Wave	8-165
8F	Alternative Antenna Switching Systems - Direct Phase Reading Interferometer	8-172
8G	Derivation of Counter Equation	8-180
8H	Gating Time Error Analysis	8-182
8I	Conversion of θ_s into Attitude	8-187
8J	Limitation of Range and Range Rate Capability	8-201
Volume 8	Program Budgetary Costs and Schedules	10-1

TABLE OF CONTENTS

VOLUME SEVEN (Continued)

Section	Title	Page
9.0	Summary	9-1
9.1	Data Flow	9-2
	9.1.1 Definition	9-2
	9.1.2 Requirements	9-2
	9.1.3 Model of the Data Flow	9-3
9.2	Telemetry System	9-8
	9.2.1 Data Handling Requirements	9-8
	9.2.2 Data Handling System Design	9-9
	9.2.3 Data Handling System Configuration	9-17
	9.2.4 Data Transmission System Design	9-23
	9.2.5 Data Transmission Link Calculation	9-28
	9.2.6 System Size, Weight and Power Estimates	9-44
	9.2.7 Equipment Implementation	9-44
9.3	Command System	9-47
	9.3.1 Definition	9-47
	9.3.2 Requirements	9-47
	9.3.3 Word Format	9-50
	9.3.4 Description and Operation of the Onboard System	9-53
	9.3.5 Estimates of Physical Characteristics	9-60
	9.3.6 Transmission Link Power Requirements	9-62
	9.3.7 Equipment Implementation	9-64
	9.3.8 Ground Equipment Requirements	9-65
9.4	Range and Range Rate Transponder	9-69
	9.4.1 Accuracy Requirements	9-69
	9.4.2 Transponder Operating Frequency Selection	9-69
	9.4.3 UHF Transponder Characteristics	9-70
	9.4.4 Equipment Implementation	9-71
9.5	Ground Station Requirements	9-72
	9.5.1 Ground Equipment Description	9-72
9.6	References	9-84
	Appendices	
	9A Commutator Channel Assignment	9-85
	9B Modulation Index Calculations (Mode 1)	9-101
	9C Solving for Receiver Noise Power and Channel Bandwidth Ratios (Mode 1)	9-103
	9D Solving for Receiver Noise Power and Channel Bandwidth Ratios (Mode II)	9-105
	9E Command Signal Catalog	9-106
	9F Telemetry Signal Catalog	9-116
	9G Data Questionnaire	9-131

LIST OF ILLUSTRATIONS

VOLUME ONE

Figure	Title	Page
1.3-1	Fairchild Hiller ATS-4 Concept	1-14
1.3-2	Reference Concept	1-15
1.3-3	Spacecraft Module Detail	1-18
1.3-4	Multiband Prime Focus Feed	1-23
1.3-5	SCS Block Diagram	1-29
1.3-6	ATS-4 Ascent Trajectory	1-31

LIST OF ILLUSTRATIONS

VOLUME TWO

Figure	Title	Page
2.1-1	Satellite Ground Track	2-2
2.1-2	Spacecraft/Sun Orientation in Transfer Orbit	2-4
2.1-3	Satellite Ground Track and Ground Station	2-12
2.1-4	Gross Data Flow Concept	2-17
2.2-1	Major Plane Location and Arts for Antenna Measurement	2-22
2.2-2	Ground Terminal Layout for Monopulse Calibration	2-33
2.2-3	Major Planes and Beam Positions for Station Pattern	2-35
	Tests	
2.2-4	Multiple Pattern Arts Using Two Ground Stations	2-41
2.2-5	Crosstalk Measurement	2-41
2.2-6	Major Plane Arts - Interferometer	2-53
2.2-7	Pointing of the Z-Axis for Interferometer Measurement	2-53
2.3-1	Typical Experiment Evaluation Profile	2-62
2.3-2	Power Profile with Additional Experiments	2-62
2.3-3	Experiment Demonstration Maximum Profile	2-63
2.4-1	Classification of Parabolic Antenna Errors	2-69
2.4-2	Reflector Errors	2-71
2.4-3	Feed Location Errors	2-75
2.4-4	Feed Location Errors ($F/D = 0.3$)	2-78
2.4-5	Frequency Limitation on Gain	2-78
2.5-1	X-Band Radiation Pattern	2-81
2.6-1	Failed Reaction Wheel Backup Subsystem	2-94

LIST OF ILLUSTRATIONS

VOLUME THREE

Figure	Title	Page
3.1-1	Antenna Feed Location	3-3
3.1-2	C.G. Location Study	3-5
3.1-3	Concept SK513-10	3-13
3.1-4	Concept SK513-12	3-15
3.1-5	Concept SK513-11	3-16
3.1-6	Concept SK513-13	3-17
3.1-7	Concept SK513-14	3-18
3.1-8	Concept SK513-16	3-19
3.2-1	Concept SK513-18	3-23
3.2.2	Concept SK513-17 (Reference Concept)	3-24
3.2-3	Spacecraft Module Detail	3-27
3.2-4	Concept Comparison Chart	3-31
3.2-5	Reference Concept on Titan IIC	3-32
3.3-1	Conic Scissors Parabolic Antenna	3-34
3.3-2	Inflatable Parabolic Antenna	3-36
3.3-3	Retentive Memory Petal Concept	3-39
3.3-4	Non-Radial Petals, Sheet One	3-41
3.3-5	Non-Radial Petals, Sheet Two	3-42
3.3-6	Petal Concept Parabolic Antenna	3-43
3.3-7	Skewed Hinge Design	3-45
3.3-8	Petal Structural Assembly and Hinge Details	3-46
3.3-9	Deployment Synchronizer	3-49
3.3-10	Mesh Segment Installation	3-51
3.3-11	Mesh Reflector Characteristics	3-52
3.3-12	Inter-Petal Locks	3-55
3.3-13	Inter-Petal Lock - Preferred Concept	3-56
3.4-1	Shaping of Mesh Reflecting Surface	3-58
3.4-2	Master Tool	3-58
3.4-3	Assembly Bonding Fixture	3-62
3.4-4	Hinge and Latch Alignment Fixture	3-63
3.4-5	Measurement of Surface Deviations	3-67
3.5-1	Truss Feed Mast Weights	3-78
3.5-2	Truss Feed Mast Frequencies	3-79
3.5-3	Single Tube Feed Mast Analysis	3-81
3.5-4	Four Tube Feed Mast Weights	3-82
3.5-5	Four Tube Feed Mast Frequencies	3-83
3.5-6	Analysis of Quadrupe Feed Mast Structure	3-84

LIST OF ILLUSTRATIONS
VOLUME THREE (Continued)

Figure	Title	Page
3.5-7	Quadruped Feed Mast Frequencies	3-85
3.5-8	Analysis of Tripod Feed Mast Structure	3-86
3.5-9	Tripod Feed Mast Frequencies	3-87
3.5-10	Reflector Petal Loading	3-94
3.5-11	Spacecraft, Injection, Motor and Adapter Structural Properties	3-94
3.5-12	Launch Integrated S/C - Analytical Model	3-96
3.5-13	Orbit Configuration - Mass Model	3-102
3.5-14	Preferred Configuration and Analytical Model	3-105
3.5-15	Petal Restraint and Stiffness	3-106
3.5-16	Mass Point Locations and Weights	3-107
3.5-17	YY Direction Mode Shapes	3-109
3.5-18	XX Direction Mode Shapes	3-110
3.5-19	Analytical Model - Orbit Configuration	3-116
3.5-20	Frequency and Mode Shapes - Orbit Configuration, Sheet One	3-118
3.5-21	Frequency and Mode Shapes - Orbit Configuration, Sheet Two	3-119
3.5-22	Frequency and Mode Shapes - Orbit Configuration, Sheet Three	3-120
3.5-23	Response to Single Finite Duration Pulse (Roll Correction Maneuver)	3-124
3.5-24	Response to Single Finite Duration Pulse (Yaw Correction Maneuver)	3-125
3.6-1	Yearly Change in Orbit Position Relative to Sun Vector	3-134
3.6-2	Petal Thermal Analysis	3-136
3.6-3	Relation of Thermal Analysis Nodes to Orbit Position	3-136
3.6-4	Feed Module Shadowing	3-137
3.6-5	Reflection Mesh Sunlight Blockage	3-139
3.6-6	Mesh and Antenna Hub Shadowing	3-141
3.6-7	Coordinate System for Thermal Analysis	3-142
3.6-8	Antenna Feed Shadowing	3-144
3.6-9	Beam Temperatures	3-147
3.6-10	Petal Beam Cross-Section	3-151
3.6-11	Mesh Standoff Fittings	3-151

LIST OF ILLUSTRATIONS VOLUME THREE (Continued)

Figure	Title	Page
3.6-12	Beam Geometry	3-153
3.6-13	Petal Thermal Model	3-159
3.6-14	Radial Displacement Geometry	3-159
3.6-15	Deformation of Radial Member	3-159
3.6-16	Reflector Surface Mesh Geometry	3-165
3.6-17	Surface Mesh Chord Position	3-165
3.6-18	Feed Mast Geometry	3-167
3.6-19	Electrical Simulation, Uninsulated Mast	3-168
3.6-20	Electrical Simulation, Insulated Mast	3-168a
3.6-21	Temperature of Node 4, Uninsulated Mast	3-170
3.6-22	Temperature of Node 4, Insulated Mast	3-170a
3.6-23	Feed Mast Shadowing on Support "A"	3-171
3.6-24	Feed Mast Thermal Model	3-171a
3.6-25	Feed Mast Distortions	3-174
3.6-26	Passive Control Areas Average Temperature versus Dissipation	3-176
3.8-1	Volume Available for Measurement Equipment	3-187
3.8-2	Mirror Position above Camera	3-187
3.8-3	Converse Mirror below Camera	3-187
3.8-4	Concave Mirror below Camera	3-188
3.8-5	Sighting Angles	3-188
3.8-6	Effective Mesh Spacing	3-188
3.8-7	Composite Converse Mirror	3-192
3.8-8	Basic Four Camera Axial System	3-192
3.8-9	Full View Camera System	3-194
3.8-10	Normal Deflection Geometry	3-194
3.8-11	Ring Viewing Angles	3-194
3.8-12	Vidicon Image Dimensions	3-196
3.8-13	Central Circle in Vidicon Image	3-196
3.8-14	Radial and Circular Scan Patterns	3-198
3.8-15	Rim Marker Pattern	3-198
3.8-16	Modified Marker Coding	3-198
3.8-17	Reversed Marker Pattern	3-201
3.8-18	Marker Pattern without 1/2 Inch Plates	3-201
3.8-19	Pattern for Third Ring	3-202
3.8-20	Pattern for Second Ring	3-202

LIST OF ILLUSTRATIONS

VOLUME THREE (Continued)

Figure	Title	Page
3.8-21	Pattern for Central Ring	3-202
3.8-22	Pattern of Perfect Match of Image and Standard Negative	3-203
3.8-23	Pattern of Mismatch of Image and Standard Negative	3-203
3.8-24	Marking Pattern from Deformed Mesh Wires	3-207
3.8-25	Deformed Wires Positioned along a Parabola	3-207
3.8-26	Illumination by Columnar Light Sources	3-208
3.8-27	Illumination by Toroidal Light Sources	3-208

LIST OF ILLUSTRATIONS

VOLUME FOUR

Figure	Title	Page
4.1-1	Flat Plate Array, Two Degrees Of Freedom	4-3
4.1-2	Flat Plate Array, One Degree Of Freedom	4-3
4.1-3	Flat Plate Array, Fixed	4-3
4.1-4	Two Flat Plates Array, Fixed	4-4
4.1-5	Three Flat Plates Array, Fixed	4-4
4.1-6	Cylindrical Array, Fixed	4-4
4.1-7	Double Faced Flat Plate Array	4-5
4.1-8	Double Faced Two Flat Plates Array	4-5
4.1-9	Double Faced Three Flat Plates Array	4-5
4.2-1	Solar Cell Radiation Degradation	4-8
4.2-2	Power Loss Due To Radiation Effects	4-11
4.3-1	Nickel-Cadmium Battery Life	4-14
4.3-2	Energy Per Unit Weight For Various Batteries	4-17
4.3-3	Energy Per Unit Volume For Various Batteries	4-18
4.3-4	Capacity vs. Temperature For Various Cells	4-18
4.3-5	Silver-Zinc Battery Cycle Life	4-19
4.3-6	Silver-Cadmium Battery Cycle Life	4-19
4.3-7	Nickel-Cadmium Battery Cycle Life	4-20
4.3-8	Umbra and Penumbra Patterns For A Synchronous Equatorial Satellite	4-22
4.4-1	Recommended % Overcharge is Temperature	4-25
4.4-2	Overcharge Pressure Vs Current	4-25
4.4-3	Maximum Limiting Voltage Vs. Temperature	4-27
4.4-4	Tapered Charge Characteristic	4-27
4.5-1	Typical Experiment Evaluation Power Profile	4-29
4.5-2	Power Profile With Additional Experiments	4-29
4.5-3	Experiment Demonstration Maximum Demand Profile	4-29
4.5-4	Power System Weight Vs. Load Duration	4-29
4.5-5	Power System Block Diagram	4-37

LIST OF ILLUSTRATIONS

VOLUME FOUR (Continued)

Figure	Title	Page
5.3-1	Ascent Trajectories	5-6
5.3-2	Earth Track of Ascent Trajectory	5-11
5.3-3	Injection Station Longitude Variation	5-11
5.3-4	Effect of Launch Azimuth on Required Increase in Characteristic Velocity	5-14
5.3-5	High Altitude, Elliptic Parking Orbit Characteristics	5-16
5.3-6	Earth Track of High Altitude Parking Orbit Ascent Trajectory	5-17
5.3-7	Ground Track of Ascent Trajectories	5-19
5.3-8	Spacecraft/Sun Orientation in Transfer Orbit	5-21
5.4-1	Payload and AIS Propellant Weight vs i_c (Burner II)	5-28
5.4-2	Payload and AIS Propellant Weight vs i_c (TE364-3)	5-28
5.6-1	Satellite Semimajor Axis Perturbation	5-42
5.6-2	Satellite Inclination Perturbation	5-42
5.6-3	Long Period Oscillation	5-44
5.6-4	Required Velocity Impulse per Year	5-46

LIST OF ILLUSTRATIONS

VOLUME FIVE

Figure	Title	Page
6-1	Reference Coordinate Frame (Nominal)	6-3
6-2a	Cell Orientation	6-13
6-2b	Cell Outputs	6-13
6-2c	Sun Sensor Signals	6-13
6-3	Meteoroid Extrapolations	6-29
6-4	Percent Open Area in Each Mesh Segment as a Function of Solar Incident Angle	6-41
6-5	Antenna Projected Surface Map	6-43
6-6	Projected Antenna Shaded Area Profile	6-44
6-7	Pitch Axis Solar Pressure Disturbance Torque	6-47
6-8	Roll Axis Solar Pressure Disturbance Torque Due to Antenna and Feed System	6-48
6-9	Roll Axis Solar Pressure Disturbance Torque Due to Fixed Solar Panels Only	6-49
6-10	Roll Axis Solar Pressure Disturbance Torque	6-50
6-11	Yaw Axis Solar Pressure Disturbance Torque	6-51
6-12	Hydrazine Thruster Output Efficiency	6-62
6-13	Liquid Hydrazine System Schematic	6-64
6-14	Block Diagram - Ascent Control	6-86
6-15	SCS Block Diagram	6-87
6-16	Phase Plane Plot Sun Acquisition - Pitch Axis	6-94
6-17	Phase Plane Plot Sun Acquisition - Yaw Axis	6-95
6-18	Phase Plane Plot Earth Acquisition Roll Axis	6-96
6-19	Phase Plane Plot Star Acquisition Yaw Axis	6-97
6-20	Open Loop Bode Plot - Roll Axis	6-99
6-21	Open Loop Bode Plot - Pitch Axis	6-100
6-22	Open Loop Bode Plot - Yaw Axis	6-101
6-23	SCS and Vehicle Dynamics Block Diagram	6-102
6-24	Roll Axis - Rigid Body Amplitude Response	6-104
6-25	Roll Axis - Rigid Body Phase Response	6-105
6-26	Pitch Axis - Rigid Body Amplitude Response	6-106
6-27	Pitch Axis - Rigid Body Phase Response	6-107
6-28	Amplitude Response Roll Axis - Flexible (.01)	6-108
6-29	Phase Response Roll Axis - Flexible (.01)	6-109
6-30	Phase Response Pitch Axis - Flexible (.01)	6-110
6-31	Phase Response Pitch Axis - Flexible (.01)	6-111
6-32	Amplitude Response Roll Axis - Flexible (.005)	6-112
6-33	Phase Response Roll Axis - Flexible (.005)	6-113
6-34	Amplitude Response Pitch Axis - Flexible (.005)	6-114

LIST OF ILLUSTRATIONS

VOLUME FIVE (Continued)

Figure	Title	Page
6-35	Phase Response Pitch Axis - Flexible (.005)	6-115
6-36	Phase Plane Plot Attitude Control During Station Keeping	6-118
6-37	Reliability Diagram	6-119
6A-1	Limit Cycle Impulse Requirements	6A-7
6A-2	Disturbance Torque Impulse Requirements	6A-8
6A-3	Maneuver Impulse Requirements	6A-9
6B-1	Micro-Rocket Applicability Thrust and Total Impulse	6B-4
6B-2	Micro-Rocket Applicability Thrust and Duty Cycle	6B-5
6B-3	Estimated System Weight as a Function of On Board Total Impulse	6B-7
6B-4	Reliability Comparison of Bipropellant or Monopropellant System	6B-8
6B-5	Hydrazine Plenum System Schematic	6B-10
6B-6	Liquid Hydrazine System Schematic	6B-11

LIST OF ILLUSTRATIONS

VOLUME SIX

Figure	Title	Page
7.1-1	Prime Focus Paraboloid Scanning Performance	7-3
7.1-2	Paraboloid Gain Loss as a Function of Beamwidths Scanned	7-4
7.1-3	Beam Scanning Capability of a Multi-Element Paraboloid Switching -Feed System	7-7
7.1-4	Beam Cross-Over Level as a Function of the Beam Scanning Increment	7-8
7.1-5	Cassegrain Antenna Gain Loss with Subdish Rotation	7-11
7.1-6	Radiation Characteristics of a Tapered Circular Aperture	7-16
7.1-7	Paraboloid Subtended Angle and Feed Size as a Function of the F/D Ratio	7-18
7.1-8	S-Band Feed-Edge Taper	7-23
7.1-9	800 MHz Prime Focus Feed	7-24
7.1-10	100 MHz Prime Focus Feed	7-27
7.1-11	Spiral Antenna Monopulse Operation	7-29
7.1-12	Parabolic Antenna Gain Loss as a Function of the Blockage Ratio	7-34
7.1-13	X-Band Radiation Pattern	7-35
7.1-14	Antenna Test Range	7-38
7.1-15	Source Tower	7-39
7.1-16	Feed Support Mast	7-44
7.1-17	Paraboloid Assembly	7-45
7.1-18	Back View of Feed Support	7-46
7.1-19	Left Side View of Feed and Feed Support	7-47
7.1-20	Right Side View of Feed and Feed Support	7-48
2.1-21	Right Side View of Feed	7-49
7.1-22	Feeds, End View	7-50
7.1-23	Feeds, Side View	7-51
7.1-24	E-Plane Radiation Patterns, Frequency 4.6 GHz	7-52
7.1-25	E-Plane Radiation Patterns, Frequency 10.5 GHz	7-53
7.1-26	E-Plane Radiation Patterns, Frequency 12.0 GHz	7-54
7.1-27	E-Plane Radiation Pattern, Frequency 18.0 GHz	7-55
7.1-28	E-Plane Radiation Pattern, Frequency 29.6 GHz	7-56

LIST OF ILLUSTRATIONS

VOLUME SIX (Continued)

Figure	Title	Page
7.2-1	Transdirective Array	7-60
7.2-2	Butler Matrix Array - Block Diagram	7-64
7.2-3	Space Fed (Lens) Array - Block Diagram	7-67
7.2-4	Stripline Diplexer	7-69
7.2-5	Stripline Latching Phase Shifter	7-70
7.2-6	Corporate-Fed Array	7-72
7.2-7	Artist Conception of Corporate-Fed Array	7-75
7.2-8	Schematic of Microwave Subsystem	7-80
7.2-9	Detail of Feed Horn Assembly	7-83
7.2-10	Possible Configuration of 4 Channel Diplexer - Circulator Strip Line Module	7-86
7.2-11	Waveguide Latching Phase Shifter	7-89
7.2-12	Array Element Layout	7-94
7.2-13	Phased Array Patterns	7-95
7.2-14	Phased Array Beam Spacing	7-101
7.2-15	Block Diagram for Digital Beam Steering Unit	7-103
7.2-16	Schematic Diagram for Bit Driver	7-105
7.2-17	Plan View of Radiating Elements	7-107
7.2-18	Side View of Corporate-Fed Array	7-108
7.2-19	End View of Corporate-Fed Array	7-109
7.3-1	RF Power vs Ground Antenna Gain	7-116
7.3-2	ATS-4 Communications System	7-119
7.3-3	Frequency Generator	7-120
7.3-4	Monopulse and Phased Array X-Band Transfer Characteristics-Series 100	7-126
7.3-5	100 MHz Relay Transfer Characteristics-Series 200	7-127
7.3-6	X-Band Transponder Output-Reflector and Phased Array Transfer Characteristics-Series 300	7-128
7.3-7	800 MHz Relay Transfer Characteristics-Series 400	7-129
7.3-8	Filter Response	7-130
7.3-9	S-Band Data Link Transfer Characteristics- Series 500	7-131
7.3-10	X-Band Frequency Generator-Representative Transfer Characteristics-Series 600	7-132
7.3-11	Multipliers in Frequency Generator, Represen- tative Transfer Characteristics-Series 700	7-135

LIST OF ILLUSTRATIONS

VOLUME SIX (Continued)

Figure	Title	Page
7A-1	Four Paraboloid Offset Feed Configuration	7-140
7A-2	Radiation Pattern of a 15-Foot Paraboloid 10 db Tapered Distribution	7-141
7A-3	Radiation Pattern Four Paraboloid Array	7-142
7A-4	Monopulse Radiation Pattern of the Four Paraboloid Array	7-144
7A-5	Four Paraboloid Array Scanning Performance	7-145
7B-1	Faraday Rotation as a Function of Frequency	7-152
7B-2	Attenuation between Arbitrarily Polarized Antenna Caused by Faraday Rotation AF - Axial Ratio	7-156
7B-3	Attenuation between Arbitrarily Polarized Antennas Caused by Faraday Rotation AR - Axial Ratio	7-158
7C-1	Helical Antenna Gain as a Function of Antenna Length	7-161
7C-2	Array Element Spacing as a Function of Array Element Gain	7-163

LIST OF ILLUSTRATIONS

VOLUME SEVEN

Figure	Title	Page
8.4-1	LF Phase Reading Interferometer	8-13
8.4-2	RMS Phase Difference Reading Interferometer Technique	8-16
8.4-3	RF Cross Correlation Interferometer Technique	8-19
8.4-4	Spread Spectrum Interferometer Technique	8-22
8.5-1	Resultant Nonambiguous Pattern after Correlation	8-26
8.5-2	Partial System Schematic of Cross Correlator Interferometer	8-30
8.5-3	Monopulse Space Angle RMS Error	8-31
8.5-4	RMS Space Angle Error Direct Phase Reading Interferometer	8-33
8.5-5	Direct Phase Reading Interferometer Relationship, Space Angle Element Separation, Unambiguous Interval vs D/λ	8-36
8.5-6	Interferometer Phase Error Due to Temperature Differential in Transmission Lines	8-37
8.5-7	Layout of Phased Array	8-45
8.6-1	Direct Phase Reading Interferometer	8-48
8.6-2	Interferometer	8-53
8.6-3	Horn Design	8-63
8.6-4	Interferometer Thermal Flow Diagrams	8-66
8.6-5	Interface between the SCS and Interferometer	8-69
8.6-6	Mode Selection and Phase Measurement	8-72
8.6-7	Timing Diagram for Phase Measurement	8-74
8.6-8	Arithmetic Unit for $\epsilon_z' + \epsilon_z''$ and $\epsilon_y' + \epsilon_y''$	8-78
8.6-9	Arithmetic Unit for $\epsilon_x' + \epsilon_x''$	8-79
8.6-10	Timing Diagram for Computational Instruction	8-81
8.6-11	Time Distribution of the Arithmetic Units	8-82
8.7-1	System Model	8-87
8.7-2	Simplified Block Diagram of Direct Phase Reading Electronics	8-88
8.7-3	Basic Interferometer Relationship	8-90
8.7-4	Geometrical Relationship of Spacecraft Position and Ground Station	8-92
8.7-5	Error in Count vs θ_s	8-96
8.7-6	Refraction Effects	8-97
8.7-7	Atmospheric Effect on Elevation Angle	8-98
8.7-8	Atmospheric Effect on the Slant Range Difference	8-99

LIST OF ILLUSTRATIONS

VOLUME SEVEN (Continued)

Figure	Title	Page
8.7-9	Spacecraft Coordinate System	8-105
8.7-10	Pitch Axis 3σ Error vs Pitch Angle, θ	8-107
8.7-11	Yaw Axis 3σ Error vs Pitch Angle, θ	8-108
8.7-12	Vector Diagram of Satellite - Ground Station Geometry	8-109
8.7-13	Orientation of R_s	8-113
8B-1	ERP vs SNR	8-140
8C-1	Space Angular Error ($\Delta\theta_m$) vs Antenna Separation (D/λ) for Different Mutual Couplings (C)	8-142
8C-2	Space Angle Error Due to Mutual Coupling - Coarse Antenna Pair	8-143
8C-3	Comparison of Antenna Elements - Mutual Coupling	8-145
8D-1	Elliptically Polarized Interferometer Antenna Pair with Elliptically Polarized Incoming Wave	8-149
8D-2	Phase Angle Error vs Axial Ratio Inequality	8-152
8D-3	Phase Angle Error vs Ellipse Tilt Angle Inequality	8-155
8D-4	Phase Angle Error vs Roll Angle (δ)	8-160
8D-5	Phase Angle Error vs Pitch Angle (θ)	8-161
8E-1	Elliptically Polarized Plane Wave	8-166
8E-2	Elliptically Polarized Plane Wave Incident at Angles θ , δ	8-167
8E-3	Receive Antenna with Inclined Polarization Ellipse	8-168
8F-1	Switched Signal Lines	8-174
8F-2	Switched Oscillator Lines	8-175
8F-3	Switched IF Lines	8-176
8F-4	Switched Multipliers	8-177
8H-1	Phase Error Distribution at Start of Count	8-186
8H-2	Phase Error Distribution at End of Count	8-186
8H-3	Phase Error Density Function	8-186
8I-1	Interferometer Illumination	8-188
8I-2	Satellite Orientation	8-193
8J-1	Geometry for Range and Range Rate Analysis	8-201

LIST OF ILLUSTRATIONS

VOLUME SEVEN (Continued)

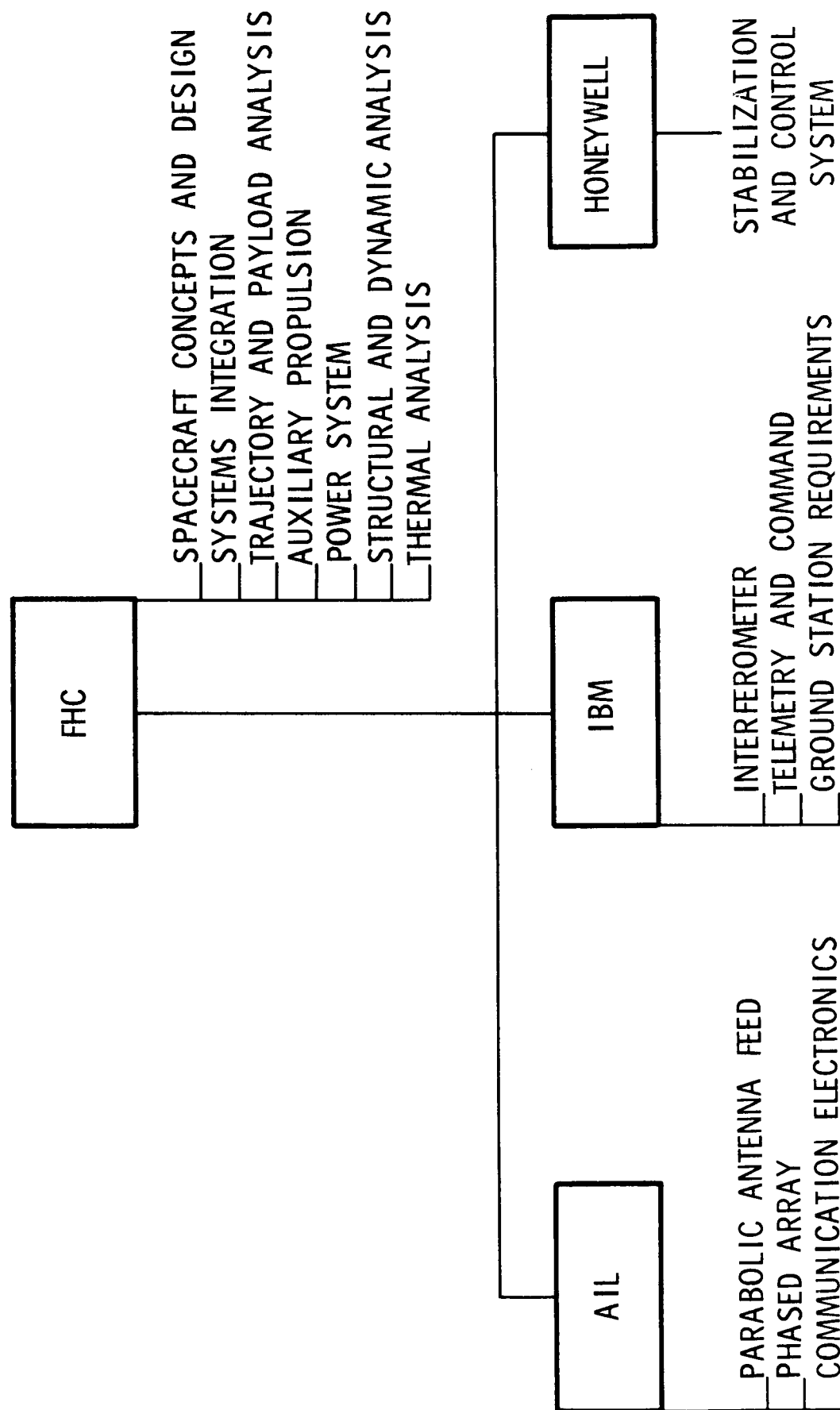
Figure	Title	Page
9.1-1	Onboard System Data Flow, Interfaces to Ground Equipment	9-4
9.1-2	Ground Station Data Flow; Interfaces to Spacecraft and Other Ground Stations	9-5
9.2-2	Basic Commutation Configuration	9-15
9.2-2	Data Handling System Configuration	9-18
9.2-3	Telemetry Data Transmission System	9-25
9.2-4	Telemetry Data Handling and Transmission Configuration	9-33
9.2-5	Block Diagram of Basic Telemetry Receiver	9-38
9.3-1	Command Word Structure	9-51
9.3-2	Command System	9-54
9.3-3	Command Decoder	9-55

PREFACE

This report covers the efforts of Fairchild Hiller Corporation and its team of subcontractors on NASA Contract (NAS-W-1411). The team organization and responsibilities during the study effort are shown on the accompanying chart. The report is divided into eight volumes, as follows:

Volume 1	Summary
Volume 2	Systems Analysis
Volume 3	Vehicle Engineering
Volume 4	Power System
	Orbital Analyses, Propulsion and Guidance
Volume 5	Stabilization and Control
Volume 6	Communication Experiments
Volume 7	Radio Interferometer Experiment
	Telemetry and Command Systems
Volume 8	Program Budgetary Costs and Schedules

ATS-4 TEAM ORGANIZATION



2.0 SYSTEMS ANALYSES

2.1 MISSION PROFILE AND OPERATIONS PLAN

2.1.1 Mission Profile

The mission profile is described in terms of events and phases. Figure 2.1-1 shows the ground track of the vehicle from lift-off to stabilization of the satellite at the desired location. Events are marked in lower case letters. Table 2.1-1 summarizes these major events of the satellite flight profile.

As illustrated in Figure 2.1-1 launch should be timed to inject into synchronous orbit at sunrise during summer and sunset during winter. This launch timing will facilitate a simple earth acquisition and the most favorable illumination of the solar panels during the transfer orbit. The transfer orbit projected in its own plane is shown in Figure 2.1-2. Superimposed on the figure is the spin orientation of the vehicle; also indicated are the major events.

The time intervals between major events and specific activities are called mission phases. Table 2.1-2 is a summary of the mission phases. The phases may overlap. For example the deployment phase and the in-orbit checkout may take place during the walk; similarly the experimentation may begin before the walk or station repositioning.

Launch Through Transfer Orbit Injection - During phases A, B, and C the satellite itself is largely inactive and control (tracking, commanding and telemetry) is exercised via the booster systems. The satellite vibration sensors are connected to the Centaur telemetry system. In phase D, however, once the satellite is separated from the Centaur, the satellite is directly controlled by the appropriate STADAN facilities. After injection into the transfer orbit (accompanied by a 7.6 degree plane change) the Centaur yaws to give the satellite a proper orientation for apogee injection. Centaur may spin the spacecraft to 1 rpm,

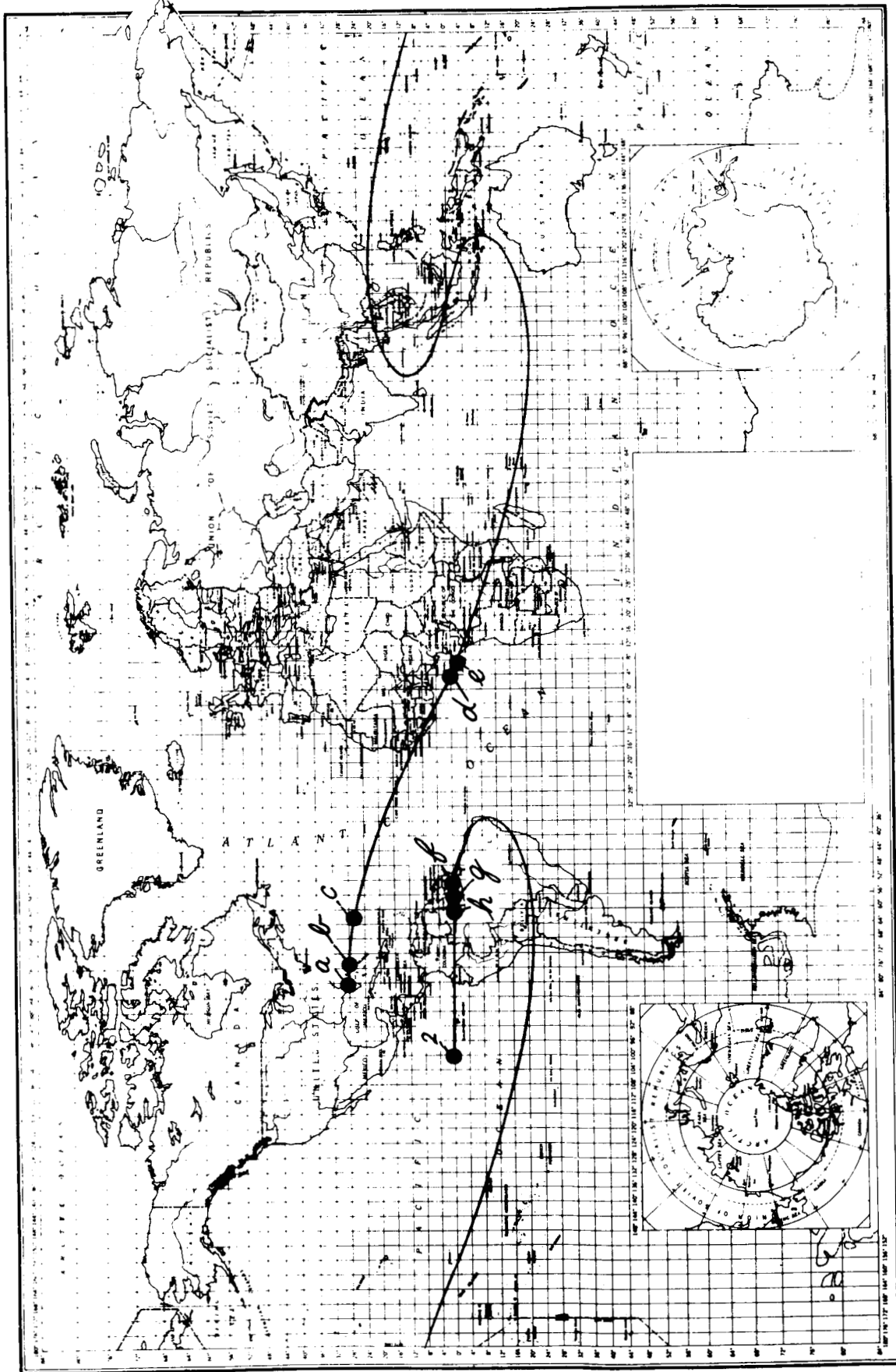


Figure 2.1-1 Satellite Ground Track

TABLE 2.1-1 EVENTS OF FLIGHT PROFILE

Event	Name	Description	Time (hrs)	Controlled by
a	Liftoff	Launch of the booster and satellite from ETR	0	Cape Kennedy
b	Separation from booster	SLV-3C separates from Centaur; during the last part of the burn the shroud has been ejected	0.07	Cape Kennedy
c	Injection into parking orbit	Centaur fires, injects into 185 km parking orbit	0.15	ETR (Bermuda)
d	Injection into transfer orbit	Centaur refires, injects into elliptical transfer orbit while reducing orbit inclination by 7.6 degrees	0.44	ETR
e	Satellite separation	Centaur rotates (yaws) vehicle to orient vehicle for proper apogee injection attitude. Centaur spins up to 1 rpm; satellite separates, spins up to 60 rpm	0.50	ETR
f	Apogee kick	At second apogee the orbit is circularized by firing kick stage	16.3	STADAN (Rosman)
g	Deployment	Satellite is despun- Kick motor is jettisoned and paraboloid deploys	16.4	STADAN (Rosman)
h	Orientation	Satellite is oriented in desired attitude	17.4	STADAN (Rosman)
i	Positioning on station	At the desired location the satellite drift is arrested	when desired	

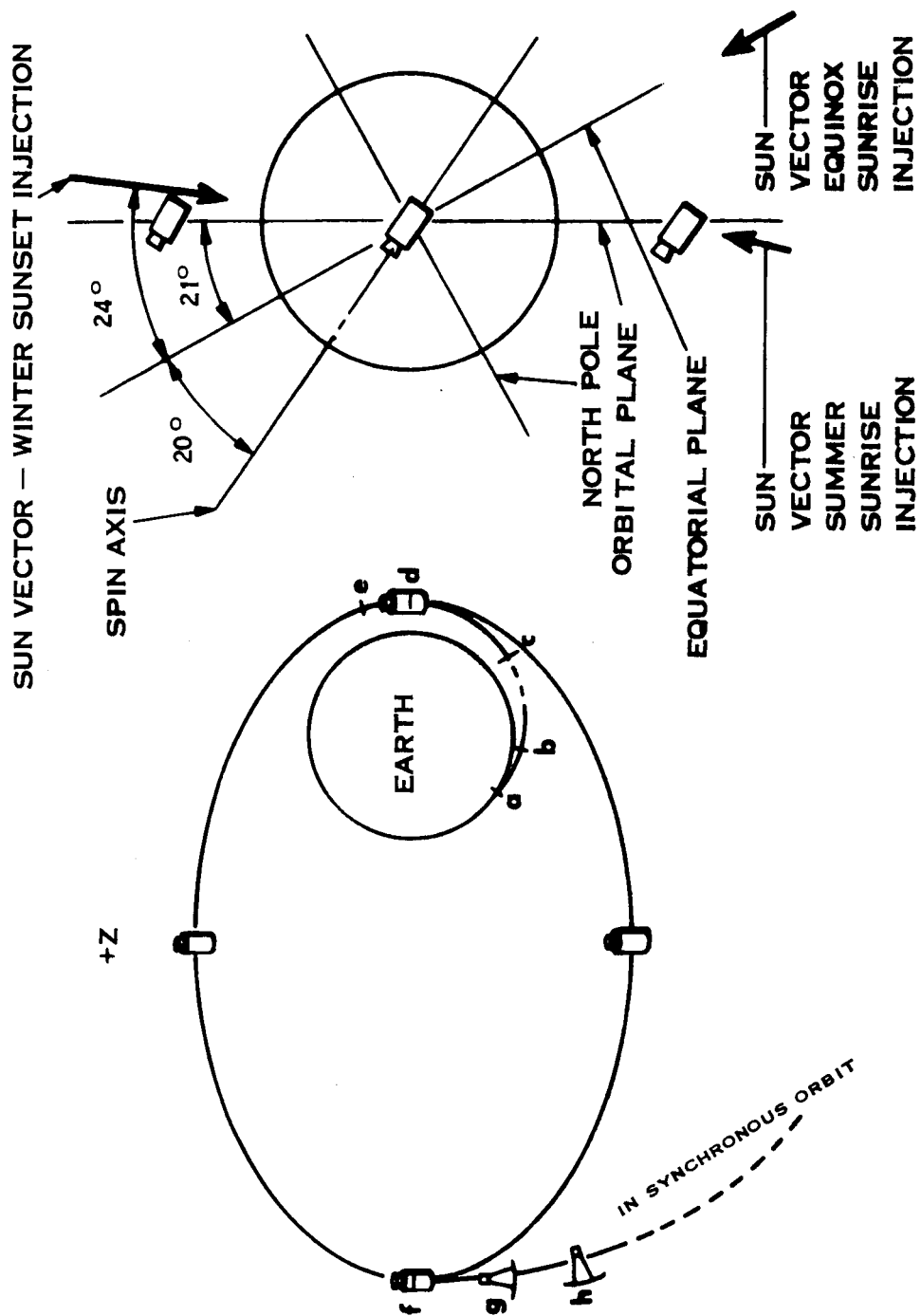


Figure 2.1-2 Spacecraft/Sun Orientation in Transfer Orbit

TABLE 2.1-2 MAJOR ATS-4 MISSION PHASES

Phase	Name	Duration	Beginning	End	Controlled by	Remarks
A	Launch	250 sec	Liftoff	Separation from SLV-3C	ETR	- Control through SLV3 command TLM system
B	Coasting	290 sec	Separation from SLV-3C	Injection into parking orbit	ETR	- Control through Centaur command and TLM system
C	Parking Orbit	1040 sec	Injection	Injection into transfer orbit	ETR	
D	Transfer Orbit	15.8 h	Injection	Apogee kick	ETR STADAN	ETR controls the spin up and separation from CENTAUR - from then on STADAN facilities are used
E	Deployment	1.0 h	Apogee kick	Completed deployment	ATS stations	- The deployment includes the orientation of the satellite
F	Checkout	3 - 6 min.	Completed deployment	Completed checkout	ATS stations	
G	Reposition	8 days	Completed deployment and acquisition	Attaining station	ATS stations	
H	Experimentation	2 years	Completed checkout	End of planned mission life	ATS stations	Performing planned experiments
I	System Demonstration	2 years	Completed checkout	End of planned mission life	ATS stations	Communication tests, tracking of low Earth satellites, coupling of interferometer with attitude control system and similar operations

separates, and the satellite spins up to 60 rpm by means of self contained solid rockets. The whole sequence is stored and executed from memory by appropriate timing. Command backup will be available.

The patterns of the telemetry and command antennas aboard the ATS-4 satellite will allow tracking from all ground stations. Also tracking via the range and range rate transponder must be possible in all different vehicle attitudes

For the last 4-hour portion of phase D, Rosman has access to ATS-4 for tracking. In this time interval the orbit parameters must be sufficiently refined to permit precise injection into the 24 hour circular orbit.

During the phases E, F, G, H and I, the satellite is tracked and commanded by the ATS ground stations (Rosman and Mojave) and telemetry data are received at these two stations.

Deployment, Acquisition and Checkout - The deployment (phase E, and events g and h) takes place in the following order:

- First the satellite is despun by a yo-yo mechanism. This is initiated following an internally sensed completion of apogee stage firing; command backup will be available.
- Secondly, the top tie squibs fire, releasing the kick-stage and the petal restraint ring. As a result, the petals deploy.
- Thirdly, the satellite undergoes the initial attitude acquisition by performing the following steps:
 1. sun acquisition using coarse sun sensor
 2. sun acquisition using fine sun sensor
 3. earth acquisition using horizon scanner by rolling about the sun line
 4. determination of Polaris angle
 5. commanded Polaris acquisition using star tracker

During the verification and checkout phase (F) the different sub-systems are checked for their proper functioning. Telemetry and command functions must be operating during the entire transfer orbit. The checkout is performed by operating the subsystems. Checkout of the satellite takes place in the following fashion:

- The configuration is checked immediately after deployment and orientation; the telemetry antenna used in the undeployed state is now shielded by the paraboloid and the second telemetry antenna on the feed structure is now utilized. The solar panel currents can be checked as an aid to verify deployment and orientation; the panel currents may also be used to determine residual rotation.
- The power system is checked next via the housekeeping telemetry.
- The next step is an electronics status checkout. This includes the communication experiment electronics and the interferometer electronics.

Orbit Correction - Following orbit injection at synchronous apogee, the attained orbit will deviate from the desired 24-hour synchronous equatorial orbit. Calculated 3σ values for the possible orbit element errors are: period error of ± 45 minutes; eccentricity error of 0.03 and inclination error of ± 1.08 degree. It is desired to correct these errors as soon as possible after injection. In particular, the period error must be corrected before the ATS-4 drifts significantly from its nominal injection station.

Within two hours after injection, the ATS-4 ground tracking complex should be able to identify the actual orbit period to an accuracy of 0.1 minute, eccentricity to an accuracy of 0.00006 and inclination of 0.02 degree. Since the attitude control subsystem will also have established the nominal earth-oriented attitude by this time, correction of the injection errors can then be initiated.

Period and eccentricity errors will be corrected in concert in order to limit velocity impulse requirements. (This may necessitate a 12-hour wait (or more) to permit a fully coordinated correction of these two errors.) Direct ground control of the proper thrust initiation time and thrust termination time for the auxiliary propulsion system (APS), based on a calculated current thrust level in accordance with received APS status data (pressure, temperature, etc.) will be employed for these maneuvers. (It is noted that a simple blowdown system is predicated for the monopropellant hydrazine APS; hence, its thrust level will decay as the system pressure drops with propellant utilization.) At the nominal design thrust level of 1 pound, the total thrusting times for the APS can be as long as 2.1 hours to provide the associated, extreme 3σ value of 150 ft/sec. for the in-plane velocity correction impulse, ΔV .

The inclination error will be independently corrected using similarly commanded North-oriented thrust impulses at the proper nodal (equatorial) points of the orbit. A total thrusting time (at a 1 pound thrust level) of as long as 2.7 hours (made up of several thrust periods) would be needed to provide the associated, extreme 3σ value for ΔV of 195 ft/sec.

Because of possible variations in the APS thrust level from the calculated current value, it may be necessary to provide a second vernier correction of the period error to realize the desired accuracy of about 0.25 min. (equivalent to a longitude drift rate of about 0.06 deg/day).

Experimentation and Demonstration - The experimentation phase (H) will commence during the repositioning maneuver. During this time experiments can be performed that take advantage of the low elevation angles from Rosman and particularly Mojave.

The following is a list of propagation experiments that can take advantage of the satellite-ground station geometry during repositioning:

- Performance of RR systems at low elevation angles:
For this experiment two RR transponders are required aboard the spacecraft; one transponder would operate at 138/148 MHz, the other at 2.1/1.7 GHz. The difference in range measured at the two frequencies can be evaluated as a function of the elevation angle and hence interpreted as a function of the ionospheric and tropospheric refraction indices.
- Polarization angle change: The polarization of the 100 MHz and 800 MHz transmission will change owing to Faraday rotation in the ionosphere. This phenomenon is a function of the elevation angle, frequency, and condition of the ionosphere. By making measurements at these frequencies during the move to the Mojave station, performance data for elevation angles from five to about fifty degrees elevation can be obtained.
- Low elevation angle pattern measurements: By determining the beam pattern for different elevation angles, especially very low ones, beam distortion due to ionospheric and tropospheric scattering can be determined. This experiment may allow inference of scattering inhomogeneities in the atmosphere for different angles of incidence. As a matter of interest it should be mentioned here that once the satellite is on station at 100° West, the great circle arc between the subsatellite point and the Alaska station is about 80.5 degrees. Therefore, such beam scattering measurements for very low elevation angles might be conducted at the Alaska ground station.
- Near the insertion point at 54° West the satellite antennas can be beamed to either Europe or Africa. It may be useful to demonstrate the communication capability from a large satellite antenna to a small ground terminal. Such demonstration may be very

favorable from political viewpoints. For example, ATS-4 could demonstrate the communication and broadcast potential of large satellite antennas to developing nations in Africa.

The system demonstration phase (I) consists of activities to verify and explore the capabilities of the ATS-4 satellite technology. It will include communication tests, tracking, and communicating with low orbiting satellites, aircraft, and small ground stations. The performance limits of the interferometer will be explored and the interferometer will be used as an attitude sensor, by interconnecting the interferometer with the ACS.

Station Keeping - The major orbit deviation which will need correction in order to provide the specified North-South station keeping is the build-up in orbit inclination caused by solar-lunar gravitational perturbations. This build-up is a long period effect amounting to 0.75 degree in a year. Hence, every three months during the first year, the observed accumulated inclination error will be corrected by a procedure similar to that described for correction of the initial inclination error. In this way, the instantaneous inclination error will be kept below 0.2 degree during the first year.

The major orbit perturbation necessitating East-West station keeping during the two year mission time is the gravitational perturbation associated with the equatorial ellipticity of the Earth. The effect of this perturbation (if uncorrected) would be to cause the ATS-4 satellite to execute simple harmonic motion about the nearest extension of the equatorial minor axis. (Based on Syncom II data, this is located at $109 \pm 6^{\circ}$ West longitude.)

Since the perturbing accelerations associated with this effect are very low, compensating pre-determined thrust impulse can be commanded every 3-4 months. A unidirectional westward drift will be induced by the Earth's terrestrial gravitational perturbation. Hence, preset westward braking impulses of the proper magnitude applied at such intervals would

reverse the natural drift and keep the satellite oscillating within $1-2^{\circ}$ of its desired subpoint longitude. Initiation of such impulses can be based on ground track data indicating that the satellite has drifted to a control boundary west of its intended station.

Use of the specified 100 ft/sec of East-West station repositioning capability is predicated upon direct on-off ground control of the appropriate APS thruster. Again, it is assumed that APS status data would be used to calculate its current thrust level for effective control of such maneuvers.

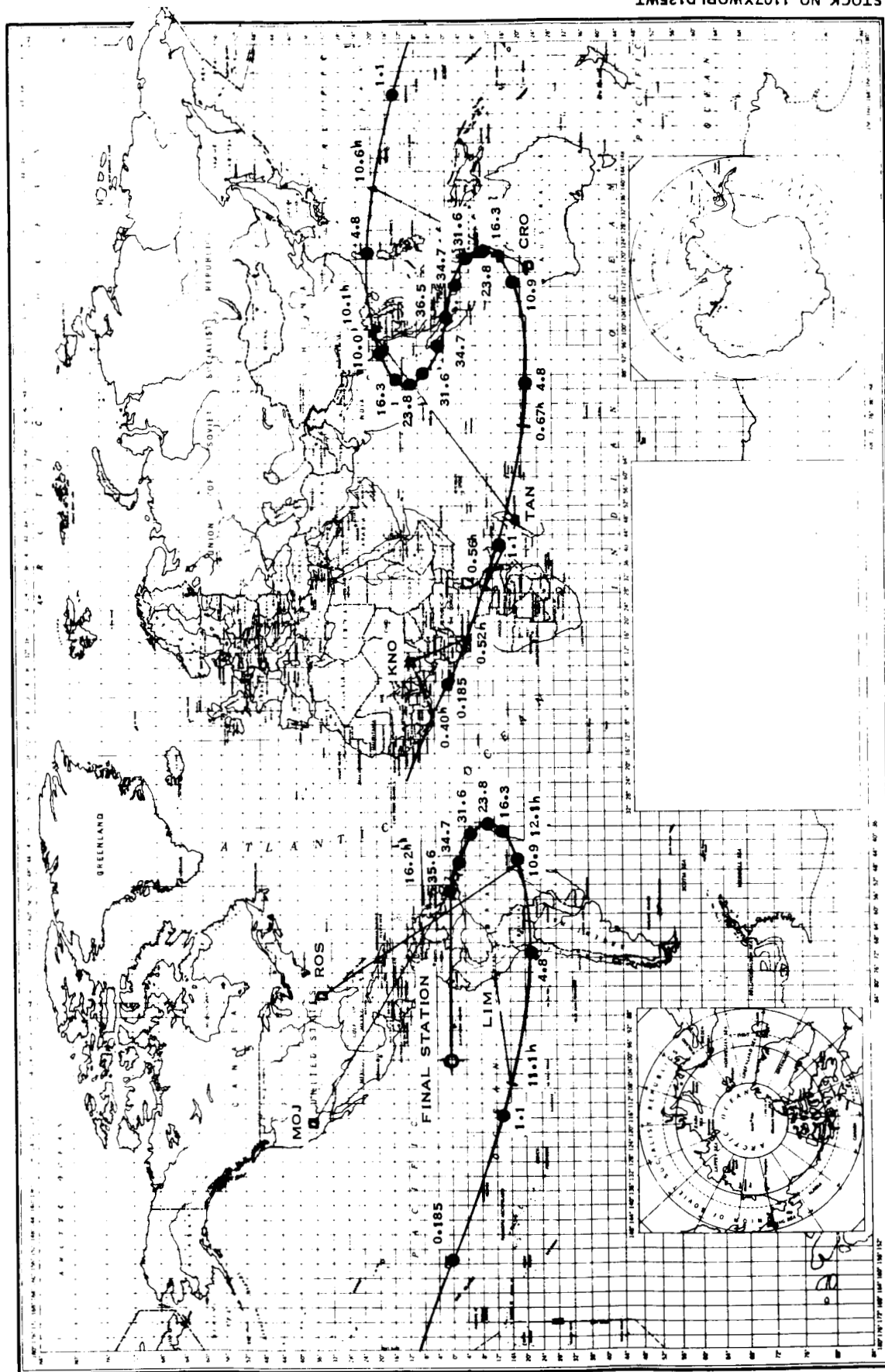
2.1.2 Operations Plan

The operations plan is described in terms of the principal ground support required for the ATS-4 Program. The ground coverage is shown in Figure 2.1-3. This figure shows the ground track of ATS-4 from the point of injection into the transfer orbit until the satellite assumes the final position over the equator at 100° W. Along the ground track of the transfer orbit the altitudes in thousands of km are indicated for several satellite positions. Also shown are ground stations, and the times of ascent and descent in hours after liftoff. Table 2.1-3 summarizes the longitudes and latitudes of several points of the transfer orbit, together with the corresponding altitudes and the time at which the satellite will be at these points; the injection point into the transfer orbit is used as the time reference.

Tracking - Different tracking aids will be used during the different phases of the satellite flight profile. For launch, from liftoff to separation of the SLV3C, the booster tracking aids shall be used. These tracking aids shall be compatible with the ETR launch complex instrumentation.

After separation, the Centaur tracking aids shall be used for coasting and parking orbit. Also during these phases (B and C) ETR shall track the satellite.

After separation of the satellite from the Centaur, the ATS-4



STOCK NO. 1107XWORLD135WT

Figure 2.1-3 Satellite Ground Track and Ground Stations

1:135,000,000

TABLE 2.1-3 GROUND TRACK DATA SUMMARY

East Longitude (degrees)	North Latitude (degrees)	Satellite Altitudes (km)	Time (hours)
4	0	185	0
41.9	-14.7	1,100	0.16
87.6	-21	4,800	0.26
112.8	-18.1	10,900	0.9
121.7	-14.7	16,300	1.19
122.6	-10.3	23,800	2.18
120.8	- 5.3	31,600	3.25
112.9	- 2.7	34,700	4.27
104	0	35,600	5.25
96.7	2.7	34,700	6.2
88.4	5.3	31,600	7.23
86.4	10.3	23,800	8.3
87.3	14.7	16,300	9.12
95.7	18.1	10,900	9.6
122	21.3	4,800	10.1
166.7	14.7	1,100	10.3
205	0	185	10.5
244.3	-14.7	1,100	10.7
289	-21.3	4,800	10.9
315.3	-18.1	10,900	11.7
323	-14.7	16,300	12.1
324.6	-10.3	23,800	13.0
322.6	- 5.3	31,600	14.5
314.3	- 2.7	34,700	15.0
306	0	35,600	15.75

tracking aid system shall be used. This tracking aid consists of an R and R transponder, meeting NASA specifications and compatible with the ground equipment available at TAN (Tananarive, Malagasy Republic), CRO (Carnarvon, Australia) and ROS (Rosman, N. C.). These three stations will produce sufficient tracking data for an apogee injection at second apogee. Table 2.1-4 summarizes the time available for tracking from the different ground sites. During repositioning (phase G) and after attaining the final position the satellite will be tracked from Rosman, N. C.

TABLE 2.1-4 TRACKING TIME PROFILE

Station	Ascent (hours after liftoff)	Descent (hours after liftoff)	Total Time Available (hours)
TAN	0.56	10.1	9.6
CRO	0.67	10.6	9.9
ROS	12.1	---	See Note

NOTE: Time available is 4.2 hours until reaching apogee and unlimited for the remainder of ATS-4 mission

Either an S-band transponder or a VHF transponder is satisfactory for tracking; a decision will be made at a later date as to what kind of transponder shall be used.

Telemetry and Command - The telemetry and command communications will be performed during phases A to C by the instrumentation aboard the SLV3C and Centaur. For obtaining vibration data from the ATS-4, there will be an interconnection of the vibration sensors on the ATS-4 to the Centaur telemetry system. After separation from Centaur, the ATS-4 telemetry and command system will be used to control the satellite and monitor its performance.

Table 2.1-5 summarizes the ground coverage of the transfer orbit for a selected set of ground stations. The coverage is shown for elevation angles to 5 degrees above horizon, except for Kano, where 3° are assumed. The table shows that the period for 0.52 to 0.56 hours is without coverage, unless lower horizon angles from Kano and Tananarive are permissible. Also the period from 9.9 hours to 11.1 hours is without coverage. This is the time when the satellite passes through perigee. After apogee injection, command and telemetry interfaces are primarily with Rosman, N. C. and Mojave, California, the selected ATS-4 ground stations.

Gross Data Flow

Figure 2.1-4 is a block diagram indicating the data flow concept. It encompasses three major elements: the ATSOCC (ATS Operation Control Center), the ground stations complex, and the spacecraft. The ground station complex consists of a primary station, Rosman, one secondary station, Mojave, and auxiliary stations, indicated by Stadan. The auxiliary stations may be used during the transfer orbit for tracking and, if necessary, for telemetry and command. Stations likely to be used are KNO, TAN, CRO and LIM (see Tables 2.1-4 and 5).

Several major categories of data and transmission signals are identified on this figure. In order to understand the figure, a description of the elements and the data categories is given below.

Ground Systems Elements

- ATSOCC: The primary function of ATSOCC is the management of ATS-4. This involves planning of operations and experiments, and scheduling of activities. Also the experiment results are collected at ATSOCC where they are evaluated and correlated.
- Rosman: This is the primary station. It receives housekeeping telemetry, transmits commands (coding of commands into

TABLE 2.1-5 TELEMETRY AND COMMAND STATION COVERAGE

Station	Ascent Time (hours after liftoff)	Descent Time (hours after liftoff)	Coverage Time Available	Command	Telemetry
Kano, Nigeria KNO	0.40	0.52	0.12	Coder: 1-CSC Xmtr 1-242-F2	136 MHz
Tananarive, Malagasy Rep. TAN	0.56	10.1	9.6	Coder: 1-CSC Xmtr 2-242-G	136 MHz
Carnarvon, Australia CRO	0.67	10.6	9.9		
Lima, Peru LIM	11.1	---	unlimited	Coders: 1-CSC 1-Vanguard 1 AVCO Xmtr 2-242-G	136 MHz
Rosman, N. C. ROS	12.1	---	unlimited	Coders: 1-CSC Xmtr 3GE 5KW 2 I. T. A. 120H	136 MHz
Mojave, Calif. MOJ	16.3	---	unlimited	Coder: 1-CSC 1-Vanguard 1 AVCO	136 MHz

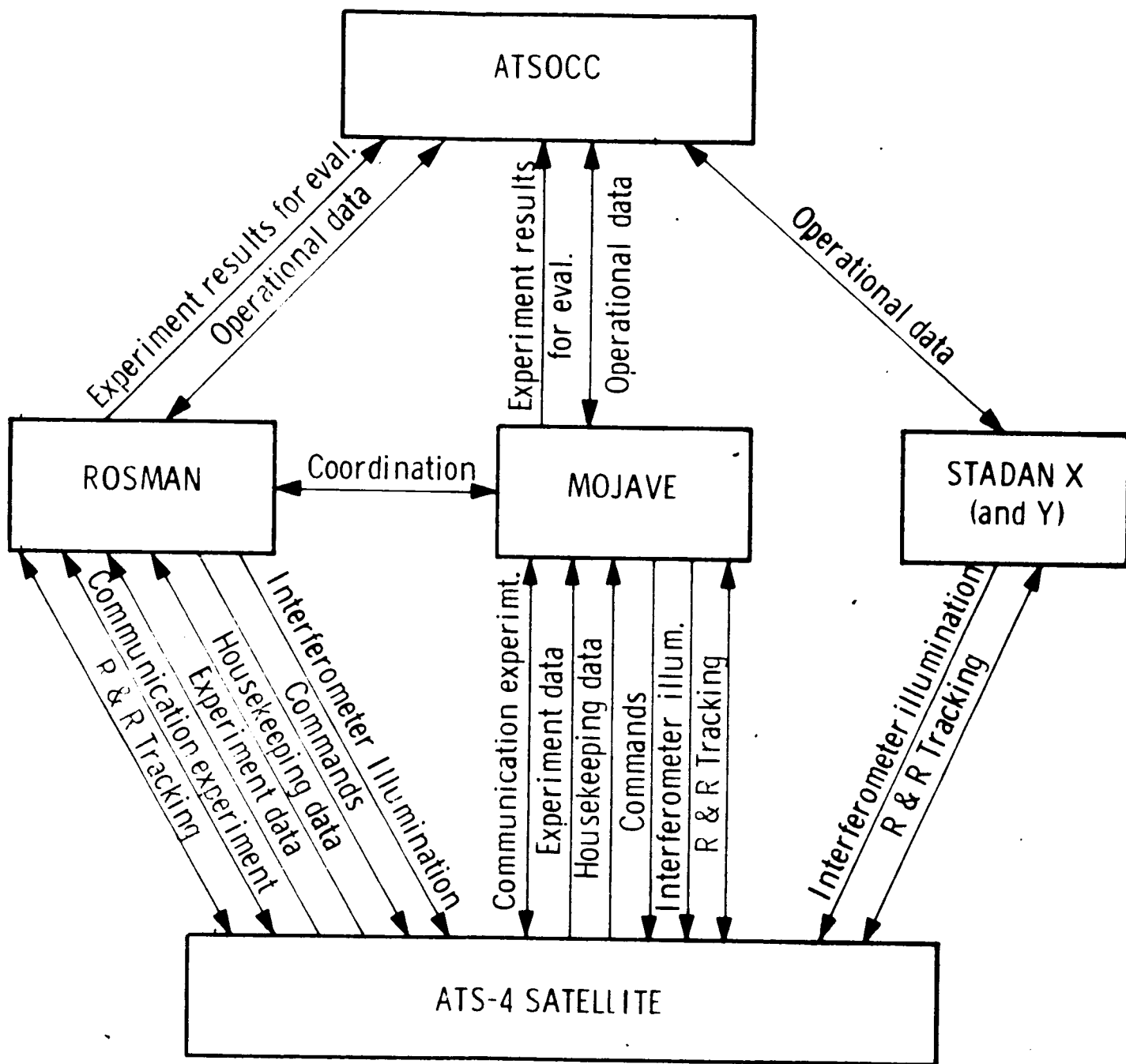


Figure 2.1-4

Gross Data Flow Concept

satellite language), receives experiment data, illuminates the interferometer and RR transponder. Among the functions performed at Rosman are data validation, experiment calibration, cursory experiment evaluation (quick look), trouble shooting, and control of satellite status. Rosman coordinates the activities with the secondary ground station.

- Mojave: This is the secondary station. It has the same capabilities as Rosman (commanding, receiving of housekeeping telemetry, experiment returns) and is coordinated with Rosman. In some experiments (antenna pattern measurement and interferometer) it will be used simultaneously with Rosman. Control of the satellite will be done from Mojave only if so advised by Rosman.
- Stadan: These are auxiliary stations. They are used on a scheduled basis.

Categories of Data

- Operational: For operational data there is a two way flow between ATSOCC and the ground stations. It consists of command lists, schedules of experiments, routine reports about satellite operations, verification of command lists. It does not carry any raw data, experimental housekeeping, or commands. Basically TTY connections are employed but SCAMA lines can be used if necessary.
- Experimental Results for Evaluation: The flow is from the primary and secondary ground station to ATSOCC. The data consists of refined experiment results and other pre-evaluated data. (No raw data is transmitted to ATSOCC). The data are the gross results and summaries. They are carried by mail or

other shipment in the form of recorded tape, letters, and reports.

- Housekeeping Telemetry: This link is a one way flow from the satellite. It contains housekeeping data, the sub-categories of which are thermal control, propulsion control, structural data, orientation control and power system data. These data do not contain experiment results, but frequently must be correlated with experiment results. These data are evaluated at the ground station and only summaries are transmitted to ATSOCC.
- Commands: This is a one way flow from ground stations (primary and secondary) to the satellite except for command verification. The command link is needed for the following subsystems: power system, structural system (deployment), auxiliary propulsion, orientation control, interferometer experiment, antenna experiments, and secondary experiments. The command link is also used to select certain operational modes required for experimental procedures, such as pre-programmed sequence of satellite motion for measuring antenna patterns. Commands in the code of the satellite systems are prepared in the ground station based on schedules and procedures transmitted from ATSOCC to the ground station.
- Experiment Data: This is basically a one way flow from the satellite to the ground station(s). It consists of raw experimental outputs that are checked immediately for validity and refined into a form suitable for transmittal to ATSOCC. The categories of experiment data are: antenna measurement signals (the pattern is determined at the ground station(s) from these signals), interferometer angle measurements (and corresponding raw data), and orientation data for precision orientation systems.

2.2 EXPERIMENT PLAN

An evaluation test approach is presented for the major ATS-4 experiments; these are the parabolic antenna experiment, the phased array experiment, the interferometer experiment, and attitude control experiment, including the evaluation of the attitude reference subsystem (ARS). These experiments will be discussed in the following fashion:

- Method What is done
- Technique How is the experiment performed
- Period of Performance When and for how long is the experiment performed
- Data Requirements What is the gross data communication requirement for the experiment
- System Interfaces How does the experiment interface ATS-4 subsystems.

2.2.1 Parabolic Antenna Experiment

The parabolic antenna experiment includes the measurement of the radiation pattern and gain.

Radiation Pattern Measurement In order to completely specify the antenna radiation pattern, field strength measurements at all polarizations are required for all spatial angles about the antenna. Measurements of this type, however, are rarely performed; exceptions are special cases where, for example, an omnidirectional pattern is specified for a telemetry antenna, or in a low noise antenna where the sidelobe level is important. Antenna patterns can be obtained either at the antenna or the ground terminal because the reciprocity principal results in identical transmission and reception patterns.

Two methods are generally available for antenna pattern measurements. The first method depends upon the satellite's ability to transmit at the test frequencies. It consists of measurements at the ground terminal of the field strength of signals radiated by the satellite as a function of its controlled attitude. These measurements are performed at the following frequencies: 100 MHz, 800 MHz, 2.3 GHz and 7.3 GHz. The second method depends upon the satellite's ability to receive at the test frequencies. It consists of telemetering to the ground terminal the AGC voltage in the channel under test for controlled vehicle attitudes. These measurements are performed at the following frequencies: 1.7 GHz, 2.1 GHz and 8.0 GHz.

The measurement will be performed in the following manner:

The satellite is pointed to a ground terminal, so that the Z-axis coincides with the line of sight. The satellite is then slewed by combined pitch and roll maneuvers which allow measurements along a minimum of four major plane cuts of the antenna pattern. Figure 2.2-1 indicates the location of the major planes with respect to the paraboloid.

The slewing maneuvers are performed in the following fashion: From the position where the Z-axis coincides with the line-of-sight, the satellite slews the Z-axis in one of the major planes in a positive direction by a specified number of degrees (see Table 2.2-1). The Z-axis is then slewed back through the line-of-sight moving in the negative direction by the same number of degrees. At the end of its negative excursion the Z-axis is moved back to coincide with the line-of-sight. This motion is shown in Figure 2.2-1, and is called a major plane cut. Measurements are made for matched, crossed, and 45° polarizations.

Table 2.2-1 summarizes the angular excursions and slewing rate requirements. The time required for a major plane cut is determined by the slewing rate and the number of degrees required for the cut. The

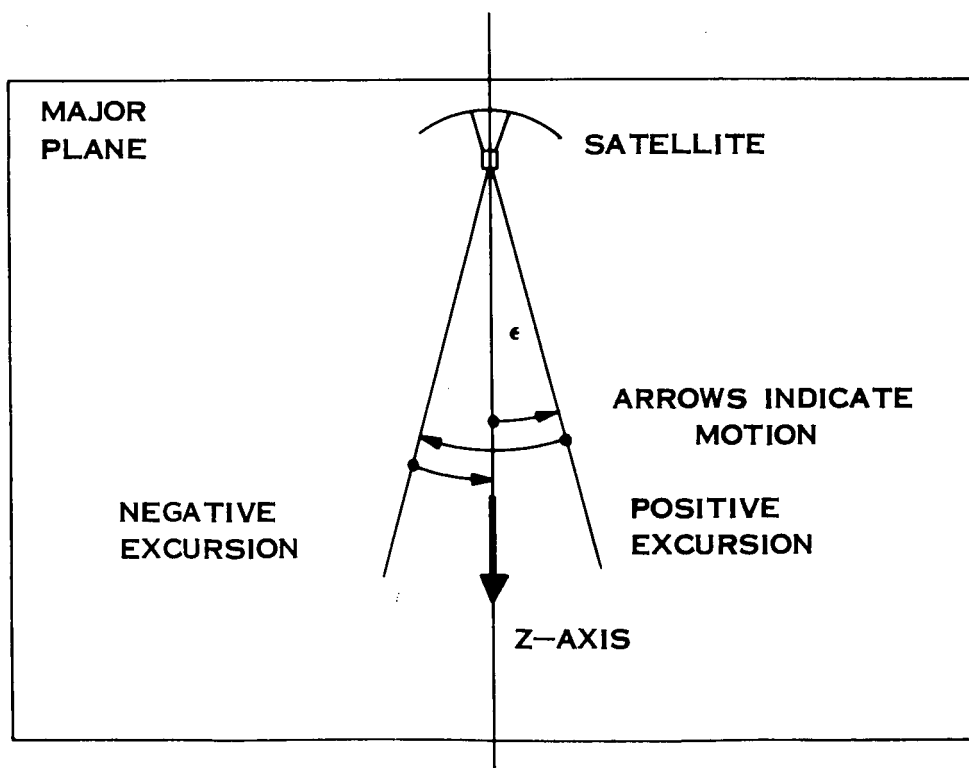
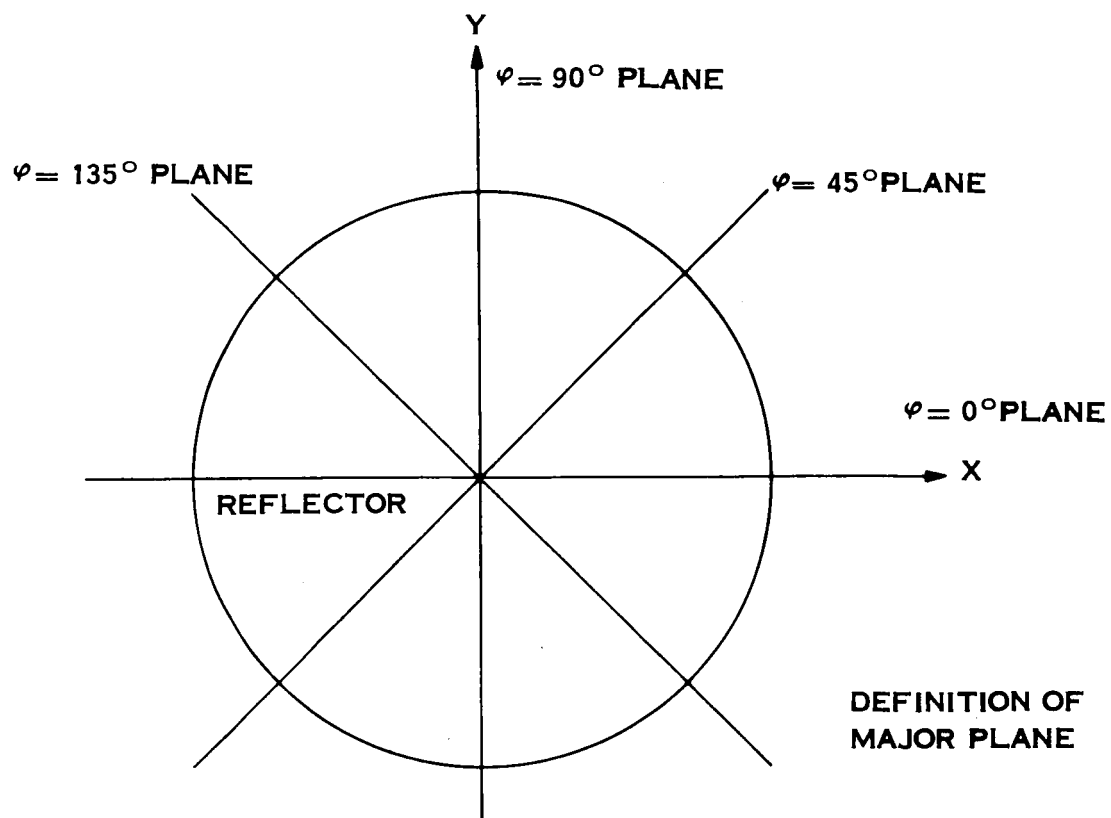


Figure 2.2-1 Major Plane Location and Cuts for Antenna Measurement

TABLE 2.2-1 SLEWING CHARACTERISTICS SUMMARY

Frequency	Beamwidth	Excursion*	Average Slewing Rate	Time for One Major Plane Cut	Estimated Reference Error	Tolerance
0.1	Degrees 22	Degrees $1/2 \text{ BW} = \pm 11^\circ$	0.6	73	Degrees 0.3	Degrees 2
0.8	3	$5 \text{ BW} = \pm 15^\circ$	1	60	0.25	0.3
1.7, 2.1, 2.3	1	$5 \text{ BW} = \pm 5^\circ$	4	5	0.02	0.1
7.3, 8.0	0.3	$10 \text{ BW} = \pm 3^\circ$	4	3	0.015	0.03

* BW = beamwidth between 3db points; the angle corresponds to ϵ in Figure 2.2-1.

error estimate is based on an 0.25 degree per hour gyro drift. The maximum error allowed during a measurement is one tenth of a beamwidth.

The monopulse capability of the paraboloid is used as an important reference in the pattern measurement. At the beginning of a measurement, pointing is established by monopulse operation. Monopulse signals are transmitted to the ACS to hold the vehicle Z-axis on the line-of-sight and then are switched off. During the slewing maneuver, as the Z-axis passes through the line-of-sight, the error is checked with the monopulse system. At the end of a major plane cut the monopulse error signal is checked again. If it is found during the measurement that the allowable error has been or is going to be exceeded, the monopulse system can be used to correct the vehicle or arrest the slewing motion.

Table 2.2-1 indicates that two modes of operation are required. The two modes, A and B, are defined in terms of the low and high frequency bands, respectively. In mode A, a slewing rate of one degree per minute is chosen along with an excursion angle ϵ of ± 15 degrees. In this mode simultaneous 100 and 800 MHz patterns will be measured. The allowable error of the Z-axis is 0.3 degrees. In Mode B, a slewing rate of four degrees per minute is chosen along with an excursion angle of ± 5 degrees. In this mode, simultaneous measurement of the 2.3 GHz and 7.3 GHz patterns in transmission, and simultaneous measurement of the 1.7, 2.1 and 8.0 GHz patterns in reception is performed. The allowable error is 0.03 degrees. Table 2.2-1 indicates that the allowable error is not exceeded in either Modes A or B.

Prior to the measurement of the first antenna pattern, which is to be used as a reference, the following conditions must be met:

- The antenna must be thermally stabilized
- The antenna surface contour must be measured
- The monopulse system must be in operation.

In order to estimate the time required for a pattern measurement, a measurement "run" is defined. A run consists of four valid major plane cuts. A Mode-A run requires approximately 4 hours whereas a Mode-B run requires approximately 20 minutes. To establish measurement repeatability a number of runs should be made and compared. During the lifetime of the satellite many antenna pattern measurements are to be made. The first measurement is the reference pattern, with later measurements verifying the pattern after an elapsed period of time, or after changes in the satellite performance and/or environment.

Table 2.2-2 summarizes the pattern measurement program proposed for the life of the mission. Additional pattern measurements are to be performed as required.

In order to perform pattern measurements on transmission, it is necessary to know the power radiated from the satellite. For this purpose, transmitter output power and the power reflected at the feed must be measured with a calibrated reflectometer and telemetered to the ground terminal. A measurement of the field strength at the ground is taken at intervals to produce at least twenty points in the main beam. In Mode A, with the narrow beamwidth of 3° and a slewing rate of one degree per minute, a reading is taken at nine-second intervals. In Mode B, the narrowest beamwidth is 0.3° and the slewing rate is four degrees per minute which then requires readings to be taken at 0.225-second intervals. For further processing, the readings are quantized into six bits to meet a 2% (0.1 db) accuracy.

The bit rates, produced on the ground, are therefore 26.6 bits per second in Mode B and 9.66 bits/second in Mode A. The same bit rates hold for reception pattern measurements where the ACG voltage is telemetered to the ground terminal rather than the transmitter power. The sampling and bit rates are summarized in Table 2.2-3.

TABLE 2.2-2 ANTENNA PATTERN MEASUREMENT PROGRAM

Approximate Time of Performance (time after liftoff)	Ground Station Used for Measurement	Purpose and Goal of the Specific Measurement	Type of Run	Estimated Time Required to Perform Measurement (Hours)
80 ^h	Mojave	Measurement at low elevation angle to determine beam scattering and polarization characteristics for low angles	Mode A Mode B Matched Polarization	5.0
5 ^d	Rosman	Measurement at maximum elevation angles at Rosman	Mode A Mode B Matched Polarization	5.0
10 ^d	Rosman Mojave	Antenna pattern measurement on location. This pattern may be used as reference for other measurements.	2x Mode A 2x Mode B 3 polarization	30.0
First Occultation	Rosman Mojave	Measurement for effects of occultation may be performed at 2 consecutive days for comparison.	Mode B Match Polarization	2.0
365 ^d	Rosman Mojave	Verification of pattern after one year has elapsed	Mode B Matched Polarization	1.0
730 ^d	Rosman Mojave	Verification of pattern after two years have elapsed	Mode B Matched Polarization	1.0

TABLE 2.2-3 SAMPLING AND BIT RATES FOR ANTENNA PATTERN
MEASUREMENTS (ON THE GROUND)

Mode	Sampling Rate	Data Rate
	Samples per Second	Bits per Second
A	0.11	0.66
B	4.45	26.6

For successful measurement of the antenna pattern, other ATS-4 subsystems must be actively employed. The requirements on these other subsystems are:

- ARS - Data is needed continuously. The ARS accuracy must be within the tolerance required for the antenna measurement. In Mode A this is 0.3 degree, and in Mode B it is 0.03 degree. ⁽¹⁾
- Monopulse - The monopulse system must supplement the ARS attitude readings. This is only possible when the Z-axis nearly coincides with the line-of-sight. In this position, the monopulse system must determine the deviation to within 0.03 degree.
- SCS - The SCS must be capable of producing the slewing motion for a major plane cut. This is 1 degree per minute for a ± 15 degree excursion (Mode A), and 4 degrees per minute for a ± 5 degree excursion. The motion along the major plane must be within the tolerances specified in Table 2.2-1. These motions are to be obtained using the reaction wheels.
- Command System - The command system must command the scanning motion for Mode A and Mode B.
- Telemetry System - The telemetry system must provide for simultaneous data transmission from the ARS, power system, thermal control system, experiment electronics, monopulse system, and the transmitted power and AGC voltage used for the measurements.
- Ground Antenna - The ground antenna must be able to vary its polarization.

Gain Measurement There are several possible methods for determining antenna gain, each varying in accuracy and complexity:

-
- (1) If 0.03 degree accuracy cannot be obtained, the monopulse system must be used as a supplemental ARS aid.

- Power Measurement: By measuring the transmitted power (P_t) and the received power (P_r), the gain (G) can be determined from the range equation

$$G = \frac{P_r}{P_T G_{gt}} \left(\frac{4 \pi R}{\lambda} \right)^2 \quad (1)$$

where R is the range and G_{gt} is the gain of the ground terminal antenna. Measurement inaccuracies are, of course, contributed by all quantities in equation 1. Since the transmitted and received power is already determined during pattern measurements, the addition of range and ground terminal gain information will serve to determine the gain.

- Comparison Method: This technique measures the gain of the paraboloid by comparison with an antenna whose gain is known. The received power of the ground terminal, radiated through the satellite transmitter-paraboloid link, is compared with power radiated through a transmitter-standard gain antenna link. Although this method has the greatest accuracy because it is a direct calibration, it reduces reliability and adds complexity to the satellite. This results from the requirement for standard gain antennas and switching circuitry.

- Indirect Measurement: This method makes use of the calculated directivity of the paraboloid, and its dissipation and mismatch losses to estimate gain. The directivity D at the peak of the main beam is given by

$$D = \frac{4 \pi}{\oint f(\theta, \phi) d\Omega} \quad (2)$$

where $f(\theta, \phi)$ is the normalized power pattern of the antenna and Ω is the solid angle. The required integration is over 4π steradians. Pattern information is available from the measurements, only over a small portion of 4π steradians. Therefore, only an estimate of the paraboloid directivity is obtained from (2).

The antenna gain is computed from

$$G = \alpha D \quad (3)$$

where α is the radiation efficiency (the ratio of the power radiated to the total power supplied to the paraboloid). The radiation efficiency is composed of dissipation losses in the feed and the reflector surface, and the feed mismatch loss. The dissipation loss, which generally runs about 2%, can be calculated from the assumed current distribution on the reflector. Mismatch loss is measured with the reflectometer.

The technique of gain measurement is as follows: In method (a) the boresight axis of the spacecraft is aligned with a ground terminal using the ARS and the monopulse system. The polarization of the ground terminal antenna is adjusted for maximum power transmission. The absolute values of the transmitted and received powers are measured. In the case of the satellite, the absolute transmitted power is measured with the calibrated reflectometer and the received power from the calibrated AGC voltage of the receiver.

2.2.2 Monopulse System Operation and Calibration

The monopulse system supplements the ARS with vernier correction signals for pointing and tracking the antenna beam. To determine the reference accuracy of the ARS, the monopulse system must be calibrated independently of the ARS.

Calibration of the monopulse system consists of constructing radiation contour maps of the azimuth and elevation error channels. This is accomplished in rectangular grid fashion by recording the signals of the error channels as a function of the position of a mobile ground station. Calibration is therefore independent of the ARS. As a consequence, the ground terminal can be located to virtually any degree of accuracy.

The satellite is pointed with its + Z-axis along the line-of-sight to a centrally located fixed ground terminal. The monopulse system then goes into operation, locking the boresight or monopulse axis of the antenna on the fixed ground terminal. After lock-on, the monopulse/SCS control loop is opened, the fixed ground terminal signal is turned off, the mobile station turned on and the azimuth and elevation error signals recorded. This measurement is repeated for the number of mobile station locations required to synthesize a contour map of the monopulse null region of the antenna beam. All positions of the mobile station are accurately located with respect to the fixed ground terminal.

The time required for calibration will depend on the number of mobile ground terminals available and the number of locations required. For the case of a single mobile ground terminal and the location layout shown in Figure 2.2-2, the time for calibration is about 23 days. This is based on an individual measurement time of about 1.5 hours. Monopulse calibration will be repeated periodically and after any severe change in the satellite environment or performance.

Boresight Alignment For the discussion of the boresight alignment, the following definitions are given:

- (1) The boresight axis is the monopulse axis.
- (2) The boresight axis error is the angular deviation with respect to the + Z-axis.
- (3) The feed alignment error is the angular deviation of the feed axis with respect to the + Z-axis.
- (4) The + Z-axis is the yaw axis as measured by the ARS.
- (5) The attitude of the + Z-axis is known within an accuracy of 0.05 degrees.

The basic idea is to measure the angle between boresight and the + Z-axis when the boresight axis coincides with the line-of-sight of a ground terminal. This will be accomplished by aligning the boresight axis with the line-of-sight

by using the monopulse system to lock on to the ground terminal. The Z-axis attitude as defined by the ARS will be noted. The boresight alignment will be measured as soon as ATS-4 is on permanent station. Deviations resulting from thermal distortions will be observed during occultations.

Pointing Accuracy - In this experiment the high resolution of the monopulse system is used to measure pointing errors under the condition of a commanded pointing direction. The objective of the experiment is to measure the angular error between the boresight axis and a commanded pointing of the + Z-axis. The technique used is to slew the vehicle into the desired attitude, such that it is pointing to the ground terminal. After the motion has been arrested, the vehicle is illuminated by the ground terminal and the resulting monopulse error signals recorded. A comparison of the recorded error signals with the monopulse system calibration will determine the pointing angle error. The measurements are made when the satellite is on station. The time required depends primarily on the slewing rate.

Tracking - Tracking is the mode in which the satellite follows a cooperative moving object, such as a low-altitude satellite or an airplane. Two methods are possible:

- Open Loop - In this method tracking is commanded according to the ephemeris of the target, which carries an 8 GHz beacon. The tracking error is measured by comparison with the monopulse system calibration.
- Closed Loop - The satellite tracks the object with a monopulse system lock-on. Error signals are transmitted to the attitude control system causing the satellite to slew and track the object. In this mode the combination of the ARS and the monopulse system as a sensor must be capable of a tracking rate of at least 0.5 degree per minute in order to follow low altitude satellites.

2.2.3 Phased Array Experiments

The following tests and experiments will be performed upon the phased array antenna in order to demonstrate that it is performing as intended, and to evaluate certain of its capabilities in the space environment.

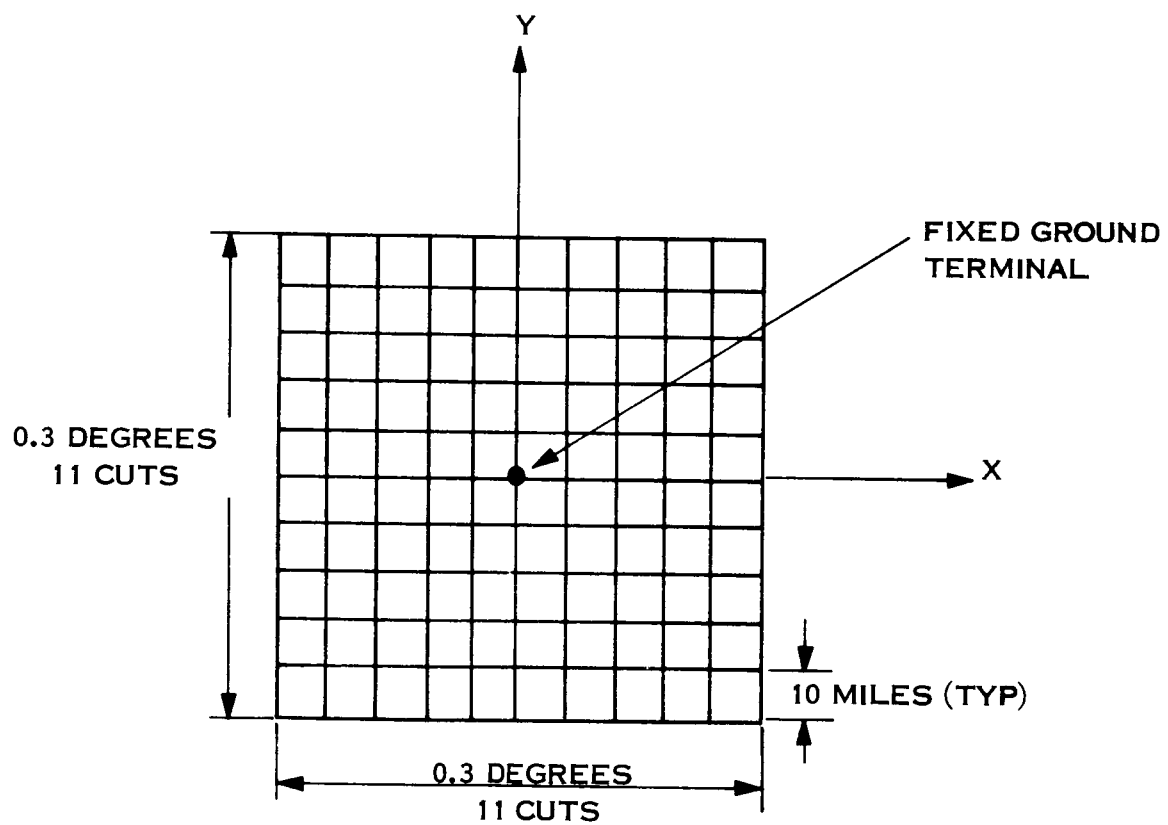


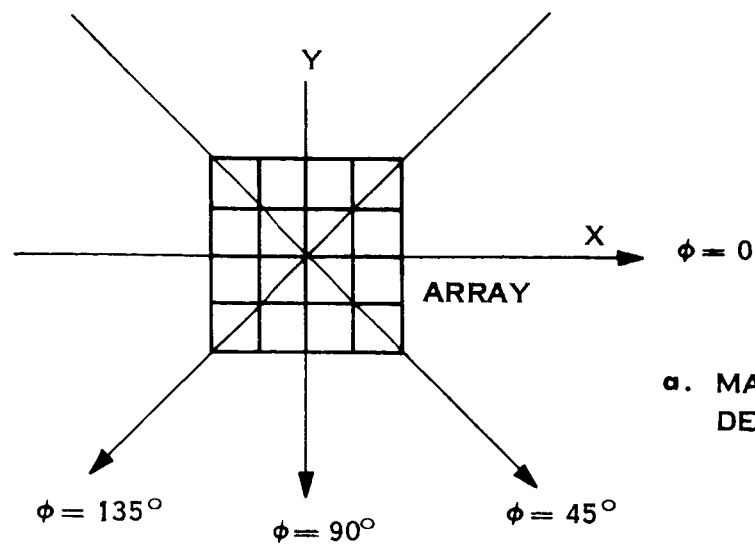
Figure 2.2-2 Ground Terminal Layout for Monopulse Calibration

- Static Patterns
- Dynamic Patterns
- Failure Mode Test
- Cross-Talk

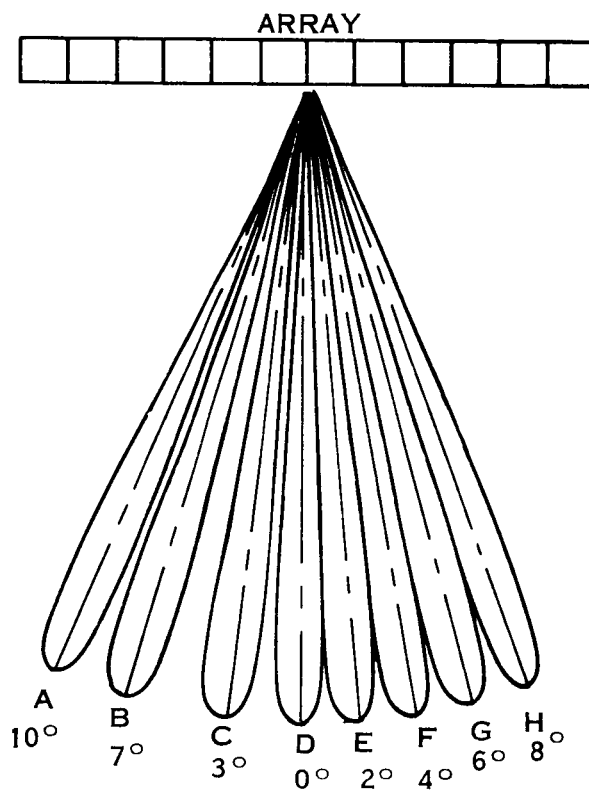
Static Patterns Static patterns of an electronically scanned antenna implies the conventional type of pattern measurement, whereby the measured beam is in a fixed position relative to the antenna, and the antenna is physically rotated relative to a fixed RF source.

Four sets of static measurements must be performed for the transmit and receive beams at the two prescribed frequencies, 7.3 GHz and 8.0 GHz. These measurements will be performed in a manner similar to those on the parabolic reflector, in which the entire satellite is moved slowly and the source antenna is at a known position on the ground. The two transmit beams may be measured simultaneously by diplexing on the ground, and likewise the two receive beams may be measured simultaneously by using two frequencies from the ground station. The beam steering data for the two beams being measured will be identical, so only one set of phase settings per beam position need be used.

Since the satellite slews very slowly, (from 0° to 4° per minute), it is possible to measure beams for a variety of pointing angles during one slewing motion. This is accomplished by switching the beam and sampling the signals. This is illustrated in Figure 2.2-3, in which the major scan planes are also illustrated. The satellite will be slewed such that its Z-axis will move in one of the major planes with an excursion of $\pm 15^{\circ}$. During slewing, the beam control unit will switch the beam at maximum speed through positions A through H repeatedly. The beam will dwell in each position long enough to allow a sample measurement to be taken for 0.9 second.



a. MAJOR PLANE DEFINITION



b. TYPICAL BEAM POSITIONS FOR STATIC PATTERNS

Figure 2.2-3 Major Planes and Beam Positions for Typical Static Pattern Tests

Stored data for 8 beams in the core memory at the satellite allows a new beam to be set every 100 milliseconds. The time between samples would be the time required to switch through and sample all the beam positions being tested. For 8 separate positions then, allowing 100 milliseconds to switch and 900 milliseconds to sample, the time between samples would be 8.0 seconds. To present the patterns to a reasonable accuracy a sufficient number of samples should be taken. A spacing between measurement points of 0.1 of a half power beamwidth, or about 0.25° is reasonable. This sets the maximum slew rate at approximately 2° per minute. The satellite must be slewed along its intended measurement axis to a tolerance of 0.3° .

The measurement along one major plane requires 15 minutes. One complete run (four major plane cuts) requires one hour. The measurement will be performed once the satellite is positioned on station: the time requirement is not critical. The measurement will be repeated periodically to determine the antenna performance as a function of satellite life-time.

The antenna pattern measurement of the phased array imposes the following requirements on the other spacecraft subsystems:

Telemetry:	Telemetering of transmission power measurements, beam switching cycle, phase shift data, ARS data, experiment electronic housekeeping data and thermal control data.
Command Systems:	Commanding of the slewing and beam switching.
Beam Steering Unit	Beam Switching.
SCS	Performance of slewing motion, at 2° per minute for $\pm 15^{\circ}$ excursions with a tolerance of $\pm 0.3^{\circ}$.

ARS:

Reference data within the tolerance of $\pm 0.3^\circ$ on the satellite attitude.

The pattern measurements will result in different data for the different beam positions. While the on-axis beam will be measured to five beamwidths, the off-axis beams will be measured asymmetrically. Consequently, for off-axis beams, more sidelobe data for one side will be available.

The gain will be determined in two fashions:

- Directly, from the measurement of transmitted power and received power.
- Indirectly, by integrating the pattern.

Dynamic Patterns Patterns will be measured on the four independent beams, two transmit and two receive. The two receive beams will be simultaneously measured as will the two transmit beams. By dynamic patterns it is meant that the vehicle is held stationary while the beam is scanned electronically, (using the beam steering system), through the ground measurement sites. The scan trace may be made to follow a straight contour for measurements of beams on one of the principal planes, or a conical contour for beams off the principal plane. This is desirable since the sidelobes will be primarily distributed along conical contours for beams off the principal axis.

Beams being measured will be scanned at the maximum rate permitted by the data link capacity which is 35 bits per second. Since the number of bits required to completely form a beam is 192, the beam position is changed every 5 seconds. The size of the beam steps will be one quarter beamwidth or about 0.6 degree. To take a full 20 degree cut therefore requires 34 steps of 0.6 degree each, for a total duration of 3 minutes. (Note, the beam moves in much finer than 0.6° steps, since each element is switched serially. The average step size is $1/64$ of 0.6° or $.009^\circ$).

In order to increase the quantity of data obtained per cut, it is proposed that the satellite be aligned for each cut in such a manner that the beam scan through two ground stations. In effect, then a pattern is measured for two boresight positions simultaneously. For example, if the satellite were fixed such that one station was at co-ordinates $(0^\circ, 0^\circ)$, and a second station was at $(0^\circ, 7^\circ)$, scanning the beams through both stations would give a measurement of the broadside patterns at the $(0^\circ, 0^\circ)$ station and patterns of the 7° scanned beams at the $(0^\circ, 7^\circ)$ station.

The broadside patterns will be measured in both principal planes and both diagonal planes. These are the $\phi = 0, 45^\circ, 90^\circ, 135^\circ$ planes in the classical spherical co-ordinate system illustrated in Figure 2.2-3 where the array aperture lies in the X-Y plane.

The simultaneous scanning of the two transmit or two receive beams is performed by applying the same phase signal to the phase shifters in both channels. This may be done by altering the address word at the start of each 192 bit phase transmission, to parallel feed the same data to both channels.

The technique utilized will be to orient the satellite to one ground station such that the phased array Z-axis passes through this station. The satellite is axially positioned such that the plane along which the beam is

to be measured passes through another station. (More than two stations may be employed if practical.) The beam steering data is telemetered to the array to form the beams 10° off-axis, and then continuously updated at the 35 bit per second rate so that the beams scan along the prescribed contour, through the Z-axis station and out to 10° off center in the direction offsite from which it started. The ground station (s) record the received signal levels.

The satellite is then axially repositioned for the next plane cut and the procedure repeated.

Every scan through the array Z-axis requires a period of 3 minutes. The prescribed four cuts will require 12 minutes of measurement plus the maneuvering time required for the satellite axial rotation. Any conical contours will require shorter durations depending upon how far from the Z-axis the particular cut is taken. A need for such cuts is not foreseen; however, if pattern abnormalities are encountered the entire space coverage of the array may be measured using this technique.

The dynamic transmit pattern measurements impose the following requirements on other spacecraft subsystems.

Telemetry:	Transmission of beam position, transmitter power output, thermal control data, ARS data and experiment housekeeping data.
Command:	Command of axial positioning and beam scanning.
Beam Steering Unit	Generation of phase shift data and on board processing.

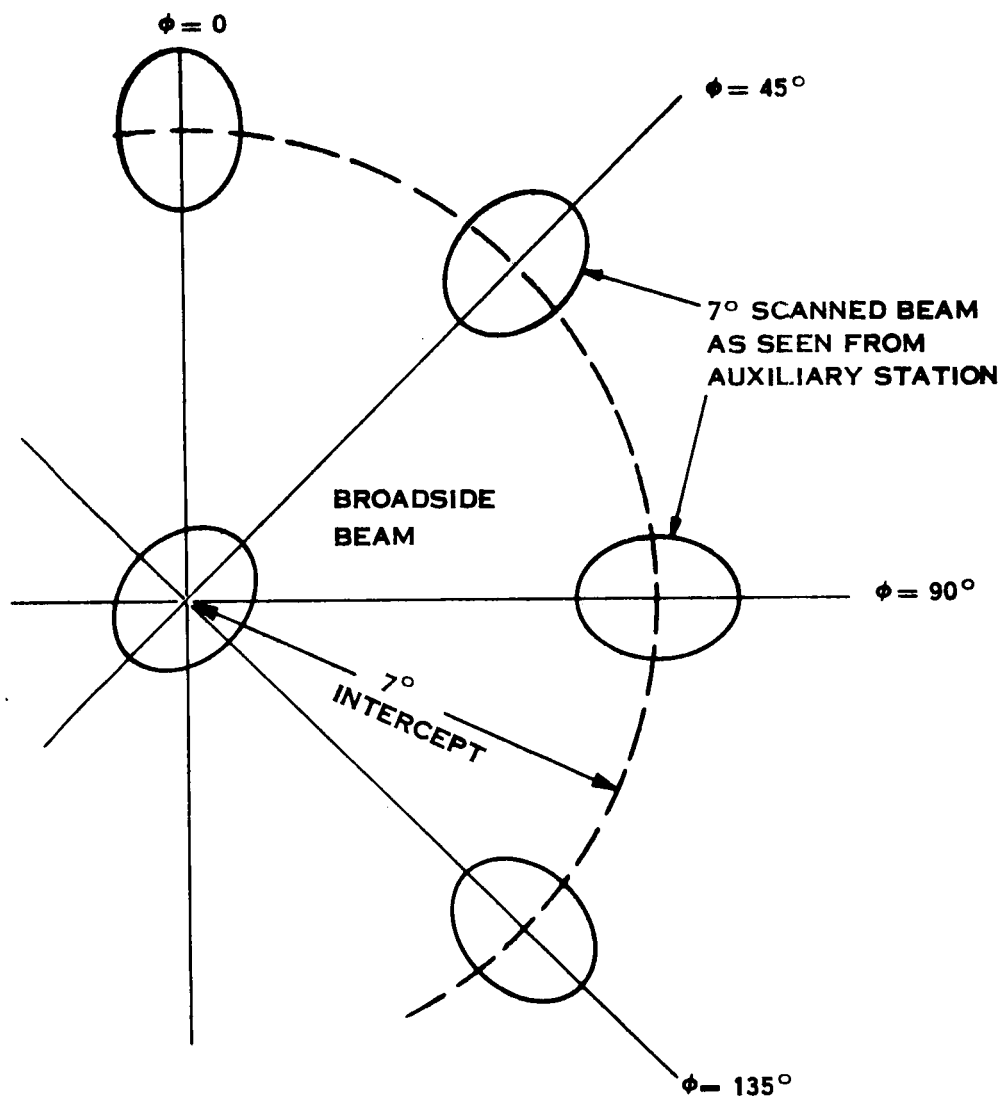


Figure 2.2-4 Multiple Pattern Cuts Using Two Ground Stations

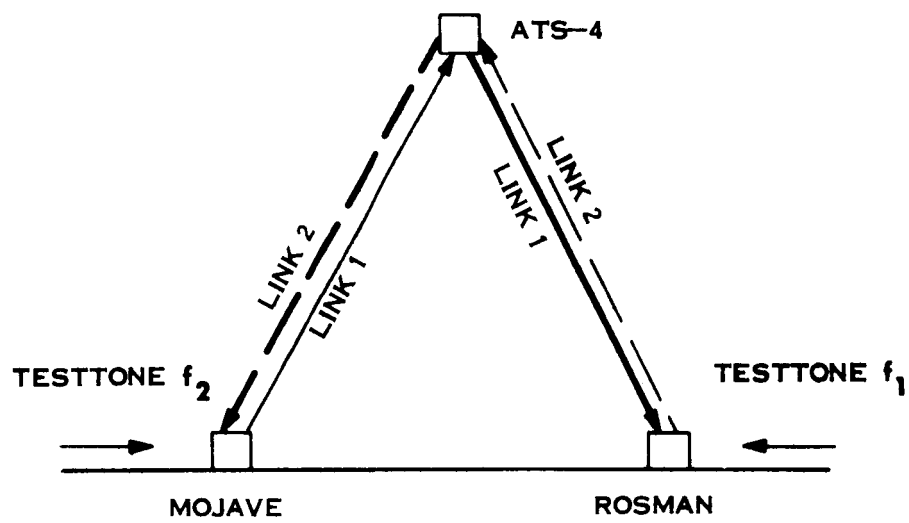


Figure 2.2-5 Crosstalk Measurement

SCS:

Positioning and stabilizing satellite.

ARS:

Reference data within $\pm 0.3^\circ$ tolerance.

Principal plane and diagonal plane cuts of the two transmit beams are obtained. In addition by using the second station, various cuts of the beam in off-axis positions are measured. Figure 2.2-4 illustrates the beam data obtained, where the lines represent the cuts taken and the circles represent the main beam positions.

Failure Mode System Test - The principal of operation of the failure mode provision of the phased array antenna is explained in Section 2.6. This failure mode involves an element by element test of the radiated signal amplitude and phase, from which many non-catastrophic type failures may be analytically diagnosed. By altering the beam steering instructions, phase corrections may then be programmed into the system to compensate for certain of these failures. This ability to make individual element tests is an important feature in the phased array since it may also be used to supply valuable reliability information about phased array components in space as the satellite approaches its life limit. It is therefore imperative that an experiment be performed to demonstrate that this mode can function effectively.

During test, the phase of a single element is cycled through its entire range of values while the other 63 elements remain fixed. The resulting modulation envelope, amplitude and phase, is analyzed to determine the performance of the particular element under test. This is repeated for all 64 elements of each transmit and each receive array network.

The satellite is oriented such that its Z-axis aligns with the ground station. Data is transmitted from the ground through the data link to fill the beam steering memory unit with the phase shifter data. This consists of 8 sets of phase shifter setting for each of 192 bits. The 8 sets of data differ only in the phase shifter settings of the element under test. The settings for this phase shifter consists of its 8 possible phase states in

rotational order. The command is then transmitted to commence cycling and the data is fed in sequence to the phase shifters. Since only one element is switched, a slight modulation envelope is impressed on the beam, the characteristics of which determine the elements function. A 1 KC cycling rate is used so that this modulation envelope is clearly distinguishable from noise. The modulation index is measured directly to determine the gain of the element relative to the array. Its phase is compared with a phase reference voltage which allows the phase of the test element to be compared to its nominal value.

Most of the time required for this test is spent filling the core memory between element cycling. The 1536 bits can be supplied at 35 bits per second, and therefore requires 40 seconds. The cycling, which runs at 1 KC requires only several seconds. An average time per element would be about 1.5 minutes, or a total of 100 minutes to test 64 elements.

The 1 KC modulation envelope, and the 1 Kc timing pulses will constitute the required data for analysis, along with the carrier level of the modulated signal. The ground beam steering programmers will supply the address of the element under test.

These measurements require the use of the following spacecraft subsystems.

Telemetry:	To transmit the data to be stored in the core memory, defining the phase shifter settings. Also to provide the start and stop cycling instructions to the satellite beam steering logic circuits.
Command System:	Command of the satellite positioning.
Beam Steering Unit	Perform the phase shifter data cycling.

SCS: Perform the satellite position and stabilization.

ARS: Provide attitude information to 0.3° tolerances.

The modulation envelope will be computer analyzed to determine the degree to which each phased array element is performing its design function. It will provide corrective data, indicate that no corrections are required, or indicate total element failure.

Cross-Talk Measurement - Cross-talk and cross-modulation measurement for both channels in duplex arrangement is accomplished by determining the transfer characteristics of two test tones of different frequencies (one tone in each channel) and by examining the resulting modulation.

A duplex link is established between Rosman and Mojave. A test tone of frequency f_1 is inserted at Rosman, and another test tone of frequency f_2 is inserted at Mojave. The cross-coupling and intermodulation is determined at Rosman and Mojave. Figure 2.2-5 shows the arrangement schematically.

The estimated time which will be required to perform the measurements is about fifteen minutes. The measurement will be scheduled when required. The following requirements exist for satellite subsystems:

Ground Equipment:	The appropriate test equipment to produce the test tones and measure cross-talk and cross-modulation is required.
SCS:	Holding the attitude for the period of measurement.
Beam Steering Unit:	Scanning of one transmitter beam in the Mode A type measurement.

2.2.4 Orientation and Control Experiment

The primary design function of the stabilization and control system (SCS) is to determine and maintain vehicle attitude as required in each mode of control. Since proper vehicle operation is dependent upon the performance of the control system, its experiment function is primarily one of design verification and performance monitor.

Design verification is determined functionally as the vehicle is methodically commanded through its modes of operation, and control subsystem status is qualitatively monitored. In addition, quantitative monitoring to assess control subsystem performance and accuracy is accomplished via TM monitor as follows:

Horizon Scanner Comparison with Fine Sun Sensor - The first step in the acquisition sequence aligns the vehicle x-axis to the sunline. In the second step, the vehicle is rolled about the sunline, permitting earth acquisition. At this point, there are two sources of pitch attitude information, one from the medium fine sun sensor and one from the horizon scanner. Since at the point of earth acquisition, pitch control is still obtained from the medium fine sun sensor, the horizon scanner pitch attitude error signal can be used to evaluate the sun sensor performance. To accomplish this, both sensor error signals are telemetered to the ground via the down-data link for comparison. In this evaluation, the sunline may not be exactly perpendicular to the local vertical, hence a non-orthogonality bias is removed from the horizon sensor pitch output signal. After verification of earth acquisition, pitch control is switched from the sun sensor to the horizon sensor, and the non-orthogonality bias is automatically removed.

Polaris Acquisition Check - After earth acquisition is accomplished and the horizon scanner is providing pitch and roll control, yaw control is switched from the sun sensor to the yaw gyro. The gyro is then torqued through a specified angle from the sunline to the equatorial plane. At this point, the

star tracker should observe Polaris directly within its instantaneous field-of view ($2^{\circ} \times 2^{\circ}$) without requiring any scanning or searching for the correct star. However, to verify that Polaris has indeed been required, the observed star magnitude is monitored to assure that it is within the Polaris star magnitude gate, the received light color spectrum is examined and the yaw gyro output signal is monitored to assure that the vehicle has traversed the proper angle for acquisition. If these tests fail, indicating that Polaris has not been acquired, a $\pm 5^{\circ}$ yaw search is commanded to locate the correct star. Since the nearest star to Polaris which is close to the same magnitude of Polaris is approximately 12 degrees away (Kochab in the constellation Ursa Minor), there appears to be no requirement for a large instantaneous field-of-view or a complex scan search for Polaris.

Yaw Gyro Performance - The star tracker provides an accurate yaw reference upon which to base the alignment, calibration, or performance monitor of other means of yaw reference. These are the yaw gyro and the interferometer. By biasing the output of the yaw gyro with the star tracker, Polaris diurnal motion bias, and telemetering the output signals to the ground, a check on gyro alignment, drift and stability is made. In a similar manner, the yaw attitude measured by the interferometer may be monitored.

Horizon Scanner Stability - A key element in the control experiment is the performance monitor of the horizon scanner. While the vehicle is holding attitude toward an offset point ground station and being controlled by the x-band monopulse antenna signals, the horizon scanner output signals are monitored by telemetry. In this manner, the horizon scanner accuracy and thermal stability is determined. This information is monitored to determine the daily predictable errors due to thermal deformation, day-night errors, and time dependent electronics degradation as well as the the random unpredictable error in the system. Similarly, the daily and seasonal horizon

definition variations may be determined by correlating the data trends with time while employing x-band monopulse control.

Pitch and Roll Gyro Performance - In a similar manner to that described above, the pitch and roll gyro drift performance is measured. When the vehicle is being controlled via x-band monopulse at an offset ground station, the gyros are torqued by a signal proportional to appropriate components of the orbital rate to maintain a null condition. The remaining output signals from the gyros is then telemetered to the ground for drift calibration and performance monitor.

Reaction Jet Performance - In an unregulated blow down hydrazine reaction jet system, the thrust output is somewhat variable and reduced with time. The actual thrust or impulse being obtained in each pulse can be determined by monitoring the wheel tachometer signal. If the jets are performing abnormally, the pulse width can be increased or decreased to affect a compensation.

Control Response - The tightness of control is measured by monitoring the wheel response to an input current correlated with the wheel tachometer signal. Also the vehicle response to a commanded impulse is determined by comparing the horizon scanner or gyro attitude signal to the input attitude command signal. These response lags are measured to verify system performance and permit appropriate changes in system gain.

Controller Performance - To monitor the performance of the controller, an identical controller logic model is to be included in a ground based computer. By monitoring the vehicle controller input and output, and comparing this with the computer model, verification is accomplished. This monitor is an essential element in the controller evaluation and redundancy diagnostics. In the event that an output discrepancy exists,

redundancy switching of the controller is commanded and a failure diagnostic routine is initiated.

Additional Experiments - In addition to monitoring the qualitative and quantitative performance of the active stabilization and control system, the spacecraft also provides a test platform for other backup or piggyback subsystems. These other piggyback subsystems, having a completely experimental or test purpose, would be included only as weight and power limitations permit. Candidate experimental subsystems, worthy of consideration, are defined as follows:

- Decomposed ammonia resisto-jets in the milli-pound class to evaluate the jet performance, control system stability, and vehicle dynamics.
- Electrically Suspended Gyro (ESG) reference system to evaluate gyro performance and accuracy.
- Developmental horizon scanners using rose pattern or alternate scanning techniques to evaluate means of obtaining improved pointing accuracy from synchronous altitude scanners. This may include data collection to determine radiometric horizon correlation with diurnal, seasonal or land-sea mass conditions.

2.2.5 Interferometer

Data obtained from tests hereinafter described will be used to evaluate the interferometer as an attitude sensor. Principal objectives are:

- Determination of interferometer resolution and accuracy over its field of view;
- Determination of operational reliability and stability of characteristics over the two year life time;
- Demonstration of the Radio Interferometer as the spacecraft stabilization and control attitude reference.

The interferometer will be evaluated in three primary modes:

- Checkout
- Sensor Evaluation
- Attitude Control Demonstration

Interferometer Checkout -- After the satellite is in orbit, the checkout mode will allow determination of onboard instrumentation operating characteristics. These first test sequences will be aimed at examining the performance in sufficient detail to establish the fact that nominal flight operation has been achieved. This validation is largely achieved through exercise via the command-telemetry interfaces and comparison with prelaunch data. Operation of the sequencer, interferometer receiver channels, zero crossing detectors and counter will be checked. Suitable checkout circuitry will be incorporated to produce standard test conditions onboard which can be used throughout the ground test and mission phases. Thus, the checkout mode will be used to both establish the electronics performance norms and to subsequently determine actual operating conditions. This facility is especially important during use of the interferometer as the attitude control reference in that it allows a repeatable, quick check which verifies stability of the sensor space angle-to-attitude calibrations.

In addition to the onboard electronics checkout, for which the test

signal will likely be injected at the first IF, antenna and mixer circuits must also be checked. To assure meaningful results, this test is performed using ground illumination; it is described as the initial part of the Sensor Evaluation pattern tests.

Sensor Evaluation -- The sensor evaluation mode corresponds to the "normal" operating condition of the interferometer sensor. Ground illuminators, computation, command and telemetry functions are active. The basic exercise required to accumulate sensor performance data consists of correlating illumination angle of arrival to measured phase angle for each interferometer axis at each operating frequency.

Boresight calibration and checkout of the interferometer array and mixer assemblies is achieved by orienting the spacecraft along the line-of-sight to a ground illuminator via the monopulse. The satellite is sequentially illuminated with each of the normal operating frequencies. The interferometer phase angles for each array axis and the processor output, are telemetered to the ground station. This data then defines the boresight alignment errors relative to the monopulse and ARS at each operating frequency for each axis.

Electromagnetic susceptibility can also be conveniently evaluated while making the boresight alignment and resolution measurements. On-board experiment transmitters are switched on in various operational combinations with test modulation while observing the interferometer error signals.

Since the interferometer array is colocated with ARS sensors, the phased array and monopulse feed canister, the interferometer boresight geometry should coincide with that of the ARS, phased array, and bear a simple relation to that of the monopulse. Hence, deviation of the ARS plus Z axis from the apparent paraboloid and interferometer axes can be directly measured. Combining this interferometer test with the monopulse calibration method (position increments of $\sim 0.030^\circ$) will produce on-axis resolu-

tion data. Dependence on ground ERP can also be determined during this test.

While the boresight errors may be completely defined, the error for other vehicle/line-of-sight orientations is not necessarily the same. Consequently, data for other test orientations are required. Rotational symmetry is expected to be good enough to permit definition of the errors everywhere in the field of view by executing radial scanning notion in 36 equispaced major plane cuts (Figure 2.2-6). The second ground station is also activated and appropriate constants, ground station and satellite positions are loaded into the processor to provide direct comparison of interferometer processor outputs with the ARS and with coordinates computed from raw interferometer data at the ground station. Since the monopulse pointing reference cannot be used beyond about $\pm 0.15^\circ$ of the line-of-sight, gyros will serve as the attitude reference during the maneuvers.

The monopulse boresight (Z-axis) of the satellite is aligned with the test ground station (as in the boresight checkout). The gyro package in the Attitude Reference System (ARS) is then caged (zeroed) and the first test swing or cut begins. The Attitude Torquing System slews the satellite Z-axis 10° off line-of-sight to the station, then swings the system back to the original position; the monopulse is used to check for gyro drift. The gyros are recaged and the system is ready for a second cut. Reaction wheels in the ATS are used for slewing the satellite. The telemetered gyro determination of attitude, the phase angles from the interferometer and the sequencer-processor output are monitored in real-time at the ground station. The gyro output is used as the input to a ground computation of the idealized interferometer readings. A running comparison of the actual and computed interferometer phase angles and attitude determination is recorded. Since the gyros are updated after each cut, the accuracy of the measurements is high. If the gyro drift is limited to 0.1° per hour and the ATS is capable of an angular rate of 4° per minute the maximum gyro drift will be less than 0.02° per cut. The error introduced by taking sequential phase measurements

while the satellite has an attitude rate will be less than 0.0003° . However, care in timing and buffering is required to assure that the compared gyroscope and interferometer readings all come from the same time frame.

The result of this sequence is calibration of the interferometer over its field of view in a form suitable to computer retrieval for subsequent pointing command preparation and attitude reference. Repeating part or all of this sequence during the two year mission will serve to evaluate component stability and reliability.

Attitude Control Demonstration-- Following the foregoing calibration exercises, the interferometer sensor and processor are ready for operational use. The demonstration consists chiefly of closing the control loop around the interferometer as the attitude reference and observing the open loop ARS response. Suitable maneuvers for this purpose are shown in Figure 2.2-7, the reference orientation being alignment of the + z-axis with the local vertical; this is the ARS reference alignment. Maximum ARS accuracy is retained throughout these maneuvers.

Commanded tracking and pointing maneuver operation can be demonstrated by inserting the desired attitude into the SCS, as normally used with the ARS. Alternatively, a backup feature of the interferometer processor can be utilized by inserting the command coordinates directly into the processor.

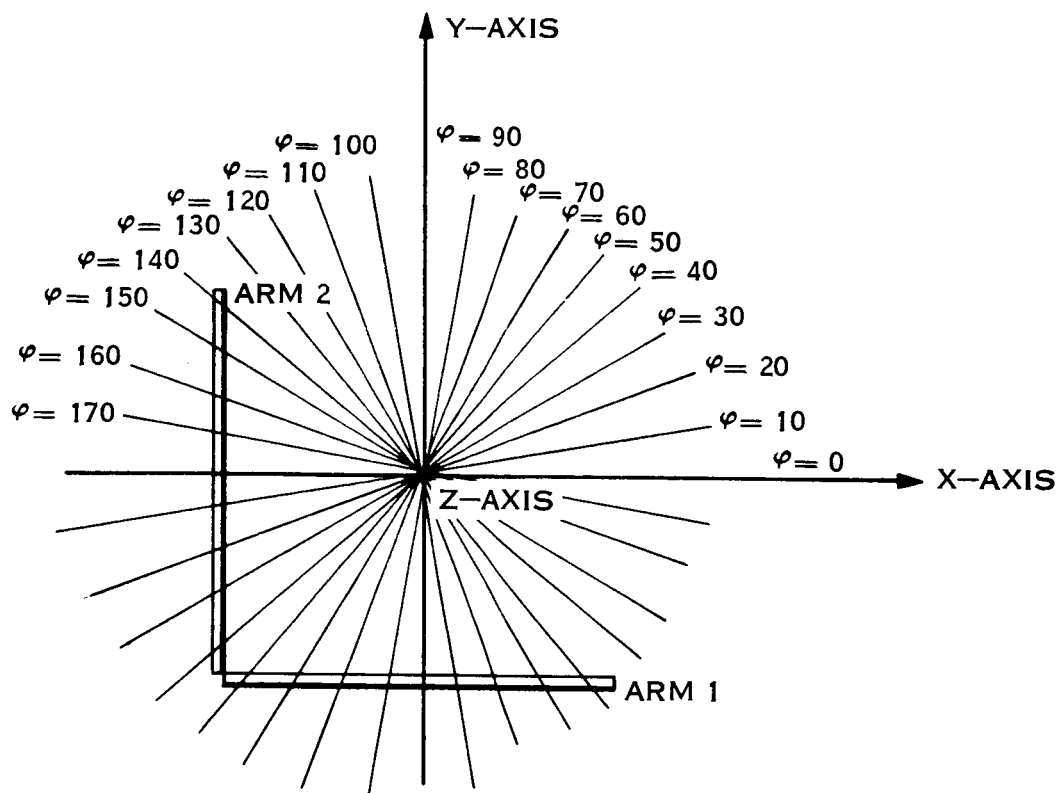


Figure 2.2-6 Major Plane Cuts, Interferometer

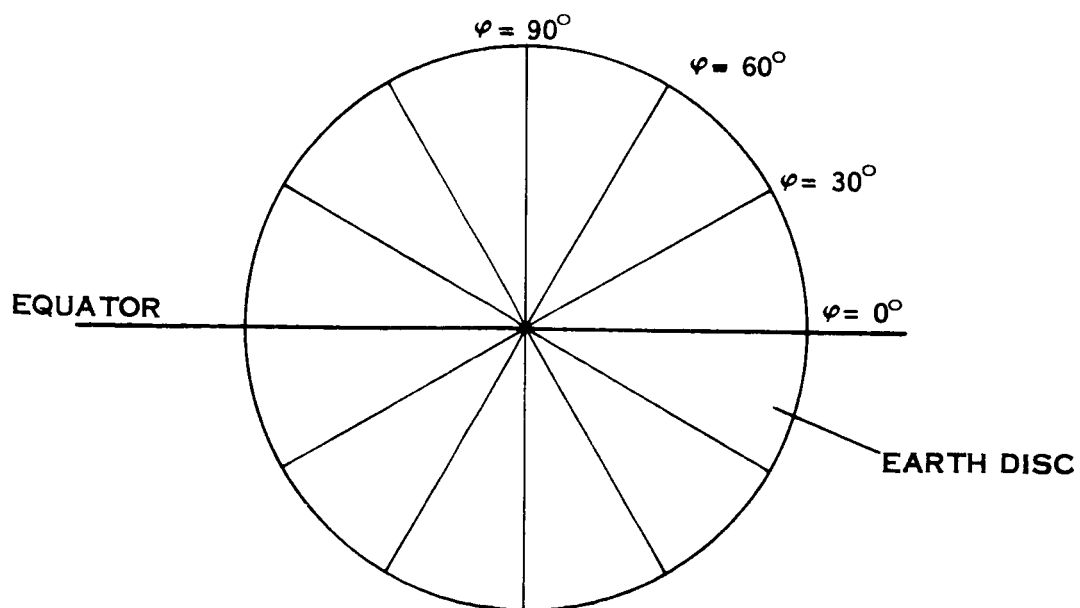


Figure 2.2-7 Pointing of the Z-Axis for Interferometer Measurement

2.2.6 Additional Communications Experiments

Demonstration of the capabilities of the ATS-4 satellite will be made by implementing those experiments listed in Table 2.2-4. These experiments are presented with a view to showing the advanced services that can be made available with the ATS-4 type of satellite.

The relay of FM and TV broadcast should originate at the control station rather than commercial stations if quantitative data is desired. The commercial signal can be used for a realistic demonstration by setting up appropriate antennas in rural communities that do not presently have FM and TV broadcast reception, for a subjective evaluation.

In the FM link, frequency response, noise level as a function of base bandwidth, emphasis-de-emphasis circuits, dispersion, and fading can be evaluated. In the TV link, test patterns provide the best vehicle for measuring resolution, contrast and signal degradation that might occur due to transmission through the satellite.

The quality of the relayed signals will compare favorably with commercial standards. Therefore, the main problem for investigation is the relay degradation and the propagation path loss.

The modulation recommended is the FCC standard, viz, modulation index of 5 and a baseband of 15 KHz for FM and vestigial sideband AM for the TV signal. Since the satellite will only transpose, it would be desirable to be able to receive the signals into standard high grade commercial receivers.

In like manner, the voice and data links can be evaluated. It is not possible to be very explicit about the experiments at this time because of the large number of possibilities the versatile phased array offers, and in conjunction with the steerable parabolic reflector, the experiments can easily multiply.

TABLE 2.2-4 ADDITIONAL EXPERIMENTS

<u>USAGE</u>	UP FREQUENCY	DOWN FREQUENCY
1. FM Broadcast Relay	8 GHz (R) ⁽¹⁾	100 MHz ^(R)
2. TV Broadcast Relay	8 GHz (A) ⁽²⁾	800 MHz (R)
3. Teletype Link to Aircraft (one way to aircraft)	8 GHz (R)	100 MHz (R)
4. Simplex Voice Link, Ground	8 GHz (A)	7.3 GHz (A)
5. Simplex Voice Link, Aircraft		
from ground to aircraft	8 GHz (R)	7.3 GHz (A)
from aircraft to ground	8 GHz (R)	7.3 GHz (A)
6. Satellite Data	2.1 GHz (R)	2.3 GHz (R)
7. Geophysical Data, Ground	1.7 GHz (R)	2.3 GHz (R)

1. (R) ATS-4 30 foot reflector

2. (A) ATS-4 phased array

A suggestion is that a teletype machine be added to an existing VHF system aboard a cross country aircraft. As the aircraft travels coast to coast, teletype weather reports can be transmitted via the 100 MC channel every 15 or 20 minutes during the entire trip. Direct communications would be available during the entire flight on 100 MC. Such an experiment will provide subjective data from the pilot and crew, especially when flying over unpopulated mountainous regions.

In the case of voice links to the aircraft, communications can be established with the control ground terminal and then contact made with other ground terminals as requested by the aircraft, and controlled by the master ground terminal. Such an experiment should be designed to show:

- That with the versatility of the phased array, the high quality link can be switched to any direction at will;
- That a cross country aircraft can maintain direct contact to any point on its route throughout the flight;
- That with the high gain of the parabolic reflector, high quality voice communication to the aircraft is feasible;
- That a quasi-random access system can be simulated by giving master control the use of one set of beams to continuously scan for calling ground terminals while communications is carried on with the other set of beams.

As pointed out earlier, such demonstrations could lead to direct links from city to city across the continent or the ocean. It can also lead to new services, such as direct telephone connections for air passengers.

For geophysical data, transmitters with geophysical sensors can be placed in nearby localities at the Mojave or Alaskan installations, for instance, so that the data relayed can be continuously checked against other sources well-established in the area.

For satellite data gathering, it may be possible to choose a multi purpose satellite designed for a low altitude orbit, or else orbit one specifically for this experiment. Either way, this experiment will require further study before a definitive program can be evolved. The function to be performed is one of maintaining contact, at the ground station, with the low altitude satellite for longer periods of time. Ultimately, with a minimum of three synchronous satellites, continuous contact with a low altitude satellite would be possible.

2.3 POWER PROFILES

2.3.1 Preorbital Power

The estimated preorbital electrical design load (Table 2.3-1) is 100 watts. From lift-off through about 3 minutes, the shroud excludes sunlight from the folded solar panels; the corresponding energy demand of 5 watt-hours is drawn from the 385 watt-hour main mission, nickel-cadmium battery (1.3% depth of discharge). Ejection of the shroud then exposes one surface of the folded solar array, and at about 1/2 hour after lift-off, the vehicle is injected into the transfer orbit, the Centaur spins up the vehicle, and separates. The total battery drain at this time is 50 watt-hours or 13%. After this sequence, the folded panels will deliver an average input to the main load bus somewhere between 130 watts (solstice launch) and 64 watts (equinox launch)⁽¹⁾. In the ensuing period, the 100 watt load remains until one hour or so before deployment which occurs at 16.3 hours. The telemetry subsystem Mode 2 is then energized, adding 34.5 watts to the total load.

Under the worst condition, i.e., equinox launch, a battery supply must support the 608.5 watt-hour drain preceding deployment⁽²⁾. Limiting the mission battery discharge to 50% (i.e. 192.5 watt-hours) would thus necessitate incorporation of a separate preorbital battery. A suitable silver-zinc unit of 50 watt-hr/lb would weigh 12 pounds.

Solstice launch panel output in the folded configuration will be sufficient to supply the entire load prior to deployment. Hence, no additional

1. Spin axis to solar vector @ Solstice:	44° ;	130 watts
Spin axis to solar vector @ Equinox:	20° ;	64 watts
Input to load buss @ Solstice:	$7.6 \times \frac{155}{2} \times \frac{1}{\pi} \sin \varphi$	$= 187 \sin \varphi$

2. $(100 - 64) 14.8 + 5 + (134.5 - 64) 1 = 608.5$

TABLE 2.3-1 ESTIMATED POWER DEMAND EVALUATION TESTS

SUBSYSTEM	Preorbital	Standby and Occultation	Deployment and Structural Evaluation	Interferometer	Parabolic Antenna Patterns	Phased Array Patterns	Occultation Parabola X-Band Pattern	Occultation Phased Array Pattern
I Parabolic Antenna								
1. Transmitters								
7.3 GHz	0				42.7	0	42.7	0
2.3 GHz	0				1.4	0		
800 MHz	0				36.0	0		
100 MHz	0				18.0	0		
2. Receivers								
8.0 GHz	0.6	4.6						
1.7/2.1 GHz	0.4	3.4						
II Phased Array								
1. Transmitters	0					85.2	0	42.7
2. Receivers	0.4	2.4						
III Orientation and Control	29.5	88.0						
IV Radio Interferometer	3.0	8.0		34.0	8.0			
V Command Subsystem	2.2							
VI Telemetry and R R	34.6		69.1	32.3				
VII Instrumentation	5							
VIII LO-Mult. Chain	13.7							
Total Load: (watts)	89.4	161.9	196.4	185.6	257.7	244.8	202.3	202.3
Design Loads:	100	175	225	200	275	275	225	225
Design Margin	12%	8%	14%	8%	7%	12%	11%	11%
2 Year Operating Margin	-	-	85	110	35	35	85	85
Initial Operating Margin	-	-	131	156	81	81	131	131

TABLE 2.3-1 ESTIMATED POWER DEMAND - DEMONSTRATION TESTS

SUBSYSTEM	PARABOLIC ANTENNA					PHASED ARRAY				
	Up Frequency	1.7/2.1 GHz	8.0	8.0	8.0	8.0	8.0	8.0	8.0	8.0
	Down Frequency	2.3 GHz	7.0	0.8	0.1	7.3	7.3	7.3	0.8	0.1
I Parabolic Antenna										
1. Transmitters										
7.3 GHz			42.5	0						
2.3 GHz			0							
800 MHz				36.0	0				36.0	
100 MHz					18.0				18.0	
2. Receivers										
8.0 GHz										
1.7/2.1 GHz										
II Phased Array										
1. Transmitters										
2. Receivers										
III Orientation and Control										
IV Radio Interferometer										
V Command Subsystem										
VI Telemetry and R R										
VII Instrumentation										
VIII I.O-Mult. Chain										
Total Load:	187.0	228.1	221.6	203.6	228.1	270.6	324.6			
Design Loads	200	250	250	225	250	300	350			
Design Margin	7%	9%	13%	11%	9%	11%	8%			
2 Year Operating Margin	110	60	60	85	60	10	-40			
Initial Operating Margin	156	106	106	131	106	56	6			

battery is required for this launch condition.

2.3.2 Experiment Evaluation

Table 2.3-1 indicates the estimated total load bus drain for various primary experiment evaluation tests. These tests group into three design load levels: 200, 225, and 275 watts.

Exercise of supplementary loads, as for additional experiments, would not be performed simultaneously with the primary ATS-4 experiments. Figure 2.3-1 is an idealized load profile which illustrates one of many conceivable sequences for performing ATS-4 tests; parabolic antenna pattern measurements, interferometer, phased array. Note that the highest load of 275 watts is below the 310 watts input available from the illuminated solar array, hence the mission battery is not discharged. Consequently this sequence, or any other imposing a peak load of less than 310 watts, could be sustained indefinitely during sunlight periods.

Figure 2.3-2 depicts the addition of supplementary experiment loads to the ATS-4 experiment evaluation sequence. To maintain the battery discharge at 10% or less, the maximum additional average load is limited to $(310 - 175) + \frac{38.5}{\mathcal{T}}$, where \mathcal{T} is the duration in hours (173.5 watts for $\mathcal{T} = 1$ hour). The minimum recharge period following a 10% maximum battery discharge is $\frac{1.5 \times 38.5}{135} = 0.43$ hours, assuming 67% recharge efficiency.

2.3.3 Experiment Demonstration

The highest power demand occurs during combined operation of the phased array two transmit beams and the parabolic antenna transmitters at 0.1 and 0.8 GHz. Figure 2.3-3 shows this demonstration load profile; load duration is limited to 58 minutes followed by a minimum recharge time of 26 minutes.

2.3.4 Power System Margin

From the standpoints of planning for additional experiments and for

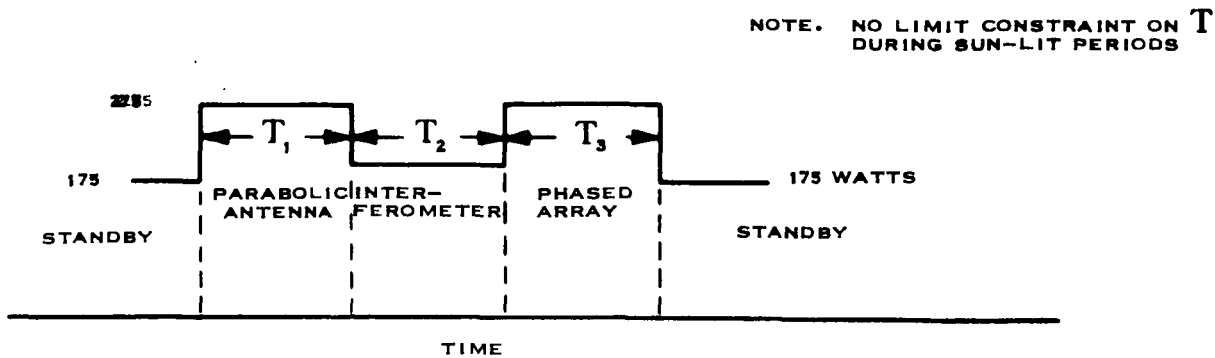


Figure 2.3-1 Typical Experiment Evaluation Power Profile²

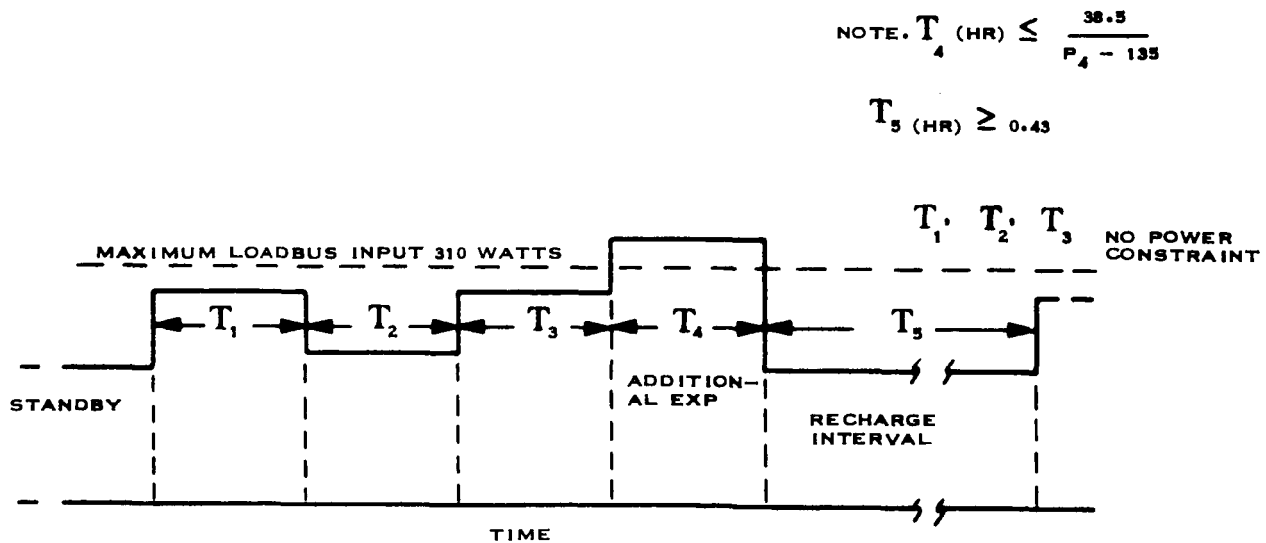


Figure 2.3-2 Power Profile with Additional Experiments

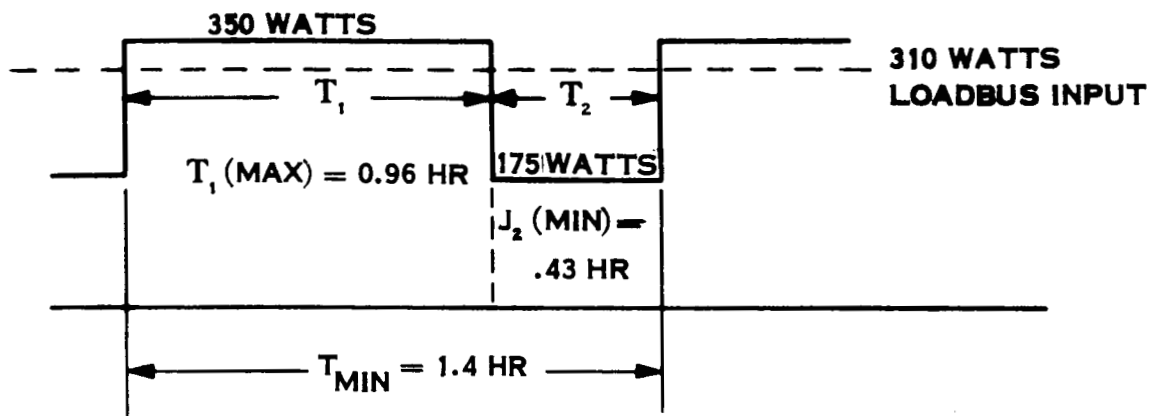


Figure 2.3-3 Experiment Demonstration
Maximum Demand Profile

defining permissible operational routines, a knowledge of the power system margin is required; i.e., excess power available over that estimated for the basic spacecraft.

The actual operating margin decreases with time as radiation effects diminish the solar array output. The fact that experiment loads are study estimates is taken into account by adding a 10% to 15% margin to the total spacecraft load for each mode to obtain the design levels. Table 2.3-1 shows the design operating margin, for each of the modes, anticipated to exist after two years of solar cell radiation degradation. Initially, the array output is 13% higher; this initial margin is indicated under the experiment demonstration column for simultaneous phased array, parabolic antenna exercise. This power is available for additional experiments early in the flight, if desired. It might also be used to power higher-power communications experiment transmitters, or to enable indefinite operation of the combined experiments.

2.3.5 Experiment Loads

Table 2.3-1 collects the various experiment loads in the operational combinations anticipated. The functional elements which comprise these loads are listed in Tables 2.3-2 through 2.3-9 with their individual standby and operate requirements.

TABLE 2.3-2 PARABOLIC ANTENNA EXPERIMENT
X-BAND

	<u>Standby</u>	<u>Operate</u>
7.3 GHz Transmitter		
1. Oscillator-Multiplier	9.7 watts	9.7 watts
2. Crystal ovens	4.0	4.0
3. Pattern test osc.	0	0.2
4. TWT amplifier	0	42.5
8.0 GHz Receiver		
1. Monopulse preamps	0.6	0.6
2. IF amplifiers	0	3.0
3. Pitch/Roll error channels	0	1.0
	14.3 watts	61.0 watts

TABLE 2.3-3 PARABOLIC ANTENNA EXPERIMENT
S-BAND

	<u>Standby</u>	<u>Operate</u>
2.3 GHz Transmitter		
1. Oscillator-Multiplier	9.7 watts	9.7 watts
2. Crystal ovens	4.0	4.0
3. PSK modulator and osc.	0	1.4
1.7/2.1 GHz Receiver		
1. RF preamplifiers	0.2	0.2
2. IF preamp. and conv.	0.2	0.2
3. IF amplifiers	0	2.0
4. Signal processor	0	1.0
	14.1 watts	18.5 watts

TABLE 2.3-4 PARABOLIC ANTENNA EXPERIMENT
0.8 & 0.1 GHz

	<u>Standby</u>	<u>Operate</u>
0.8 GHz Transmitter	0	36.0 watts
0.1 GHz Transmitter	0	18.0 watts

TABLE 2.3-5 PHASED ARRAY EXPERIMENT
X-BAND

		Operate		
		<u>Standby</u>	<u>Beam No. 1</u>	<u>Beams Nos. 1 & 2</u>
7.3 GHz Transmitter				
1.	Oscillator-Multiplier	9.7 watts	9.7 watts	9.7 watts
2.	Crystal ovens	4.0	4.0	4.0
3.	TWT amplifiers	0	42.5	85.0
8.0 GHz Receivers				
1.	Preamps (2 ea.)	0.4	0.4	0.4
2.	IF amplifiers (2 ea.)	<u>0</u>	<u>2.0</u>	<u>2.0</u>
		14.1 watts	58.6 watts	101.1 watts

TABLE 2.3-6 STABILIZATION AND CONTROL EXPERIMENT

		<u>Average</u>	<u>Peak</u>
1.	Polaris Star Tracker	4 watts	20 watts
2.	Horizon Scanner	3	6
3.	3-Axis Gyros	20	30
4.	Inertia Wheels	21	60
5.	Wheel Drive Electronics	4.5	12
6.	Reaction Jets	0.5	20
7.	SCS Controller	30	30
8.	Inverter	<u>5</u>	<u>20</u>
		88.0 watts	198 watts

TABLE 2.3-7 RADIO INTERFEROMETER EXPERIMENT

		<u>Standby</u>	<u>Operate</u>
1.	RF preamplifiers	1 watt	1 watt
2.	IF preamplifiers	2	2
3.	Sequencer	0	4
4.	IF amplifier	0	3
5.	Counter and clock	0	10
6.	Phase lock loop	0	5
7.	LO/Multiplier	0	5
8.	Programmer	0	2
9.	Coordinate resolver	<u>0</u>	<u>2</u>
		3 watts	34 watts

TABLE 2.3-8 COMMAND SUBSYSTEM

	<u>Standby</u>	<u>Operate</u>
1. Main Receiver	0.5 watt	0.5 watt
2. Redundant Receiver	0.5	0.5
3. Select Logic	0.2	0.2
4. Main Decoder	0.5	11.0
5. Redundant Decoder	0.5	11.0
	<u>2.2 watts</u>	<u>23.2 watts</u>

TABLE 2.3-9
TELEMETRY AND TRACKING TRANSPONDER SUBSYSTEM

	<u>Standby</u>	<u>Mode No. 1</u>	<u>Mode No. 2</u>
1. Main Transmitter	0.5 watt	10 watts	10 watts
2. Redundant Transmitter	0.5	0.5	0.5
3. Main Power Amplifier	0.5	0.5	35
4. Redundant PA	0.5	0.5	0.5
5. Main SCO's	0.4	0.4	0.4
6. Redundant SCO's	0.4	0.4	0.4
7. Main Encoders	1.0	14.0	14.0
8. Redundant Encoders	1.0	1.0	1.0
9. RR Transponder	4.0	7.3*	7.3*
	<u>8.8 watts</u>	<u>34.6 watts</u>	<u>69.1 watts</u>

* 15 watts operate power functions on ground command at approximately 30% duty factor to injection, 8% thereafter

2.4 ANTENNA ACCURACY CONSIDERATIONS

Antenna performance is adversely affected by mechanical inaccuracies in the antenna. Inevitably, the reflecting surface of the parabolic antenna will contain irregularities; in addition, it will deviate from the ideal by an amount dependent on structural tolerances. Further, the reflecting surface will change from its original position due to forces of acceleration and to forces generated by thermal changes. The location of the feed for the parabolic reflector is also subject to error, for the same reasons cited. Another source of errors may be in design. For example, the deployable parabolic antennas that are based on umbrella-like schemes suffer from an error caused by the fact that the reflecting sheet stretched between two radial ribs differs from the desired double curvature surface. The errors associated with the parabolic reflector antenna are classified and summarized in Figure 2.4-1.

In the following sections the various errors are discussed. The degradation of antenna gain is by far the most important effect of inaccuracies, for the ATS-4 mission. The increase in sidelobe levels caused by deviations and irregularities is not important, and consequently will not be discussed.

2.4.1 Reflecting Surface Errors

The effects of random errors in the surface of the reflector are described in statistical terms. The gain reduction with random errors is given by ⁽¹⁾:

$$\frac{G}{G_0} \simeq 1 - \frac{3 \pi^2 C^2 \delta^2}{4 \lambda^2}, \quad C < \lambda$$

(1) Hansen, R. C., Microwave Scanning Antennas, Academic Press, New York (1964), Chapter 1




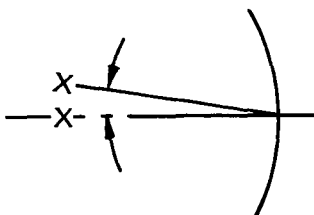
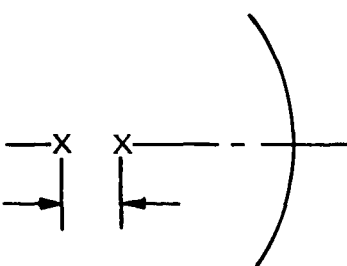
Category	Type and Typical Cause
Reflecting Surface Errors	<p>Random - Surface irregularities due to manufacturing processes and tolerances.</p> 
	<p>Systematic - Surface deformation due to thermal stresses, acceleration forces, solar pressure, and gravity gradient effects.</p> 
	<p>Periodic - Surface inaccuracies due to design or incomplete deployment.</p> 
Feed Location Errors	<p>Off-Axis - Feed location errors due to manufacturing tolerances and environmental forces.</p> 
	<p>On-Axis - Feed location errors due to manufacturing tolerances and environmental forces.</p> 

Figure 2.4-1 Classification of Parabolic Reflector Antenna Errors

Here λ is the wavelength and δ is the RMS aperture phase error. The RMS reflector error is half of δ , due to the reflection process. The correlation interval is denoted by C and is that distance, on the average, where the errors become essentially independent of one another. The antenna with a smaller correlation distance gives lower sidelobe levels than an antenna with a larger correlation distance. An error extending across a major portion of the antenna will have a greater adverse effect than an error which is localized, such as a bump or dent of greater amplitude. Continuous disturbances (e.g., gores) which extend across the antenna have large correlation distances and will have much greater adverse effects.

In Figure 2.4-2a the reduction in gain is plotted as a function of reflector deviation. If the reduction in gain must be limited to 1 db, an RMS reflector error of 0.1 inch will allow operation at all frequencies up to 10 GHz. In this example, the RMS reflector error is about one-tenth of the operating wavelength. If the surface tolerance were 0.050 inches RMS and if this error were random, with small correlation interval, Figure 2.4-2a would apply again. In this case the gain reduction at 10 GHz would be 0.3 db, and somewhat less at 8 GHz. This loss of gain is tolerable, for most applications.

At the extreme of large correlated random errors, a more severe degradation results. In reference (1), p. 78, Figure 47, a gain reduction of 1.5 db is found, for an 0.050 inch RMS error, at 10 GHz. This value applies for a correlation distance much larger than the wavelength.

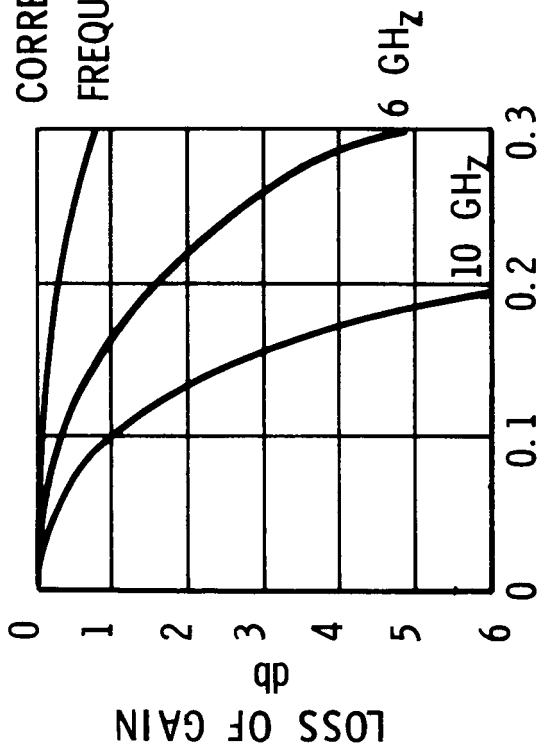
The systematic (or non-random) errors encountered in the large reflecting surface of the parabolic antenna are due to deflections caused by temperature differences in the structure. Deformations due to acceleration forces occur when attitude control jets are operating. However, as shown in Section 3.5, these deflections are negligible compared to ones of thermal origin.

For symmetrical deflections of the reflecting structure, the res-

Figure 2.4-2

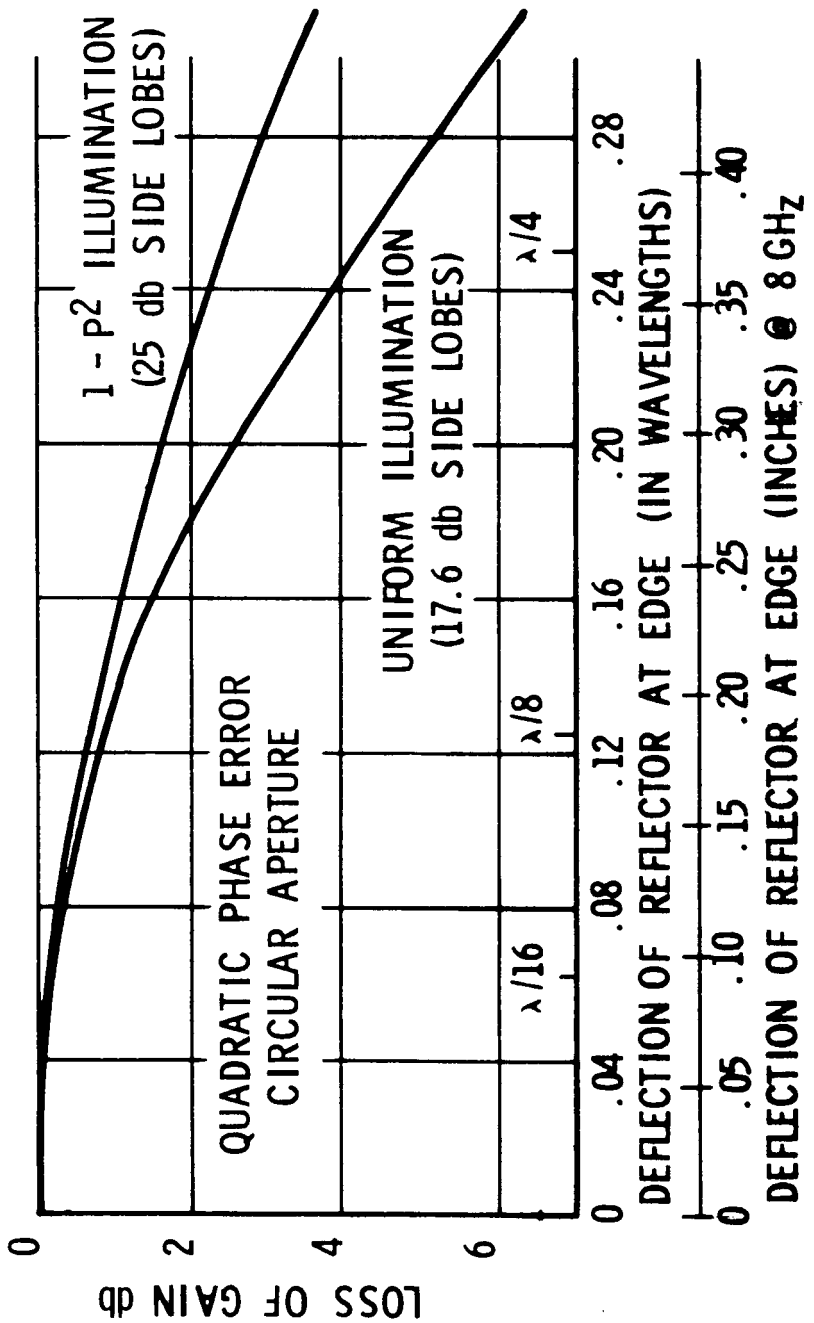
REFLECTOR ERRORS

CORRELATION INTERVAL = $\lambda/2\pi$
 FREQUENCY = 3 GHz



a)

RMS RANDOM REFLECTOR ERROR (INCHES)



b)

ulting aperture phase defect can be approximated by a quadratic curve. Two cases of aperture illumination have been considered - uniform and tapered. The uniformly illuminated circular aperture has 17.6 db sidelobes. The second type of illumination which was considered was tapered and provides 25 db sidelobes. It is, of course, somewhat less efficient aperture - wise than is the uniform aperture illumination. Figure 2.4-2b shows the reduction of gain resulting from the quadratic phase defect, for the two illumination distributions. The gain reduction is more serious for the uniformly illuminated aperture but the difference is rather small. If a degradation of gain of about 1 db is tolerable, a maximum edge deflection of somewhat over $\lambda/8$ is allowable. A deflection at the edge of $\lambda/32$ (0.05 inches at 8 GHz) causes a degradation in gain of less than 0.5 db for either tapered or uniform illumination. Sidelobe level is degraded about 3 db for the uniformly illuminated case and considerably more for the $(1-P^2)$ distribution.

The analysis of deflections due to thermal stresses is described in Section 3.6. Results from those calculations may be used in connection with Figure 2.4-2b to estimate the gain degradation.

Other systematic errors have been analyzed by Silver⁽²⁾. The linear phase error causes the beam to tilt off axis. The quadratic phase errors raise the sidelobe intensities and fill in the nulls, while at the same time reducing the gain. The cubic phase error causes a beam tilt similar to that due to the linear phase error and increases sidelobes in an asymmetrical manner.

The periodic error produces spurious beams at angles off broadside. The angular location and amplitude of the spurious beams depends on the error amplitude and spacing. The spurious beams are analogous to the

2. Silver, S., Microwave Antenna Theory and Design, McGraw-Hill New York (1949)

grating lobes of array theory; grating lobe theory thus can be applied to the analysis of the periodic error. A source of periodic errors may be traced to the design. For example, deployable parabolic antennas that are based on umbrella-like schemes suffer from an error caused by the fact that the reflecting sheet stretched between two radial ribs differs from the desired double curvature surface. This error belongs to the periodic class and can be handled analytically, at least for certain distributions. Another example of design errors is afforded by a wire mesh reflecting surface. Where one wire crosses over another, a small perturbation in reflecting surface occurs. This is another example of a regular (or periodic) error.

Linear, cubic, and periodic errors can be handled analytically (see reference 2 for details). For the ATS-4 application and reflector design, it is felt that the two types of errors graphed (random and quadratic) are sufficient for evaluation of antenna performance.

2.4.2 Feed Location Errors

The feed for the parabolic antenna is attached to the reflector by a feed mast support structure, which is made of aluminum tubes. Thermal deflections caused by temperature differences in the support structure will displace the feed from the focus. The displacement is, in general, made up of two motions - one along the antenna axis and the other orthogonal to the antenna axis. It is convenient to analyze feed location errors by considering the two motions separately. The net effect of a general feed displacement error is simply the sum of the two individual effects, at least approximately so, if the displacement error is small.

When the feed is displaced off-axis, the antenna beam is shifted off-axis, by roughly the same angle, and in a direction opposite to the feed. As a consequence, the antenna beam is pointed erroneously, and a loss of gain results. This is the major source of gain loss.

A second-order effect is the loss of gain at the beam peak, which

results when the feed is scanned off-axis. This so called scan loss is treated in Section 7.1, and is a negligible amount, for the small feed displacements under consideration here.

An approximate expression for the loss of gain resulting from an off-axis feed displacement error is given by

$$P = \frac{12 \delta^2 \lambda^2}{(F/D)^2}$$

Here P is the gain loss (db), F is the focal length, D is the antenna diameter, δ is the feed displacement error, λ is the wavelength, and β is the beam deviation factor.

In Figure 2.4-3a are shown curves of gain loss vs. displacement, for various values of the F/D ratio. An error of $\lambda/10$ causes a gain loss of 0.4 db, for F/D = 0.5. As the F/D ratio decreases, the antenna becomes more sensitive to feed location errors.

If the feed is displaced along the axis of the antenna, the resulting aperture phase error is of a quadratic nature - similar to the reflector deformation caused by thermal gradients, which was discussed in the preceding sections. The resulting defocusing of the beam causes a loss of gain, an increase in sidelobe levels, and a blurring of the pattern nulls. The beam location, however, is not moved from its original angular position. A feed location error of $\lambda/10$ causes a gain loss of about 0.4 db, for F/D = 0.3 (Figure 2.4-3b).

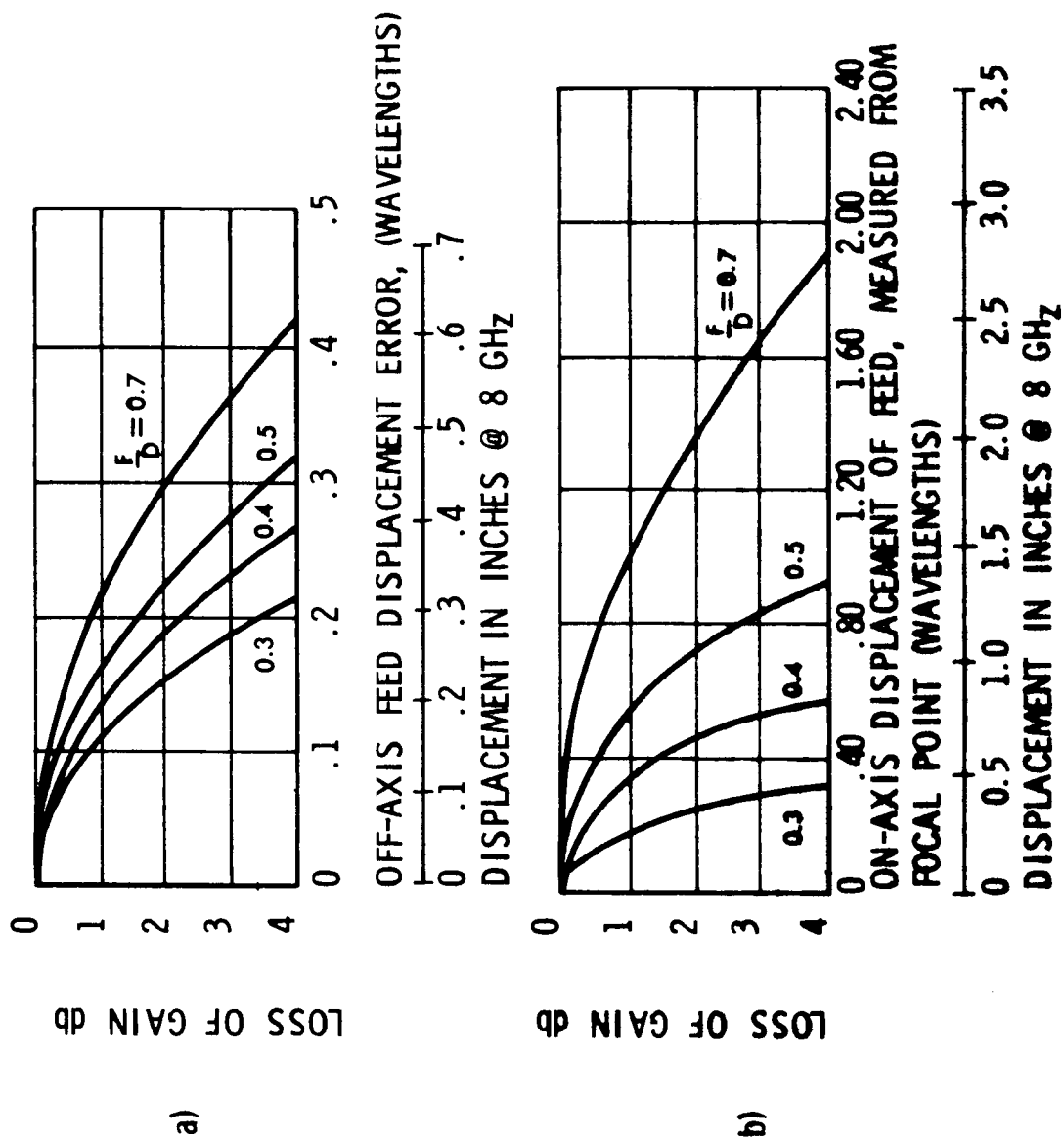
A second graph of feed displacement errors has been prepared to show in more detail the characteristics for the selected F/D ratio of 0.3. Here (Figure 2.4-4), both on-axis and off-axis errors are shown together. The sensitivity to off-axis displacements is almost twice that to on-axis errors.

2.4.3 Frequency Limitations on Gain

The various antenna errors - random, systematic, feed positional-

Figure 2.4-3

FEED LOCATION ERRORS



combine in a complicated fashion to reduce the antenna gain. An approximate equation for gain loss is arrived at by estimating the net error to be the root-sumsquare of the individual errors, thus:

$$\sigma^2 = \sigma_p^2 + \sigma_m^2$$

Here, σ^2 is the net error variance, σ_p^2 is the path-length error variance at the edge of the paraboloid, and σ_m^2 is the path-length error variance due to random type errors. The net-gain-loss will then be as follows:⁽³⁾

$$\frac{G}{G_0} = \exp \left[- \left(\frac{4 \pi \sigma}{\lambda} \right)^2 \right]$$

where λ is the operating wavelength and G_0 is the gain in the absence of errors. This equation is not exact, but it may be used to illustrate the frequency limitations on gain. Curves of gain vs. frequency have been calculated from the above equation and the results are shown in Figure 2.4-5. The increase in gain is proportional to the square of the wavelength, at low frequencies. As the frequency increases, the exponential term begins to dominate and eventually the gain peaks and then drops. The peak gain is inversely proportional to $(\sigma/D)^2$, where D is the diameter of the antenna.

The errors for the 30-foot diameter case are tabulated in Table 2.4-1. Errors for the other diameters have been scaled, by the ratio of the diameters, to arrive at the values of tolerances indicated in Figure 2.4-5.

The curves show that the largest antenna (35 feet in diameter) has the smallest gain, at 8 GHz. At lower frequencies, however, the larger gain characteristic of the larger antenna is realized.

2.4.4 Summary of Antenna Error Effects

The tolerances for the recommended parabolic antenna configuration

(3) Potter, P.D., Merrick, W.D., and Ludwig, A.C., "Big Antenna Systems for Deep Space Communications," Astronautics & Aeronautics, Oct., 1966, p. 86.

of diameter 30 feet, are summarized for ready reference in Table 2.4-1. Justification for the tabulated values are found elsewhere in this report.

TABLE 2.4-1 SUMMARY OF ANTENNA ERROR EFFECTS

Source of Loss	Amount of Error (inches)	X	S	Gain Loss (db)	
				800MHz	100MHz
Reflector Deviations					
Random	0.060 (RMS)	0.4	0.1	0	0
Thermal	±0.070 at tip	0.1	0.0	0	0
Feed Location Errors					
On-axis	±0.15	0.3	0.0	0	0
Off-axis	±0.10	0.5	0.1	0	0

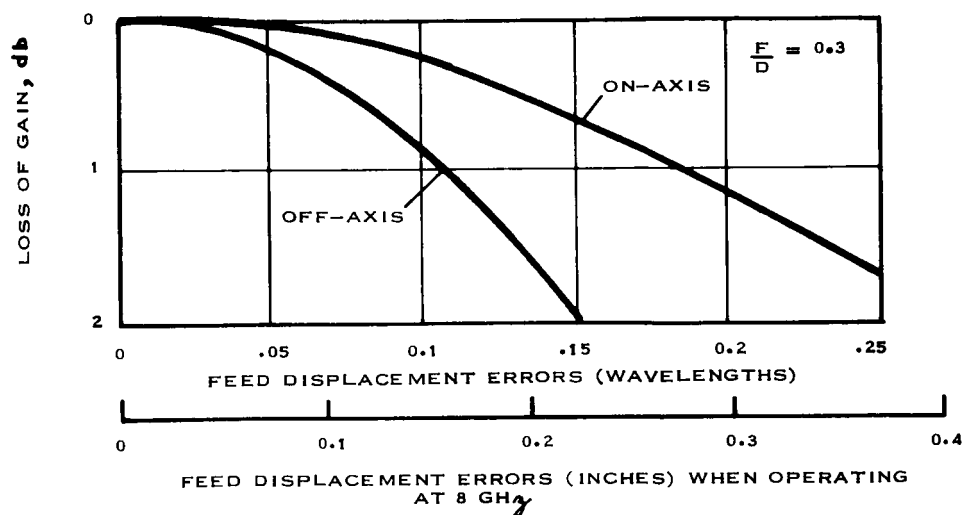


Figure 2.4-4 Feed Location Errors ($F/D = 0.3$)

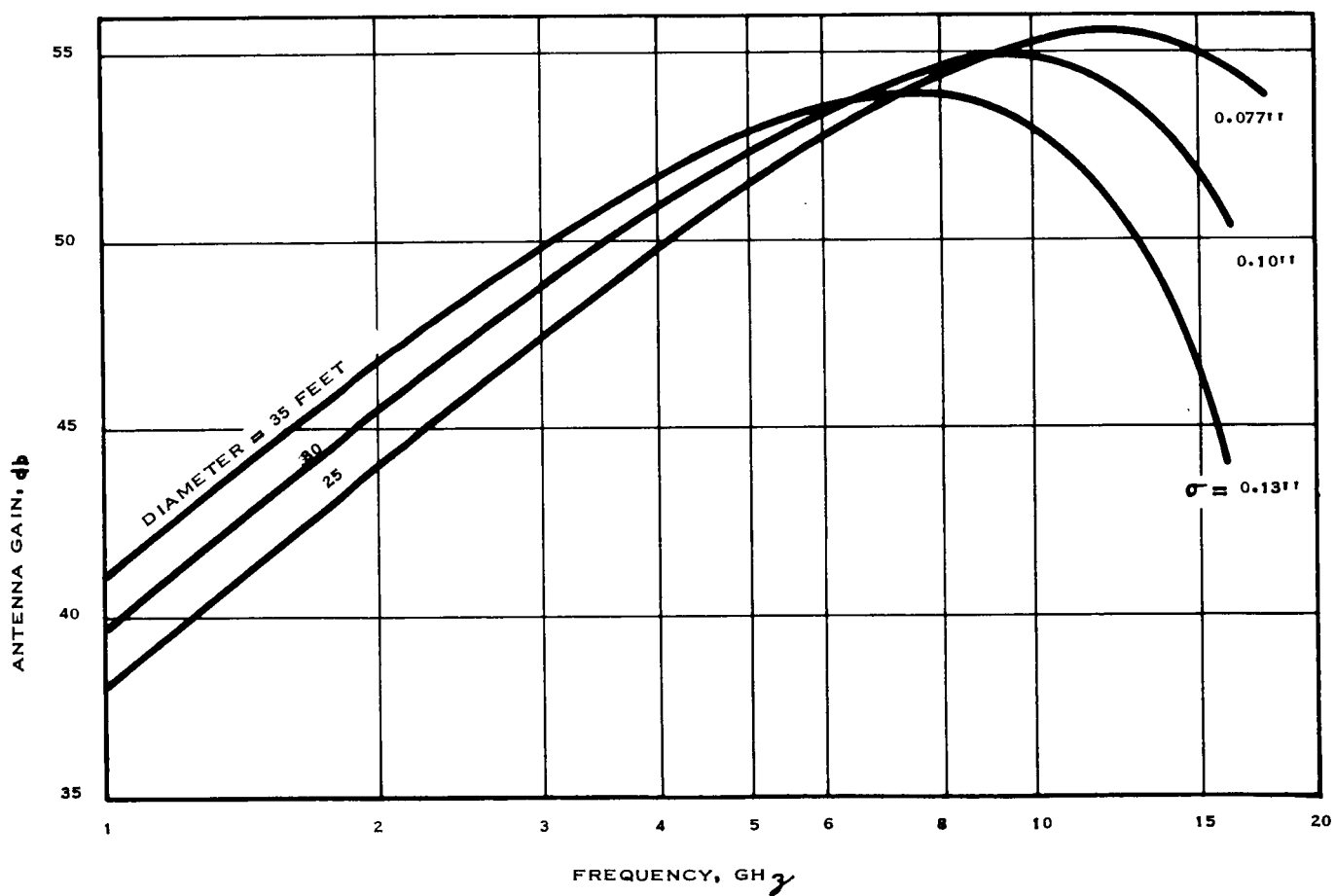


Figure 2.4-5 Frequency Limitation on Gain

2.5 ANTENNA EFFICIENCIES

2.5.1 Parabolic Antenna

The following items contribute to the losses which are inherent to parabolic antennas:

- Aperture taper
- Spillover
- Spacecraft blockage
- Support mast blockage
- Feed phase error
- Polarization
- Systematic reflector distortion
- Random reflector distortion
- Feed axial displacement error
- Feed lateral displacement error
- Reflector and feed dissipation loss
- Feed reflection loss

The aperture taper of the paraboloid depends upon the feed pattern and the F/D ratio. A deviation from a constant field distribution across the aperture results in a loss of gain.

Spillover loss is that energy radiated by the feed which is not collimated by the reflector. Since a feed cannot be designed to have a truncated pattern (no spillover loss) there is a trade-off between the spillover loss and the aperture taper loss. A 10 db aperture taper has been found to give the best compromise between the two.

Since the spacecraft electronics compartment is located in the aperture of the paraboloid, it contributes to the degradation by blocking a portion of the radiating aperture. This loss can be estimated by considering the blocking member to be a radiation which is 180° out of phase to the

reflector signals. The gain loss is then given by

$$\eta_b = 20 \log \left\{ \frac{1 - \int_0^b [A + B(1 - \rho^2)^p] \rho d\rho}{\int_0^1 [A + B(1 - \rho^2)^p] \rho d\rho} \right\} \quad (1)$$

where A, B and p are constants describing the aperture distribution, b is the blockage ratio and ρ is the normalized radius of the paraboloid. At X-band, A, B and p are respectively 0.4, 0.6 and 1.5. The gain degradation is then

$$20 \log (1 - 1.82 b^2 + .82 b^4). \quad (2)$$

Figure 2.5-1 indicates the effect on the X-band pattern.

The feed support mast contributes to the blockage loss as does the spacecraft. The support mast, however, also affects the primary feed pattern. Since the combined effect of altering the feed pattern and blocking the aperture is impractical to calculate, a test evaluation was performed. Preliminary measurements of a scale model of the tripod support have been performed and are described in Section 7. Gain losses ranging between 1.0 and 2.5 db were measured.

Feed phase error occurs when the feed is anything other than the hypothetical "point source." Phase errors are in general very hard to estimate so that measurement techniques must be used.

Polarization losses are contributed by the feed and reflector. For a dipole-type feed the reflector polarization loss is given by P. D. Potter¹ as

$$\eta_p = 10 \log \left(1 - \frac{\psi^4}{96} \right) \quad (3)$$

where ψ is one half of the included angle of the paraboloid. Polarization losses caused by the feed depend upon the polarization required. The

¹ Potter, P. D., JPL Technical Report 32-149, 1960

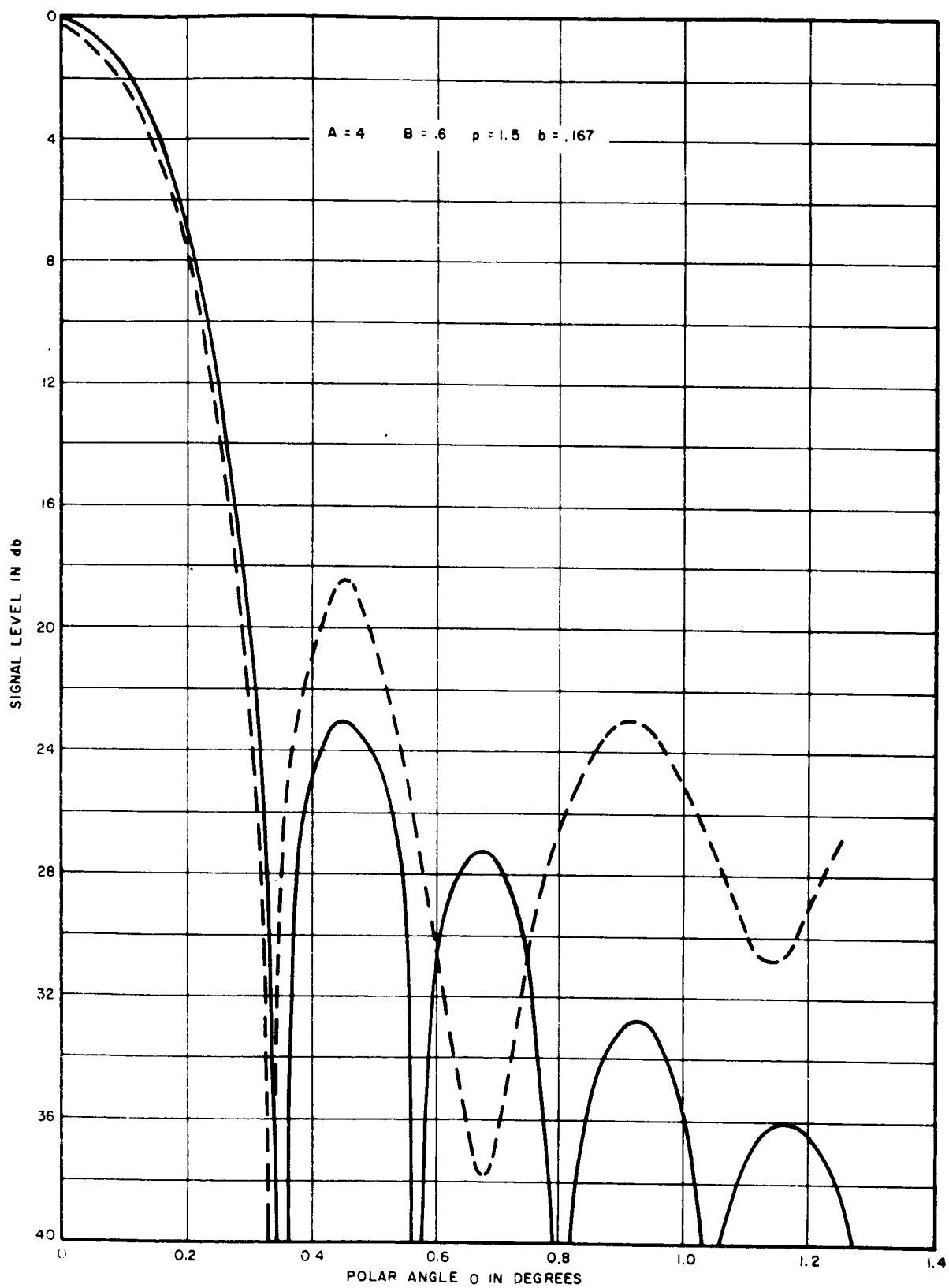


Figure 2.5-1 X-Band Radiation Pattern

greatest loss will occur in the 100 and 800 MHz bands where the feeds are circularly polarized. These feeds have patterns which are circularly polarized only on-axis, and become elliptically polarized off-axis.

Systematic reflector distortions caused by thermal gradients and random reflector distortion caused by manufacturing errors change the aperture phase distribution. This results in a loss of gain because the differential elements of aperture area do not radiate in phase.

Feed positioning is critical with respect to gain loss especially in systems using small F/D ratios. Lateral feed displacement results in linear and cubic phase errors. The linear component causes an undistorted beam shift, equal to the feed squint. The cubic component, which is known as primary coma, causes a loss in gain and a beam shift in a direction opposite to the linear component. Axial displacement of the feed causes a quadratic phase error. This also results in loss of gain. These effects were discussed in the preceding section.

Reflector and feed dissipation losses are a result of their construction from materials of finite conductivity. Dissipation losses in large reflector systems generally run about 2% (0.1 db).

Feed impedance mismatch causes a reflection loss. For a VSWR of 1.5:1 the loss is about 0.2 db.

All gain losses are summarized in Table 2.5-1. In the cases where the gain degradation cannot be calculated, and has not been measured, an estimate is given. The efficiency of the parabolic antenna ranges from a low value of 22% at 100 MHz to a high value of 43% at S-band.

2.5.2 Phased Array Figures of Merit

- Introduction A variety of array techniques have been singled out for study and analysis under this program. These include the transdirective array, the Butler matrix array, the space fed (lens) array and the corporate

TABLE 2.5-1 PARABOLIC ANTENNA EFFICIENCIES

LOSS CONTRIBUTOR	X	S	800 MHz	100 MHz
Aperture Taper and Spillover	1.0 db	1.2 db	1.5 db	3.0 db *
Spacecraft Blockage	.4	.4	.4	.4
Support Mast Blockage	1.4	1.25	2.25	2.5 *
Systematic Reflector Distortion	.1	0	0	0
Random Reflector Distortion	.4	.1	0	0
Feed Lateral ** Displacement	.5	.1	0	0
Feed Axial Displacement	.3	0	0	0
Feed Phase Error *	.3	.3	.4	.4
Polarization	.05	.05	.05	.05
Dissipation	.1	.1	.1	.1
Reflection	.2	.2	.2	.2
TOTAL	4.75 (1) 4.25 (2)	3.7 db	4.9 db	6.65 db
Efficiency	33 % (1) 38 % (2)	43 %	32 %	22 %

(1) without monopulse
* estimated

(2) with monopulse
** zero loss when monopulse
system is in operation

series fed array. In order to establish a rationale for a meaningful comparison of these prime candidates, a tentative design has been generated for each, with a set of least common denominators that are fundamental to the mission requirements.

- Differences in Systems Affecting Figures of Merit The Butler matrix, space-fed and corporate-fed arrays have certain hardware similarities, viz, each uses a single antenna, four sets of phase shifters, two transmitters, two receivers, and a beam steering unit commanded by a coded signal from a single terminal station. On the other hand the transdirective array requires two separate antennas, one for transmit frequencies and one for receive frequencies. Element spacing for each of the two sets of frequencies is critical for accurate use of the self phasing technique. The system requires a chain of frequency converters for signal processing and phasing. It has, essentially, a separate receiver for each element of the receive antenna. Two transmitters (RF amplifiers) are also required. The beam steering mechanism is an integral part of the circuitry. It is commanded by a CW signal originating from each of the terminal points using the relay link.

In order to compare the transdirective array with the other three types of arrays the following parameters were assumed identical for all four systems.

- | | | |
|---------------------|---------------|---------|
| <u>Antenna Gain</u> | Receive mode | 36.6 db |
| | Transmit mode | 35.9 db |

Note 1 - This does not include any system losses and represents the directivity of a 64 element array.

Note 2 - Since the transdirective array requires two separate antennas, both may be optimized. Thus, an average gain of 36.3 db will be used for both the transmit and receive cases. This

assumes an average aperture size equal to the single aperture required by the other three systems.

- Transmitter Output 10 watts average

All systems use two TWT amplifiers, one for each transmit channel.

- Receiver Noise Figure 8.5 db

Note 1 - The transdirective array requires 64 separate, wide-band, mixer-preamplifier front ends. Although the use of 64 tunnel diode amplifiers could enhance the noise figure by as much as 2.5 db, their addition to the system at this time or in the near future appears to be prohibitively complex. A low level of confidence in the achievement of reasonable levels of stability, gain and phase tracking among 64 preselector-TDA combinations does not warrant their consideration in a system that demands very high levels of reliability.

Note 2 - In the remaining systems only two narrow-band receive channels are required. Since gain and phase tracking are not criteria (each channel is independent) TDA's will be assumed for a 2.5 db receiver noise figure enhancement.

- Bandwidth

All four candidate systems will be assumed to have the same RF and IF information bandwidth.

In addition to the above parameters which are used to calculate the figure of merit of the systems, the factors which most affect system performance are losses and weight.

The most serious limitations in the ERP of the transdirective array technique is the high conversion loss (-11.5 db) associated with the wide band output mixer. It is possible that the use of varactor diode up-converters could improve this loss by 2 to 3 db without a serious degradation in phase tracking between units. Since development effort in this area has been limited to very narrow RF bandwidths and small temperature excursions, it would not be safe to assume more than a 1.5 db improvement in the near future. Thus, a projected figure of -10 db will be used.

System weights are based upon currently available hardware. The weight of the transdirective array is obtained from Reference 1. The Butler matrix, space fed and corporate-fed arrays include weight allowances for beam steering units. These weight estimates are based upon the following conditions.

- All beam steering computations will be made by a ground terminal computer. This maximizes programming flexibility, minimizes on-board electronics and requires a data rate in most modes of operation of less than 12 bits per second.

- Command signals are received aboard the spacecraft via reception equipment that exists for use by other subsystems. Thus the weight of this time and/or bandwidth shared command receiver, cannot be totally associated with the overall weight of the phased array.

The Transmit Mode Figure of Merit (Table 2.5-2) The transmitter figure of merit has been calculated by taking the antenna gain on transmit (A), subtracting the loss (B), between the transmitter and the antenna, multiplying it by a transmitter output of 10 watts and dividing the result by the

Reference 1.- "Design Review Report for High Gain, Self Steering Antenna Systems," March 1966, Contract NAS5-10101, Report P66-68, Hughes Aircraft Company

TABLE 2.5-2 ARRAY FIGURE OF MERIT - TRANSMIT

Figure of Merit (Transmit) = $\frac{10 \text{ watts}}{C (\text{System Weight})} \times \text{Antilog (A-B)}$				
	Transmit Antenna Gain (A)	Transmit System Losses (B)	System Weight (C)	Figure of Merit ERP (watts/lb)
Transdirective Array	36.3 db ⁽¹⁾	13.8 db ⁽²⁾	120 lbs	14.8 ⁽⁴⁾
Butler Matrix Array	35.9	9.5	188	23.2 ⁽⁵⁾
Space Fed (lens) Array	35.9	4.0 ⁽³⁾	169	91.8 ⁽⁵⁾
Corporate Fed Array	35.9	2.5	166	131.5 ⁽⁵⁾
<p>(1) Includes antenna gain optimization of 0.4 db.</p> <p>(2) Includes projected loss reduction of 1.5 db.</p> <p>(3) Includes amplitude taper and spillover losses.</p> <p>(4) Total RF power out is limited to 50-100 milliwatts per radiating element due to varactor upconverter saturation.</p> <p>(5) Total RF power output is limited only by the availability of TWT's and total DC power available.</p>				

estimated system weight (C). This number is expressed as ERP per unit weight (watts/pound).

Receive Mode Figure of Merit The receive mode figure of merit is a means of rating the performance of the respective systems. It is expressed as the signal-to-noise ratio for one cycle of bandwidth per unit system weight (see Table 2.5-3). Calculations were made by assuming a source (terminal) ERP of + 60 dbm and a space loss of 202 db. (No fade margin nor atmospheric losses were assumed.) To this resulting number (-142 dbm) the antenna gain (A) is added and the system losses (B) from the antenna terminals to the input of the receiver are subtracted. The output noise power per cycle (in db) is subtracted from the total power into the receiver, and the resulting number divided by the system weight. The noise figure of the basic mixer is assumed to be 8.5 db. Expressed as an equation, the receive mode figure of merit is written as:

$$\frac{S}{N} \frac{\text{db for 1 cycle}}{\text{weight}} = \frac{\text{ERP} - \text{SL} + \text{A} - \text{B} - \left(\frac{\text{K T} - \text{N F}}{\text{cycle}} \right)}{\text{weight}}$$

In the last column of the table, the signal power (per unit weight) received in the spacecraft is listed. It was calculated from the following:

$$\frac{S}{W}, \text{ power per unit weight} = \frac{\text{ERP} - \text{SL} + \text{A} - \text{B}}{\text{weight}}$$

Conclusions - The most significant data in the above tables illustrates that the corporate-fed system delivers the greatest ERP per unit weight and the transdirective array has the highest signal-to-noise ratio per unit weight (for a 1 cps bandwidth). Comparing just these two systems, it is seen that for the transmit mode (down-link) the corporate-fed array has almost 10 db/lb. greater ERP than the transdirective array whereas in the receive mode (up-link) the transdirective array has 0.123 db/pound greater signal-to-noise ratio than the corporate-fed array.

TABLE 2.5-3 ARRAY FIGURE OF MERIT - RECEIVE

	Antenna Receive Gain A	Receive System Losses Before Receiver B	Receiver Noise Figure N.F.	Weight C	Receive Figure of Merit	
					S N db for 1 cy. lb.	Watts lb.
Transdirective	36.3 db	1.8 db	8.5 db	120 lbs.	.483	137×10^{-18}
Butler Matrix	36.6	9.5	6.0 ⁽²⁾	188	.273 ⁽³⁾	27.6×10^{-18} (4)
Space Fed	36.6	4.5 ⁽¹⁾	6.0 ⁽²⁾	169	.356 ⁽³⁾	88×10^{-18} (4)
Corporate Fed	36.6	3.0	6.0 ⁽²⁾	166	.360 ⁽³⁾	11×10^{-18} (4)

1. Includes illumination taper and spillover losses.
2. Includes 2.5 db tunnel diode amplifier enhancement of noise figure which is not considered practical for the transdirective system.
3. As a short term projection, the use of non-cooled parametric amplifiers in each of the two channels could enhance these numbers by an additional 1-1.5 db in the Butler matrix, space fed and corporate fed arrays.
4. Upgraded 2 db because of improved receiver noise figure (compared to transdirective noise figure).

Since all satellite communications systems are down-link limited because of the restriction of DC power availability, the 10 db/pound transmit superiority of the corporate-fed array far outweigh the (S/N)/pound receive advantage of the transdirective approach.

This has been one of the key factors in selecting the corporate-fed array as the prime choice for the ATS-4 mission application.

2.6 FAILURE MODES

2.6.1 System Considerations

The ATS-4 spacecraft is designed for a two year life. However, since lifetime predictions are probabilistic in nature, the possibility of failures still exists. In this section some of the failure modes will be discussed and their impact on the spacecraft operation estimated.

To maximize operational reliability, some systems aboard ATS-4 have redundancy built into them. An example is the telemetry system which consists of two transmitters and two commutators, one each in a standby mode. By switching between the transmitters and the commutators, full operational capability can be maintained even if one should fail. Another example is the attitude sensing system which has completely redundant elements. The torquing subsystem has redundant nozzles and, in the event of reaction wheel failure, limited operation is possible with the thrusters.

Table 2.6-1 shows some of the ATS-4 subsystems failure modes and back-up provisions. Occurrence of any subsystem failure does not preclude a useful mission. For the recommended design concepts, failure of one subsystem or experiment does not result in a loss of the other experiments.

2.6.2 Parabolic Antenna

The most serious failure is non or incomplete deployment of the reflector. To guard against this possibility a redundant deployment motor is incorporated, backing up the spring extension system. In addition, the hinging arrangement insures extension of all petals by positive contact if the deployment synchronizer should fail or if one petal should jam during extension.

The inter-petal locks are primarily used to achieve an accurate reflector surface contour. The ring continuity that they provide is not used in the dynamic analysis to determine the petal natural frequencies in orbit. Con-

TABLE 2.6-1. FAILURE MODES AND BACK-UP PROVISIONS

Subsystem	Failure Mode	Back-up Provisions
Structure	Antenna reflector fails to deploy.	Redundant deployment motor
Auxiliary propulsion system	Jet failure: failure to open or failure to close	Only drift would result - not fatal
Attitude reference system.	Sensor failure.	Redundancy of sensors: the interferometer experiment can be complete back-up for ARS; gyros back up sensors.
Attitude control system	Wheel failure.	Jet thrusters, but with degraded accuracy and limited life.
Power	Battery failure, load switch failure	Redundancy; the power system has 100% redundancy.
Interferometer	Electronics failure	Some elements of the phased array may be used as back-up.
Phased array	Phase shifters	Update beam steering computer by ground command
Communications Equipment	Transponders	Redundancy and switching capability
Instrumentation	Electronics Failure	Telemetry and command system have 100% redundancy

sequently, the failure of one or more locks to function will not have a disastrous effect on reflector performance. The effect of no radial growth capability of adjacent petals (sticky lock) has been analyzed and the resultant thermal distortion is small. (0.14 inch maximum compared to .070 inches under normal conditions)

The failure of a hinge lock to function is not serious if a sufficient number of inter-petal locks function properly. This lock only serves to stop petal rotation about the hinge line. This degree of freedom is eliminated by the interpetal lock since the hinge lines are skewed relative to the plane of the reflector.

In the event of a deployment failure the mission can still be a partial success by the operation of the phased array and interferometer if the apogee injection motor is jettisoned properly. The basic sensors will be unobscured and stabilization is actually enhanced by a more favorable gravity gradient configuration. Difficulty will arise in the operation of the partially obscured reaction jets. Reduced power output will be available from the partially obscured and improperly oriented solar panels.

2.6.3 Stabilization and Control System

Torquers

In event the reaction wheels fail, operation can be continued at a reduced pointing accuracy (but sufficient for S Band operation) using the reaction jets with the logic and switching circuits employed during acquisition. This reduced pointing accuracy will be 0.3° in pitch and roll and 0.50° in yaw. The resulting system is shown in Figure 2.6-1. The limit cycle rate is the key quantity determining the jet "on" time and in conjunction with the dead zone and compensation time constants determines the jet "off" time. These two time intervals will determine the duty cycle and thus the gas consumption rate. The limit cycle may be expressed as follows:

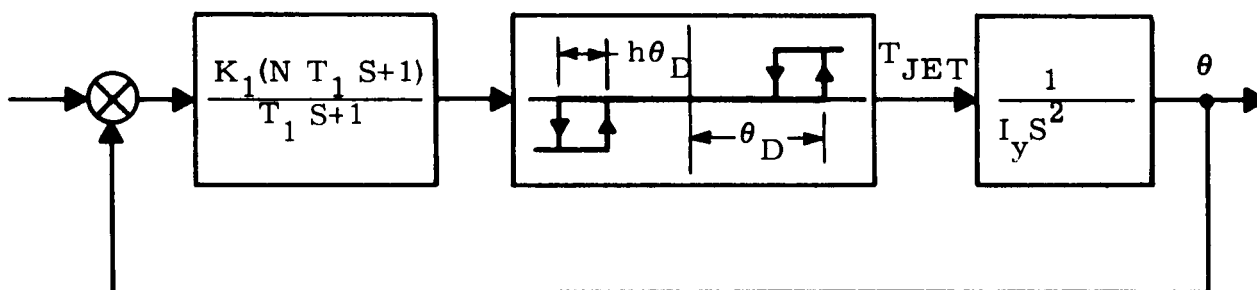


Figure 2.6-1 Failed Reaction Wheel Backup Control Subsystem

$$\theta_{LC} = \frac{h\theta_D + \lambda_o (N-1) T_1 T_R - \lambda_o \frac{T_R^2}{2} + \lambda_o (N-1) T_1^2 \left(1 - e^{-\frac{t_o}{T_1}}\right)}{2 \left[(N-1) T_1 - \frac{T_A + T_R}{2} \right]}$$

where:

- h = Hysteresis of level sensing (.05)
- θ_D = Level sensing ($\pm 0.1^\circ$ roll and pitch, $\pm 0.2^\circ$ yaw)
- λ_o = Angular acceration ($0.002^\circ/\text{sec}^2$ roll)
 $(0.0035^\circ/\text{sec}^2$ pitch)
 $(0.00257^\circ/\text{sec}^2$, yaw)
- N = Ratio of lead to lag time constants (10)
- T_1 = Lead network time constant (1 sec)
- T_A = Time delay in jet thrust application (0.1 seconds)
- T_R = Time delay in jet thrust removal (0.2 seconds)
- K_1 = Gain of lead network (1.0)
- t_o = $\frac{2\dot{\theta}_{LC}}{\lambda_o} - T_R$ Elapsed time from jet thrust application
to commanded removal

The initial calculation is made assuming $e^{-\frac{t_o}{T_1}} = 0$. For the roll axis, the first limit cycle rate is found to be 0.001443 degrees/sec. The value of t_o is calculated from:

$$t_o = \frac{2\dot{\theta}_{LC}}{\lambda_o} - T_R = \frac{2(.001443)}{.002} - 0.2 = 1.24 \text{ seconds}$$

Using this time $e^{-\frac{t_o}{T_1}}$ is calculated:

$$e^{-\frac{t_o}{T_1}} = e^{-1.24} = 0.29$$

This value is now used to calculate a new limit cycle rate ($\dot{\theta}_{LC}$). This iteration process is continued until successive evaluations of $e^{-\frac{t_o}{T_1}}$ show little change. Using this technique, the resulting limit cycle rates are found to be:

$$\begin{aligned}\text{Roll} & - 0.0011^{\circ}/\text{sec} \\ \text{Pitch} & - 0.00154^{\circ}/\text{sec} \\ \text{Yaw} & - 0.00172^{\circ}/\text{sec}\end{aligned}$$

The rate increment provided by the jets at each firing is twice the limit cycle rate. The momentum imparted to the vehicle per cycle in each axis is:

$$\begin{aligned}\text{Roll} & - (2)(2) \frac{(0.0011)(2150)}{57.3} = 0.165 \frac{\text{ft lb sec}}{\text{cycle}} \\ \text{Pitch} & - (2)(2) \frac{(0.00154)(1226)}{57.3} = 0.132 \frac{\text{ft lb sec}}{\text{cycle}} \\ \text{Yaw} & - (2)(2) \frac{(0.00182)(1677)}{57.3} = 0.213 \frac{\text{ft lb sec}}{\text{cycle}}\end{aligned}$$

The cycle time is:

$$\begin{aligned}\text{Roll} & - 366 \text{ seconds} \\ \text{Pitch} & - 262 \text{ seconds} \\ \text{Yaw} & - 443 \text{ seconds}\end{aligned}$$

This results in an average use of momentum capability which is stored in the gas system of:

$$\begin{aligned}\text{Roll} & - \frac{(24)(3600)}{366} \times 0.165 = 38.9 \text{ ft lb sec/day} \\ \text{Pitch} & - \frac{(24)(3600)}{262} \times 0.132 = 43.6 \text{ ft lb sec/day} \\ \text{Yaw} & - \frac{(24)(3600)}{443} \times 0.213 = 41.5 \text{ ft lb sec/day}\end{aligned}$$

In addition to the limit cycle, gas will be used to hold vehicle attitude in presence of the cyclic disturbance torques (normally stored by the wheels) and the average

value of disturbance torques. These are:

Roll (cyclic)	-	3.44 ft lb sec/day
Roll (average)	-	3.45 ft lb sec/day
Pitch (cyclic)	-	9.8 ft lb sec/day
Pitch (average)	-	0.82 ft lb sec/day
Yaw (cyclic)	-	2.16 ft lb sec/day

If all wheels failed at the beginning of the mission and control by reaction jets is used, the days of operation can be found by dividing total gas storage capability (9849 ft lb sec) by the sum of the average use listed above. This is:

$$\frac{9849}{144} = 68.4 \text{ days}$$

If only one wheel should fail, operation may be continued for a longer period. Further, if the auxiliary propulsion system fuel is diverted for the reaction jet system, operation can be extended further. The time of operation on jets only is dependent upon the amount of gas remaining at the time of failure.

Horizon Scanner and Gyro Reference Unit - The redundant horizon scanner is backed up with the gyro reference unit as a means of maneuvering the vehicle from one offset point to another or for satellite tracking acquisition. Conversely the horizon scanner may be used in place of the gyro reference unit in some maneuvers. The gyro unit is to be used for vehicle attitude monitor while performing antenna pattern measurements out to $\pm 15^\circ$ from a particular ground station.

Star Tracker - Failure of the star tracker and its redundant unit result in loss of an accurate yaw reference. Back-up means of yaw reference is provided by the yaw gyro with periodic updating via the interferometer. In this failure mode, yaw pointing accuracy is based on the drift rate of the gyro ($0.1^\circ/\text{hr}$, 3σ , stable to $0.01^\circ/\text{hr}$) and the update performance of the interferometer (0.05°). Further failure of the yaw gyro results in direct inter-

ferometer command control, limited to data rate and vehicle drift between commands.

Controller - Failure of the controller results in loss of capability to diagnose the failure and switch to the redundant controller elements. Ground monitor of controller input and output permits the ground station to perform redundancy switching within the controller itself. In the event that both the primary and the redundant controller have similarly failed assemblies, there may be the possibility of limited operation. Loss of acquisition logic, diagnostic logic, or monitor assemblies would continue to permit limited operation. Failure of the autopilot control drive electronics, however, results in loss of wheel or jet drive command capability. Therefore this critical link will require significant reliability and redundancy study.

2.6.4 Phased Array

The freedom of a phased array antenna from massive failure depends upon the degree of independence between elements designed into the system. Single component failures cause no more than slight deterioration in performance. In the phased array system being recommended for this mission, several factors contribute toward simplifying the problem of failure backup:

- Much of the logic is performed at the ground station rather than in the satellite. Thus maintenance is readily available.
- Driver circuits operating the phase shifters are independent, resulting in graceful degradation.
- Branch RF feed networks use matched and isolated tee junctions, which minimize the mismatch effect of one RF failure upon other elements.

It is conceivable that a failure could occur in an RF component, which could be compensated for by the proper settings of the electronic phase shifters. Certain failures of finite phase shifters, power dividers, adapters, and radiating elements could be corrected (at least partially) by the failure analyzing mode. In order to permit this up-dating of the phase shifter settings, an element failure analyzing mode will be built into the beam steering system. The system will contain a core memory circuit whose capacity is the phase shifter settings for 8 beams, a total of 1536 bits. Associated with this memory are the necessary logic circuits for consecutively cycling the contents of this storage through the phase shifter drive register, and an oscillator for timing the cycling.

In order to test an element, the memory is supplied with 8 sets of phase shifter settings for a broadside beam. All settings are identical except for the phase shifter associated with the element under test. In each of the sets of data, the phase shifter of the test element is in a different one of its 8 states. When the data in this memory is cycled through the phase shifters, the phase of all elements in the array with the exception of the test element, remain fixed. The test element is cycled through its phase states in rotational order, so that a quantized sine wave amplitude modulation is introduced into the RF carrier along with a small phase modulation. Its amplitude ideally will be about 0.2 db, since it represents a rotating vector of unit length adding to a stationary vector 63 units long. With controlled timing of the data cycling from the ground, the effective phase of the test element may be determined. This can be compared to the ground-computed nominal phase shift setting.

The data link system is used to carry the phase shifter data which is stored in the core memory. After the testing of one element

is completed, the memory is blanked, and the settings for testing the next element are loaded into the memory unit. The data link channel also carries the signal which starts and stops the cycling oscillator.

Should an analysis of all elements in the array indicate that a failure which changes the phase of an element had occurred, the beam steering computer is supplied with the proper modifications to optimize array phasing.

The technique described above has been successfully utilized in the self-testing circuitry of the Sperry "HAPDAR" phased array antenna. More than 2000 elements are automatically tested in less than 1 hour, and the element phase accuracy measured to within 5° .

2.6.5 Antenna Experiment Electronics

A preliminary reliability study indicates a 0.98 reliability of the antenna experiment electronics, including the monopulse receiver, for the two year life of the ATS-4 mission. This reliability figure is based on operating 3 hours per day and includes selected redundancy. To discuss the failure modes and back up operation, the electronics equipment is divided into 5 groups.

- X-band monopulse receiver
- X-band reflector crossband relay with 100 MC output
- X-band phased array relay with 800 MC output

- S-band relay
- Frequency generator

The monopulse receiver error channels will be equipped with redundant standby modules to be switched in by command. (Communications system block diagram, Figure 2.6-2.) The sum channel, similarly equipped with redundant modules, can be replaced via ground control switching by employing one of the phased array channels. This extra precaution is added because the sum channel has more functions to perform.

The sum channel, besides being part of the monopulse system, will also receive and transpose the FM signal to transmit on 100 MHz and voice links to transmit on 7.3 GHz. The A beam of the phased array will receive and transpose the TV signal for transmission on 800 MHz, and a voice link for transmission on 7.3 GHz. The B beam of the phased array will receive and transpose a voice link to a transmission frequency of 7.3 GHz.

Modular redundancy will be the same within each of the transponder channels, except for the TWT. One, possibly two, standby TWT's will be available to switch into the output of any of the three X-Band transmitters.

Thus, the X-band transponder, which includes the sum channel of the monopulse receiver, and is the most active of the three, can be replaced by either of the phased array channels equipment. The two phased array channels are redundant to each other.

The 800 MHz linear amplifier will be redundant and can be attached to either the A beam channel or the B beam channel receivers of the phased array. Similarly, the 100 MHz chain will be redundant but will remain connected to the sum channel position though the channel equipment is switched.

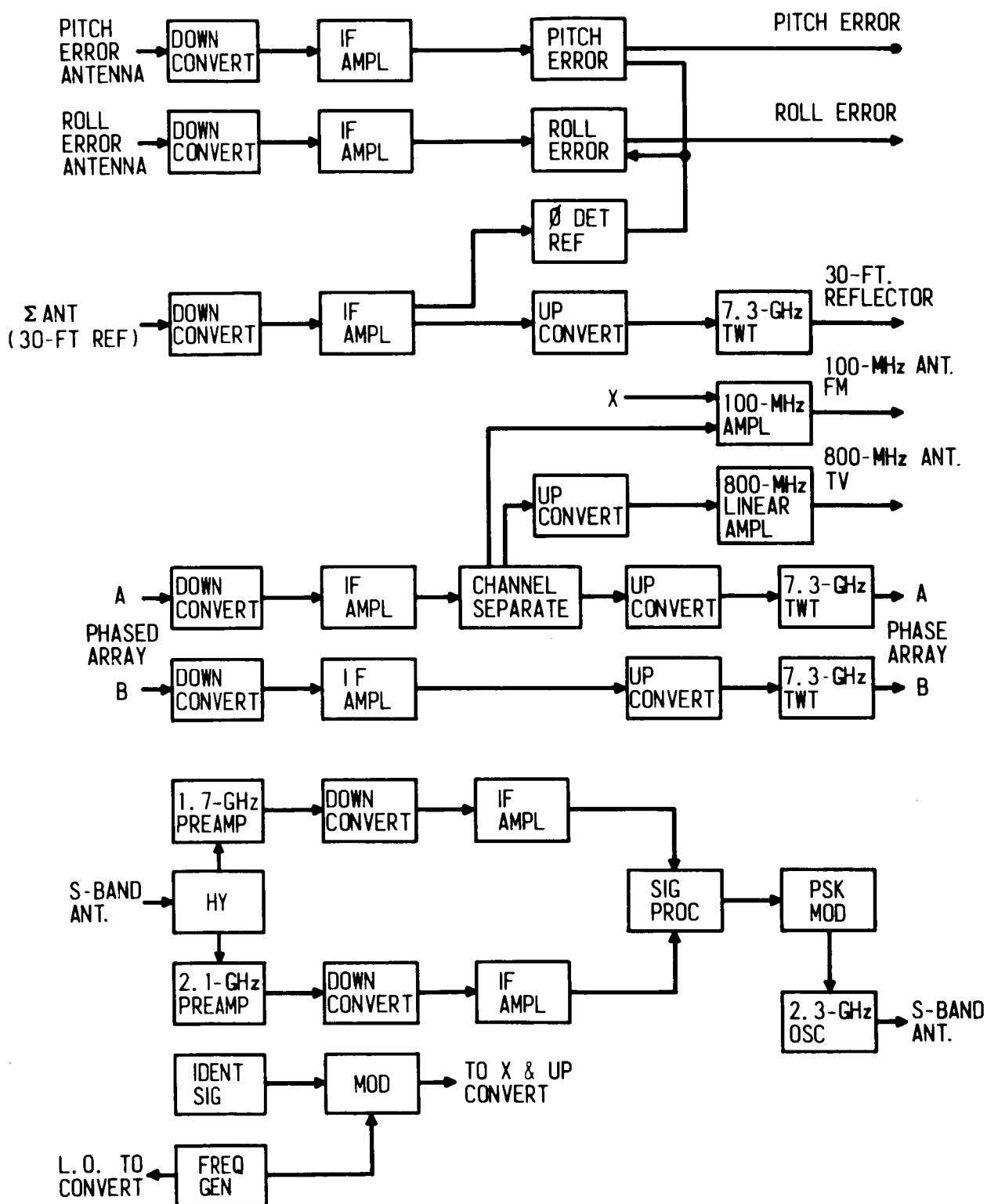


Figure 2.6-2 ATS-4 Communications Systems

The S-band receivers will have modular redundancy similar to the X-band receivers, but no channel switching. The signal processor and 2.3 GHz oscillator will have standby units.

In the frequency generator, the local oscillator signals will be generated by two master oscillators. One will generate all the X-band local oscillator signals and the other will generate the S-band, 800 MHz and 100 MHz signals. Each oscillator will have a standby circuit which will be switched in on command. The simple identification signal for antenna pattern measurements will not be redundant, but the oscillator for generating signals from the transmitting portion of the transponder will have a standby oscillator. While identification of the signal is desirable, it is not essential to the pattern measurements, whereas the oscillator signal is necessary to generate an output from the RF power amplifiers. Without the oscillator, a slightly degraded performance on pattern measurements is available by sending a signal up to the satellite and receiving the transposed signal on the ground.

All switching will be done with semiconductor switches and will be controlled from the ground. The voltage, current and temperature of each module will be telemetered to the ground along with such parameters as diode RF output current in the frequency converters, and SWR from the power amplifiers to their respective antennas. Decision to switch in redundant modules or channels will be made by ground control.

2.6.6 Phased Array Monopulse Operation

The beam steering unit on the satellite contains a 1536 bit case memory, in which the phase shift data for up to 8 separate beams may be stored. Upon command these may be rapidly cycled through the phase shift register as is done in the static pattern measurements (Section 2.2.3) and in the failure mode element phase tests (Section 2.2.3). A further use for the versatile phased array antenna utilizing this beam cycling function is to provide an emergency back-up for the monopulse tracker in the reflector antenna feed.

Phase data for a set of four beams which overlap at the proper angles to form a sequential lobing cluster may be transmitted to the core memory in about 25 seconds. These four beams when rapidly cycled through the phase register are used to supply accurate tracking information.

Once the data is in the memory, the data link system is used to carry the cycling timing information. Two possible instances in which this tracking capability is valuable are:

- Monopulse circuit failure. Should a failure occur which disables the tracking capability of the reflector feed, the phased array can be placed in the sequential lobing mode. The error signal generated can be supplied to the satellite attitude control system which performs as if it were supplied monopulse data. The accuracy would be about 0.03° which is poorer than that obtained from the monopulse (0.003°).
- Attitude Control System Failure. A malfunction in the attitude control system renders the monopulse system useless. Accurate attitude information might be obtained however by first scanning the phased array beam to a ground station location for an approximate "fix". About this beam axis then, the sequential lobing mode is used to obtain a coarse error indication. Using this error a new set of four beams are fed into the storage and a finer error obtained. Several iterations which take about 1 minute each could result in otherwise unobtainable attitude sensing accuracy.

2.7 WEIGHT SUMMARIES

The spacecraft and its subsystem weight summaries are collected in this section for easy reference. Tables 2.7-1 and 2.7-2 contain the spacecraft weight summary. Subsystem weights are given in Tables 2.7-3 through 2.7-11.

TABLE 2.7-1 SPACECRAFT WEIGHT SUMMARY - ORBITAL CONFIGURATION

	<u>Weight (lb.)</u>
Reflector (Including Deployment System, Locks, Etc.)	274
Stabilization and Control	192.8
Auxiliary Power System	172
Phased Array	166
Interferometer	30.5
**Solar Panels (Fixed)	103.0
Battery And Power Conditioner	77
Feed Mast	46
Communication Equipment	55
Structure And Mechanism	150
Telemetry, Command & Tracking	40
Cabling And Miscellaneous	30
Feed	15
	<hr/>
TOTAL	1351.

**Oriented Solar Panels Weight 50 Pounds Instead
of 103 Pounds For The Same Power Output.

TABLE 2.7-2 LAUNCH WEIGHT OF SPACECRAFT

	Weight	
	(lb)	(lb)
Nominal Payload To Synchronous Apogee, W_{san}		4,000
ΔW_{san} Due 10' Shroud Extension	50	
ΔW_{san} Due Δi Of 7.6° By Centaur	560	
Payload To Synchronous Apogee, W_{sa}		3,390
Centaur-To-Spacecraft Adaptor	150	
*Spin-Up And Spin Axis Control During 17 Hr. Coast	25	
Apogee Start-Burn Weight, W_{sb}		3,215
Propellant Weight, W_p	1,440	
Apogee End-Burn Weight, W_{eb}		1,775
Rocket Motor Expended Inerts	15	
**Despin Elements And Apogee Control Expendables	10	
Rocket Motor Inerts	145	
Final Orbit Payload, W_{pl}		1,605
In Orbit Spacecraft Weight	1,351	
Available For Additional Experiments	254	
*Table 2.7-11 Shows This Value To Be 10# Indicating This Value Is Conservative		
**Table 2.7-11 Shows This Value To Be 5# Indicating This Value Is Conservative.		

TABLE 2.7-3 REFLECTOR WEIGHT

	Weight (lb.)
Petals (32)	
24 at 3.69 lb = 88.6 lb	164
8 at 9.43 lb = 75.44 lb	
Hinges and Springs	35
Mesh	25
Inter-Petal Lock (32)	15
Down Lock (32)	15
Rate Control System	15
Insulation	5
TOTAL	274

TABLE 2.7-4 STABILIZATION AND CONTROL SYSTEM WEIGHTS

	<u>Weight (lb)</u>
Polaris Star Tracker	20.0
Z-Axis Horizon Scanner	18.0
Acquisition Sun Sensor	3.0
3 Axis Gyro Unit	10.0
Wheel Drive Electronics	5.0
Inertia Wheels	34.2
Reaction Jet Subsystem	54.0
SCS Controller	30.0
Power Inverter	<u>18.6</u>
TOTAL	192.8 lb.

TABLE 2.7-5 AUXILIARY PROPULSION SYSTEM WEIGHTS

	<u>Weight (lbs)</u>
Fuel	135
Tanks	25
Nozzles	3
Miscellaneous (Valves, Tubing Etc.)	<u>9</u>
TOTAL	172

TABLE 2.7-6 PHASED ARRAY WEIGHTS

	<u>Weight (lbs)</u>
256 Phasors, 64 Quadriplexers	64.0
64 Horns and Support Strut	13.2
64 Diplexer Circulator Package @ 5 oz.	20.0
8 Way Wave Guide Power Dividers	31.5
2 Transmitters (TWT's)	14.0
2 Receivers	1.5
1 Beam Steering Unit And Drivers	15.0
Miscellaneous (Cables, Connectors, Supports)	<u>7.0</u>
TOTAL	166.

TABLE 2.7-7 INTERFEROMETER WEIGHTS

	<u>Weight (lbs)</u>
Interferometer	15.0
Electronics	<u>15.5</u>
TOTAL	30.5

TABLE 2.7-8 POWER SYSTEM WEIGHTS

	<u>Weights (lbs)</u>
Solar Panels	103
Batteries	62
Power Conditioning	<u>15</u>
TOTAL	180

TABLE 2.7-9 COMMUNICATIONS EQUIPMENT WEIGHTS

	<u>Weight (lbs)</u>
X-Band down and up converters	2.50
100 MHz IF amplifiers	2.60
1.7 GHz Preamplifiers	0.37
Monopulse attitude error & detector	1.12
Identification signal	0.25
Modulator	0.25
Frequency generator	2.00
Stand down converter	1.00
800 MHz up converter	0.37
Signal processor & PSK mod.	0.50
2.3 GHz oscillator	3.00
100 MHz amplifiers	3.00
800 MHz amplifier with power converter	6.00
TWT with power supply	7.50
Channel separation filters and IF filters	2.00
Boxes, connectors, RF gasketing, cables, brackets, switches, etc.	7.54
Redundant Elements	15.00
	<hr/>
TOTAL	55.00

TABLE 2.7-10 TELEMETRY, COMMAND AND
TRACKING EQUIPMENT WEIGHT

	<u>Weights (lbs)</u>
Telemetry Antenna	4.2
Telemetry Electronics	14.8
Command Electronics	11.0
Tracking Antenna	2.0
Tracking Electronics	8.0
	<hr/>
TOTAL	40.0

TABLE 2.7-11 TRANSFER ORBIT CONTROL WEIGHTS

	<u>Weights (lbs)</u>
Spin-up jets	3.8
Control jets	6.3
Sun Sensor	1.5
Despin Yo-Yo	2.6
Cabling Connector	1.0
	<hr/>
TOTAL	15.2